Bimolecular charge transfer reactions at and through the liquid-liquid interface

Thèse N° 9658

Présentée le 8 novembre 2019

à la Faculté des sciences de base
Laboratoire d'électrochimie physique et analytique
Programme doctoral en chimie et génie chimique

pour l'obtention du grade de Docteur ès Sciences

par

Grégoire Clément GSCHWEND

Acceptée sur proposition du jury

Prof. J. Vanicek, président du jury
Prof. H. Girault, A. J. Olaya Avendano, directeurs de thèse
Prof. E. Vauthey, rapporteur
Prof. R. M. Corn, rapporteur
Prof. J.-E. Moser, rapporteur

2019

ÉCOLE POLYTECHNIQUE
FÉDÉRALE DE LAUSANNE

Remerciements

La réalisation de ce travail n'aurait pas été possible sans les apports essentiels et complémentaires de nombreuses personnes de talent. À cet égard, je tiens à exprimer tout particulièrement ma gratitude au Professeur Hubert Girault qui m'a accueilli dans son laboratoire aussi bien durant mon master que durant mon doctorat. Je lui suis reconnaissant de m'avoir accordé sa confiance et de m'avoir donné l'opportunité de mener librement mes recherches, tout en bénéficiant de son encadrement. Par ailleurs, j'ai également eu la chance d'être son assistant pour le cours d'électrochimie des solutions pendant trois années. Cette expérience s'est révélée particulièrement intéressante et enrichissante, car c'est aussi en transmettant des savoirs que l'on parvient à une meilleure compréhension de ces derniers.

Je souhaite aussi remercier ma codirectrice de thèse, la Doctoresse Astrid Olaya. Elle m'a non seulement montré et expliqué les bases de la spectroscopie aux interfaces liquide-liquide, mais elle a su m'apporter force conseils et solutions qui m'ont aidé à mener à bien mon projet. Son expérience s'est avérée bénéfique lorsque qu'il s'est agi de confronter mon travail au monde de la publication scientifique, qui suit ses règles propres, bien différentes de celles de l'électrochimie. Je remercie aussi le Professeur Pierre-François Brevet avec lequel j'ai eu le plaisir de discuter de mes résultats, mais aussi de spectroscopie et de science en général. Ses apports ont été nombreux et décisifs.

Mon travail n'aurait certainement pas été possible sans les connaissances et la disponibilité de M. Frédéric Gumy, qui a mis au point toute la partie technique de mon installation laser. J'ai appris énormément à ses côtés et son départ du laboratoire fut une grande perte pour moi. Je le remercie pour tout le temps qu'il a consacré à mon projet.

Tous mes remerciements aussi à M. Stéphane Voeffray et à M. Robin Delèze, qui ont mis au point plusieurs prototypes de cellules "spéctro-

électro-photochimiques" résistantes à toutes les agressions chimiques mais néanmoins d'une compacité remarquable, ainsi qu'à M. Patrick Favre, qui s'est occupé, entre autres choses, de l'électronique desdites cellules. À ce sujet, si l'électrochimie ne peut pas se passer d'électronique, la poursuite d'un doctorat ne peut se passer d'informatique. C'est donc naturellement que mes remerciements vont aussi à Cédric Passerini et Jean Perruchoud qui ont dépanné mon ordinateur à de nombreuses reprises. Je remercie aussi Mme Annabelle Coquoz et M. Laurent Seydoux, les responsables du "magasin de chimie", qui sont indispensables à réalisation de tout projet à l'EPFL de Sion.

Je remercie enfin tous les membres du LEPA qui m'ont aidé, directement ou indirectement, durant ces quatre années. Il serait impossible de citer ici l'intégralité de leurs innombrables contributions, mais c'est précisément dans ces occasions que l'on prend conscience qu'un travail s'inscrit toujours dans la continuité de celui des autres. J'espère ainsi leur avoir apporté autant qu'ils m'ont donné.

Résumé

Les interfaces sont omniprésentes dans la Nature. Parmi elles, les interfaces entre fluides sont des constituants essentiels des tissus biologiques. C'est à ces interfaces qu'ont lieu de nombreux phénomènes et réactions électrochimiques. A cet égard, les interfaces entre deux solutions d'électrolytes non miscibles (Interface Between Two Immiscible Electrolytes Solutions (ITIES)) constituent des modèles intéressants pour étudier ces phénomènes car elles sont notamment plus faciles à mettre en place du point de vue expérimental. Néanmoins, certains aspects théoriques régissants leur comportement restent à clarifier avant de pouvoir éventuellement les extrapoler aux systèmes biologiques. Ainsi, la présente thèse se propose de faire bénéficier l'étude des ITIES des progrès techniques réalisés dans le domaine de la spectroscopie de génération de seconde harmonique en temps résolu et dans le domaine des simulations de mécanique moléculaire.

Dans un premier temps, une étude par simulation moléculaires de la structure des ITIES est présentée. On y montre que, contrairement aux prédictions des modèles classiques de type "Goüy-Chapman" , les ITIES sont dépourvues de couches diffuses et que l'essentiel de la chute de potentiel se fait à l'interface, sur quelques nanomètres. En se basant sur ces résultats, une approche qualitative des courbes de capacitance de ces interfaces est proposée et montre qu'elles peuvent être vues essentiellement comme des condensateurs plans, à condition de prendre en compte le profile d'énergie des ions organiques proches de l'interface.

Dans un deuxième temps, la possibilité de réaliser des réactions de transfert d'électron aux ITIES est revisitée à l'aune des conclusions du premier chapitre expérimental. Il est montré que de telles réactions sont en effet possibles mais que la structure de l'interface impacte significativement leur cinétique. Ici, la possibilité de contrôler directement un transfert d'électron inter-moléculaire est discutée et proposée comme étant une

nouvelle manière de réaliser des réactions chimiques.

Enfin, le dernier chapitre présente une étude originale d'une réaction bimoléculaire contrôlée par la diffusion entre molécules adsorbées dans le plan de l'interface. La cinétique de cette réaction a la particularité d'être influencée par le changement de type de diffusion en fonction de la concentration interfaciale en molécules adsorbées. Ainsi, à faible couverture de l'interface, la diffusion dans le plan est normale et la cinétique peut être décrite par le modèle de Smoluchowski transposé aux systèmes bi-dimensionnels. Néanmoins, avec l'augmentation de la densité de couverture de l'interface, la diffusion devient "anormale", et la cinétique ne peut plus être décrite par une approche classique. L'évolution du type de diffusion est aussi observée dans des simulations de mécanique moléculaire conduites sur des échelles de temps comparables.

Ainsi, nous pensons que cette thèse présente des résultats intéressants, qui éclairent certains aspects de l'électrochimie des ITIES. Aussi, elle devrait constituer une base utile pour la poursuite de l'étude de ces interfaces et, ultimement, de celles des interfaces biologiques.

Abstract

Interfaces are ubiquitous in Nature. Among them, soft interfaces are essential constituents of biological tissues. Indeed, many electrochemical reactions and phenomena take place at these interfaces. In this respect, ITIES are an interesting model to study such phenomena because they are notably easier to experimentally setup. Nevertheless, some theoretical aspects governing their behaviour are still to be clarified before they can be possibly transposed to biological systems. Thus, the present thesis aims at bringing the progress accomplished in the domains of Time-Resolved Second Harmonic Generation (TRSHG) and molecular mechanics simulations to the study of ITIES

First, we present a molecular mechanics study of the structure of the polarised soft interfaces. It is shown that, contrary to the predictions of classical Goüy-Chapman type models, ITIES are devoid of diffuse layers and that the main part of the potential drop occurs at the interface, over few nanometres. Based on these results, a qualitative description of the capacitance curves of these interfaces is proposed and shows that they can be essentially seen as a plan capacitor, given that account is taken of the free energy profile of the ions close to the interface.

Secondly, based on the conclusions of the first experimental chapter, we revisit the possibility to carry out electron transfer reactions at ITIES. It it shown that such reactions are indeed possible but that the interface structure significantly impact their kinetic. Here, the possibility to directly control an intermolecular electron transfer is discussed and proposed as a novel way to realise chemical reactions.

Finally, the last chapter presents an original study of a diffusion-controlled bimolecular reaction between molecules adsorbed in the plan of the interface. Interestingly, the kinetic of this reaction is influenced by the concentration dependent diffusion regime. Thus, at low surface

coverage, the kinetic can be described within the Shmoluchowski model transposed to two-dimensional systems. Nevertheless, with the increase of surface coverage, the diffusion becomes "anomalous" and can no longer be described with a classical approach. The progressive change of diffusion regime is also observed in molecular mechanics simulations realised on similar time-scales.

Thus, we think that this thesis presents interesting results that shed light on some aspects of electrochemistry at the ITIES. Also, it should be a useful basis for further studies of these interfaces and, eventually, of biological interfaces.

Keywords: ITIES, electrolyte solutions, second-harmonic generation, molecular mechanics, capacitance, electron transfer, anomalous diffusion, triplet-triplet annihilation

Contents

Glossary

BSPBPy 1,1'-bis(4-sulfophenyl)-[4,4'-bipyridine]-1,1'-diium.

DCE 1,2-Dichloroethane.

DFT Density Functional Theory.

DMFc Decamethylferrocene.

DMRc Decamethylruthenocene.

ECSOW Electron Conductor Separating Oil-Water.

FLE Fractional Langevin Equation.

GCM Goüy-Chapman model.

IMPS Intensity Modulated Photocurrent Spectroscopy.

ITIES Interface Between Two Immiscible Electrolytes Solutions.

LLI Liquid-Liquid Interface.

MSD Mean Squared Displacement.

NLO Non-Linear Optical.

OA Operational Amplifier.

OPLS Optimized Potentials for Liquid Simulations.

PB-PMF Poisson-Boltzmann Potential of Mean Force.

PZC Point of Zero Charge.

SECM Scanning Electrochemical Microscopy.

SHG Second Harmonic Generation.

TCNQ 7,7,8,8-tetracyano-p-quinodimethane.

TFT α,α,α-trifluorotoluene.

TRSHG Time-Resolved Second Harmonic Generation.

TTA Triplet-Triplet Annihilation.

TTA-UC Triplet-Triplet Annihilation Up-Conversion.

ZnTMPyP Zinc-5,10,15,20-(tetra-N-methyl-4-pyridyl)porphyrin.

Introduction

The particularity of liquid-liquid interfaces LLI, in comparison to other interfaces, is that the two condensed phases they separate are fluid. In this respect, they can be continuously deformed and allow matter diffusion. One of the difficulties in studying liquid phases, and therefore liquid interfaces, is that unlike solids they do not have a crystal order, and unlike vapour phases, intermolecular interactions are of critical importance. Thus, no assumption of periodicity or homogeneity of their structure can be made. For these reasons, the molecular structure of the LLI has long remained controversial. However, using different experimental approaches like neutron reflectivity [1], X-ray reflectivity [2] or molecular mechanics simulations [3], their structure could be elucidated and it is now established that the liquid-liquid interface is molecularly sharp but roughened by capillary waves, with an amplitude of approximatively one nanometre [1–3].

The relevance of the LLI to electrochemistry was shown in 1968 by Gavach *et al.* who demonstrated that ion transfer could be observed at the ITIES [4]. Later, Samec *et al.* reported the observation of an electron transfer at the polarised ITIES[5]. These two fundamental studies showed that electrochemistry at the ITIES was actually more diverse than that at the Electrode-Electrolyte Interface (EEI) since both ionic and electronic currents are allowed to take place. Since then, many others such charge transfer phenomena have been reported, however the mechanisms by which they operate are still open questions. This situation is mainly the consequence of the absence of accepted models of the polarised ITIES. Indeed, how can interfacial electrochemical reactions be understood without a reliable molecular description of the polarised interface?

Structure of the polarised ITIES

In the early years of the study of the ITIES, their structure was deduced from surface tension measurments and was found to be well described by two back-to-back diffuse ionic layers separated by oriented solvent molecules [6–9]. This model – called the Modified Verwey-Niessen model (MVN) – was also able to qualitativelly describe the trends of the capacitance curves of the polarised ITIES [10, 11]. However, these studies were limited mainly to the water/nitrobenzene interface and to a restrained choice of organic supporting electrolytes, typically tetraalkylammonium/tetraphenyl borate. Such systems offer a relatively narrow potential window, which does not allow to test the validity of the MVN in various experimental conditions or at large polarisations. Thus, the limitations of the MVN model appeared clearly when the capacitance of the ITIES was systematically studied with different organic solvents and various aqueous and organic supporting electrolytes at different concentrations. In particular, several authors questioned the relevance of an ion-free layer of oriented solvent molecules and it became clear that ion penetration inside the solvent layer was necessary to take account of the experimental results [12–16]. Indeed, they showed that the surface tension of a non-polarised ITIES was dependent on the aqueous electrolyte type and concentration [13], which implies that ions are present at the interface, since they change its physical properties, but also that the capacitance of the ITIES could not be decomposed in the sum of diffuse and of compact layer contributions[14, 15].

The importance of the ion–solvent interaction was highlighted by computer simulations of the polarised ITIES. This was first shown using a lattice gas model. Indeed, despite their crude representation of the intermolecular interactions, such models could show that the capacitance of the ITIES was dependent on the ion Gibbs energy of transfer but also that there was a significant overlap of the aqueous and organic ionic layers at the interface [17, 18], in agreement with the experimental results. Then, molecular mechanics simulations were coupled to the Poisson-Boltzmann equation in the Poisson-Boltzmann Potential of Mean Force (PB-PMF) model. This approach was able to successfully describe the electron density at the polarised ITIES measured by X-ray reflectivity. Compared to the previous theories based on the MVN model, the PB-PMF predicts sharp ion densities on both sides of the interface and, similarly to the lattice gas models, an overlap of the ionic densities [19–23]. Thus, in almost

fifty years, the representation of the polarised ITIES evolved from that of two diffuse ionic layers separated by oriented solvent molecules, to that of sharp ion profiles strongly coupled to the solvent densities. Nowadays, the PB-PMF model constitutes one of the most accurate representation of the polarised ITIES. Nevertheless, despite its success for some systems, this theory sometimes predicts unrealistic ionic profiles at zero or negative polarisations, implying that it could still be improved [24].

Ion transfer at the ITIES

As mentioned above, the polarised ITIES, contrarily to the EEI, offers the possibility to observe both electron transfer and ion transfer reactions. Before the advent of reliable models of the ITIES, ion transfer was studied mainly from a pure electrochemical point of view, *i.e.* authors were mainly interested in the description of the kinetic of the ion transfer in order to relate it to the observed interfacial currents [25–27]. It was quickly suggested that the ion transfer was an activated process, although the origin of the activated step was debated. Indeed, some authors thought the transfer as a chemical reaction, [28–31], while others considered it as a mass transport phenomenon [25, 32]· The difference between these two approaches is that in the former case, a molecular description of the interface is not necessary, while in the latter case, a good understanding of the interface structure and ion solvation is needed [33].

Similarly to the studies of the structure of the ITIES, the understanding of ion transfer beneficiated from the progress of computational chemistry. Interestingly, in some molecular mechanics simulations, the transfer of charged species at the LLI appears as a non-activated process, *i.e.* the enegy of the ion rises smoothly from one phase to the other [34–37]. These conclusions are in contradiction with the electrochemical measurements presented above, but also with the lattice gas models, that indeed clearly show a potential dependent activation barrier at the polarised ITIES [38, 39]. Although lattice gas models are simpler than molecular mechanics simulations, the conclusions they draw are probably more reliable because firstly they are in agreement with experimental results, and secondly they take into account the whole ITIES structure (solvents, supporting electrolytes and counter-ions) and do not simply consider a single ion. Unfortunately, lattice gas models did not reached the same popularity than

the molecular mechanics simulations, and they are only a small number of studies using them to simulate the ITIES. Nevertheless, improvements of the molecular mechanics methods, in particular simulations using polarisable force fields [40] or carried out in an external electric field, showed non-linear energy profiles, with energy minima at the interface, or even activation barriers, given a different definition of the transfer reaction coordinate [41, 42].

One of the limits of the molecular mechanics simulations is that they did not take account of the presence of other ions in the system because of the limitations of the computational ressources. However, several experimental results demonstrated later that indeed, supporting electrolytes are of critical importance in explaining the ion transfer mechanism. Using nanometer-sized interfaces – an experimental configuration that allows to work without supporting electrolytes[43] – Laforge *et al.* showed that organic phase electrolytes where necessary to "shuttle" the transfer of alkali metal ions from the aqueous phase to the organic phase [44]. Using the same method, Sun *et al.* suggested that the transfer of strongly hydrophilic ions did not take place from the aqueous to the organic phase, but rather to aqueous clusters in the organic phase [45]. Therefore, these results highlight that it is necessary to include all the molecular constituents of the ITIES in the simulations to properly describe the mechanism of ion transfer at the ITIES.

Electron transfer at the ITIES

Since its first observation at the nitrobenzene-water interface between $Fe(CN)_6^{3-}$ and ferrocene by Samec, Marecěk and Weber in 1977 [5], the electron transfer reaction at liquid-liquid interface has been the object of numerous debates and questioning. Indeed, this phenomenon had to be explained while the precise structure of the interface was not precisely known. Could the kinetics be described by classical Butler-Volmer theory or does it require a new model? Is the electron transfer actually heterogeneous or homogeneous, involving therefore subsequent ion transfer? What is the role of the polarisation of the interface on the kinetics? At the time, all those questions were difficult to address because of the lack of experimental methods specific enough to the peculiar nature of the liquid-liquid interface. Now, almost forty years after the article of Samec *et al.*, there is a better

understanding of the electron transfer reaction at the ITIES but, nevertheless, unambiguous results are still needed to get a complete understanding of this phenomenon.

Early years

The early years of the study of the electron transfer reaction at the liquid-liquid interface were mainly devoted to the development of theoretical models describing the kinetics of the charge transfer. The first theoretical description was proposed by Samec in 1979 [46] followed by Girault&Schiffrin in 1988 [33] and Marcus in 1990 [47]. Although they are derived from different considerations, the models of Samec and Girault&Schiffrin are quite similar. The main differences being that the model of Samec does not take account of the work due to the change of chemical potential and activity coefficient of the reactants as they approach the interface, nor of the formal redox potential difference between the reagents. Thus, according to Girault&Schiffrin, the observed second order rate constant can be expressed as:

$$k_{obs} = \delta r \, \nu_{eff} \, e^{\frac{1}{RT}\left(-\frac{\lambda}{4}-(1-\alpha)w_p^{\ominus}-\alpha w_s^{\ominus}-z_{o1}F\Delta_1^a\phi-z_{r2}F\Delta_2^b\phi-\alpha zF\left(\Delta_b^a\phi-\Delta\phi_{o1/r2}^{\prime\ominus}\right)\right)} \tag{1}$$

In the equation 1, the first pre-exponential terms, δr and ν_{eff}, are respectively the range over which the electron transfer is taking place and a factor depending on the frequency of the nuclear motion along the reaction coordinates. The first term in the exponential depends on the vertical reorganisation energy, the next four terms describe the work necessary to form the precursor and successor complexes and the last terms take account of the reaction driving force, both as the difference of Galvani and formal redox potentials between the reactants. The main conclusion from this equation is that if the distance separating the reactants is small compared to the distance over which the Galvani potential drop occurs, or, in other terms, that only a small fraction of the potential drop acts on the reactive complex, most of the interface polarization contribution to the kinetics will be on bringing the reactants to the interface. This highlights one of the main questions concerning the electron transfer reaction at ITIES: is the polarisation dependent current due to a change of the driving force or to a change of the interface reagents concentration?

Indications concerning the role of the polarisation were published by Geblewicz&Schiffrin in 1988 [48] in a study of the electron transfer between a lutetium biphthalocyanine and $Fe(CN)_6^{4-}$ at the DCE-water interface by voltammetry which concluded that, for this system, the double layer effects were negligible, and that the reagents were probably relatively far from each others, explaining therefore an irreversible kinetics. These observations supported the idea that the work terms in equation 1 were negligible and that the main factor contributing to the kinetics was the potential difference between the reagents. Nevertheless, as mentioned by the authors, more accurate determinations of the rate constant were required to test their hypothesis. Indeed, this study was carried on by cyclic voltammetry, the rate constants being calculated using the Nicholson method[49]. However, this method was developed for the electrode-electrolyte interface. Its application to liquid-liquid interface was therefore to be considered carefully. In 1991, Cheng&Schiffrin [50] found results comparable to those of Geblewicz&Schiffrin[48]. They studied the electron transfer between ruthenium and iron tetraphenylporphyrins by voltammetry and concluded that, when the concentration of one of the redox species is high enough, its respective phase can be considered as metallic, supporting therefore the validity of the Nicholson method. Like Geblewicz&Schiffrin[48], they found a rather slow kinetics — compared to what could be expected at a true metal-electrolyte interface — and explained this difference by the need to displace the porphyrin ligands before the electron transfer takes place.

The model derived by Marcus [47][51] gives the following equation for the electron transfer rate constant:

$$k_r = \kappa\nu \exp\left(-\frac{1}{k_b T}\left(w_p + \frac{(\lambda + \Delta G'^{\ominus} + w_s - w_p)^2}{4\lambda}\right)\right) \qquad (2)$$

The equation 2 contains the same parameters than the equation 1, that is a pre-exponential factor depending on the nuclear vibrations, the work terms to bring the reagents to the reaction point and to separate them after the reaction, the reorganization energy and the reaction free energy. This expression is however remarkable because it quadratically depends on these terms. Thus, assuming that w_p, w_s and λ are independent of the reaction Gibbs energy, the rate constant will increase with decreasing $\Delta G'^{\ominus}$, reach a maximum and then start to decrease. This behaviour, signalling the entry

in the "inverted region", is characteristic of the electron transfer theory developed by Marcus.

Using impedance spectroscopy, Cheng&Schiffrin [52] found in 1993 a quadratic dependence of the rate constant on the applied Galvani potential difference. Analysing the results with the help of the Marcus theory, they however found that the observed quadratic dependence was better explained by a diffuse layer effect than by a true quadratic dependence of the activation energy on the driving force as expected from the theory. Indeed, measuring the interface capacitance, they found significant ion pairing between the organic and aqueous phase that induced a dependence of the transfer coefficient on the potential difference. This observation is critical because it shows that a model such as that of Girault&Schiffrin[33] can also lead to non linear dependence of the rate constant on the driving force. Thus, observation of a quadratic relation does not necessarily imply that the Marcus model is applicable and a careful evaluation of the other parameters and assumptions underlying the models has to be made.

New experimental approaches

The first studies on the electron transfer reaction at the ITIES were limited to classical electrochemical techniques such as cyclic voltammetry or impedance spectroscopy. Sometimes, different approaches were proposed like for instance a photoinduced electron transfer between ruthenium tris-bipyridine and 7,7,8,8-tetracyano-p-quinodimethane (TCNQ) [53]. Nevertheless, the classical tools of electrochemistry were not optimal to study the redox reactions across a liquid-liquid interface. Indeed, voltammetry does not discriminate between current due to ion or to electron transfer. Thus, the kinetic parameters derived from those studies were always plagued by the uncertainty concerning the origin of the current actually measured.

In 1996, Selzer&Mendler [54] published an article where they showed that Scanning Electrochemical Microscopy (SECM) could be used in the study of the electron transfer across the liquid-liquid interface. They emphasised that the previous methods were limited by the difficulty to separate ion transfer from electron transfer, as well as by the need to compensate the large iR drop in the organic phase. Furthermore, the range of organic solvent that could be used was restricted to those able to dissolve organic electrolytes. The use of SECM solved these problems

because the measured current was only the one related to the regeneration of one of the redox species, while the interface polarisation is ensured by the presence of a potential determining ion in both phases. Briefly, SECM consists in the generation of a redox species at the tip of a glass-coated micro-electrode (either oxidation or reduction). The so-generated compound then diffuses and reacts at the interface. By approaching the electrode closer and closer to the interface, the current measured at the tip of the micro-electrode increases because the reactive species must diffuse through a shorter distance. The results are then plotted as a current over distance (to the interface) graph — so-called "approach curves" — that, when fitted with an appropriate model, provides information on the kinetics at the interface. This last point is actually one of the weaknesses of the SECM. Indeed, it relies on the ability to build a theoretical model of the experiment, as well as to fit the results with this model.

Although Selzer&Mendler[54] were the first to present SECM as a "new tool" to study the electron transfer at the liquid-liquid interface, this technique had already been used earlier by Solomon&Bard in 1995 [55] in a short but critical publication where they studied the reaction between $Fe(CN)_6^{4-}$ (generated at the tip of the electrode) and TCNQ at the 1,2-Dichloroethane (DCE)-water interface. This experiment was interesting because, as the authors said, the reaction was "uphill", *i.e.* not thermodynamically spontaneous. Indeed, according to the author, the formal redox potential between the two species was -190 mV. Therefore, the reaction needed an extra driving force to proceed. Thus, the measurement of a current that they reported had two strong implications for this system: firstly the electron transfer was heterogeneous because a homogeneous reaction is not thermodynamically possible, and secondly a significant — significant enough to overcome the thermodynamic limitations — fraction of the Galvani potential difference was present between the reagents to allow the reaction to proceed.

The conclusions of Solomon&Bard[55] were nevertheless slightly moderated by another study of Wei *et al.*[56] claiming that the reaction could not be only heterogeneous because of a significant partitioning of the reagents. Indeed, using SECM, they studied the oxidation of ferrocene by the tip-generated $Ru(bpy)_3^{3+}$ at the nitrobenzene-water interface, they found that roughly 10% of the current could come from the homogeneous oxidation of ferrocene. This proportion was however of the same magnitude that the

experimental error and they did not correct their results for this artefact. This experiment highlights another problem encountered when studying the electron transfer at the liquid-liquid interface. Indeed, each system is, at least to some extent, peculiar, and general conclusions on the mechanism or kinetics of the reaction can be drawn only if one is sure that the experiment is generic enough. In the case of Wei *et al.*[56] the use of ferrocene as electron donor in the organic phase could be questioned because a significant partitioning of ferrocene and ferrocenium in the aqueous phase had already been reported years ago [57].

Apart from the publication of Wei *et al.*[56] the mechanism of the electron transfer was assumed to be most of the time heterogeneous and the main interrogation became the elucidation of the role of the interface potential difference. Tsionsky *et al.*, in two articles published in 1996[58] and 1997[59], analysed by SECM the influence of a Galvani potential difference on the electron transfer between the zinc tetraphenylporphyrin cation (generated at the tip of the microscope) and various aqueous redox couples. They found that the kinetics of the reaction was strongly correlated to the potential difference, with Tafel plots having a slope of roughly 0.5. Furthermore, based on the incompatibility of their work with that of Katano *et al.* [60] they tentatively excluded possible double or inner layer effects. Nevertheless, they pointed that any correction to the observed kinetics would be difficult owing to the lack of information concerning the structure of the interface. For instance, they reported the formation of a film at the interface by pairing of hydrophobic and hydrophilic ions. Such phenomenon could obviously influence the kinetics but was hard to include in a model.

Tsionsky *et al.* also reported for the first time — according to the authors — the observation of the "Marcus inverted region" at the liquid-liquid interface by varying the driving force both by changing the formal redox and Galvani potential differences [59]. They also excluded double layer effects by working with a neutral organic redox species and with a high ionic strength in the aqueous phase. This result provided further evidence that the electron transfer was heterogeneous and dependent on the driving force. Furthermore, it supported the idea that a theory such as that of Marcus was necessary to describe the reaction.

In the years following the work of Tsionsky *et al.*[59] several publications introduced new techniques to probe the electron transfer at the ITIES, most of them based on spectroscopy [61–64]. They overall confirmed the

previous results on the heterogeneous character of the reaction and its dependence on the Galvani potential. The main interest of those studies was to show that a specific probing of the reactions taking place at the interface was possible beyond SECM.

In 1999, Liu&Mirkin [65] and Shi&Anson [66] independently, using different experimental approaches and systems, reported the observation of a Galvani potential difference independent electron transfer and even a redox potential difference independence (for Shi&Anson). Liu&Mirkin studied the system zinc tetraphenylporphyrin - $Ru(CN)_6^{3-}$ by SECM, while Shi&Anson used the decamethylferrocene - $Ru(NH_3)_6^{3+}$ couple with the thin layer technique. Briefly, this approach consists in depositing a small drop of organic phase on a graphite electrode and immersing it in the aqueous phase, where a counter electrode is placed. This method resembles SECM but avoid the ion transfer following the electron transfer necessary to maintain the electroneutrality. The advantage is that the electron transfer kinetic that is measured is free of possible limitations due to ion transfer. The main argument of Liu&Mirkin[65] compared to Tsionsky *et al.*[59] was that their system was truly neutral in the organic phase. Indeed, compared to Tsionsky *et al.* their micro-electrode was located in the aqueous phase and generated $Ru(CN)_6^{3-}$ while in Tsionsky *et al.* experiment it was the porphyrin that was oxidized. Therefore, it was concluded that the measurement of Tsionsky *et al.* could have been induced by double layer effects. The conclusions of Shi&Anson[66] are that the limiting step in the electron transfer is the formation of the precursor complex at the interface. Both articles supported their conclusions with a new model derived by Schmickler in 1997 [67]. In his model, Schmickler explicitly made the assumption that the potential drop between the reagents was small, and that most of the kinetic effects were due to changes in concentrations. However, these assumptions were valid only for solutions of low ionic strength, more precisely as long as the Debye length was shorter than the width of the interface. Using his model, Schmickler showed that effects similar to those predicted by Marcus theory — that is the "inverted region" — could, in some cases, be explained by concentration changes. Indeed, let's take as example an electron transfer from a negatively charged donor to a neutral acceptor. Increasing, the Galvani potential difference will increase the driving force but also decrease the concentration of the donor, the later effect can eventually overcome the former and lead to an apparent slower

kinetic with increasing free energy difference.

The main conclusion that could be drawn from the work of Schmickler[67], Liu&Mirkin[65] and Shi&Anson[66] was that the electron transfer was probably more difficult to explain that what could be expected from the work of Tsionsky *et al.*[58, 59]. In particular, the role of the ionic strength on the kinetics was highlighted. In this respect, Zhang&Unwin in 2000 [68], and Ding *et al.* in 2001 [69] published studies were, among other parameters, they studied the influence of the supporting electrolyte concentration on the rate constant. Both articles showed that the dependence of the kinetics on the potential difference decreased with the ionic strength. While Zhang&Unwin[68] explained this observation by a "salting-out" effect — that is a decrease of the solubility of the compounds with the ionic strength — , Ding *et al.*[69] concluded that it could be due to many phenomena, and possibly a combination of several of them. Among the possible explanations were specific adsorption of ions, ion transfer-electron transfer coupling, double layer effect, etc. They, however, refuted the hypothesis of Zhang&Unwin[68], arguing that the ionic strength dependence could be observed even when salts not acting as "salting-out agent" were used. The same year, Shi&Anson [70] also emphasized that the formal redox potential of the chemical species was dependent on the ionic strength and that it should always be measured in the experimental conditions. This suggestion was confirmed a year later when Zhang&Unwin [71] published the results of a study where they showed that, at least for the ferro/ferricynanide couple, the change of formal redox potential with the ionic strength could explain the lower dependence on the polarization.

Thus, it appeared that the electron transfer at ITIES was harder to describe than what one could expect from the earlier studies. In particular, it was recognized that contradictory results could be obtained with similar systems simply by changing some experimental parameters that could seem, at first sight, of lower importance. Furthermore, the need of more precise models, taking account of a larger number of parameters was required. Applying the technique of Intensity Modulated Photocurrent Spectroscopy (IMPS) to the liquid-liquid interface, Fermin *et al.* in 1999 [72] and then Eugster *et al.* in 2002 [73], published results that could for the first time discriminate between forward and backward electron transfer. Even if IMPS relied on data fitting according to a rather crude model of the interface, they could show a clear dependence of both the electron transfer and back

transfer on the Galvani potential difference. Nevertheless, Fermin *et al.* moderate their conclusions by suggesting that the aqueous redox species — a negatively charged zinc porphyrin — could have changed the kinetics by a concentration effect and specific adsorption. This problem was, however, not present in the experiment of Eugster *et al.* where both redox species were neutral. The data that they published were consistent with the Marcus theory — including the "inverted region" — and they found an average distance of 8Å between the reagents. This result lead them to question the generally admitted picture of the liquid-liquid interface where only a small fraction of the total Galvani potential difference occurs between the reagents.

In their studies, Fermin *et al.*[72] and Eugster *et al.*[73] polarized the interface with a four-electrode potentiostat and not with a common ion, as it was usually the case for SECM experiment. This method allowed the measurement of the kinetics over a wider potential window and with smaller potential steps. Furthermore, ion transfer-electron transfer coupling is avoided. This permits the construction of graphs showing the rate constant recorded at many potential differences while, with the common ion method, only few points were shown. This lack of data was insufficient to, for instance, unambiguously highlight a Marcus "inverted regions". In 2002, Zhang *et al.* [74] showed that a similar system could be used to polarise the interface in SECM studies. Using this modified procedure, Sun *et al.* [75] reported in 2003 the measurement of a clear "inverted region" at the DCE-water interface. Their experiment was carried out with different organic redox species and at various organic ionic strengths. The Marcus prediction could be observed in all cases, while it appeared that the organic electrolyte concentration effect was mainly to level off the kinetics without significantly change its dependence on the Galvani potential difference.

The years following the work of Sun *et al.*[75] did not see the emergence of new conclusions, experimental approaches or models concerning the electron transfer at the ITIES. One can, however, cite a publication of Hotta *et al.*[76] in 2003 claiming that the electron transfer at the liquid-liquid interface was a homogeneous process. This article jeopardized what seemed to be a "well admitted" idea, following the work of the past years, that the transfer was indeed heterogeneous. Hotta *et al.* studied the ferrocene - $Fe(CN)_6^{3-}$ system at the nitrobenzene - water interface by Electron Conductor Separating Oil-Water (ECSOW). This method consist

in kipping the aqueous and organic phases physicaly sperated but to connect them with an electron conductor to allow electron transfer. Thus, electron transfer is allowed between the phases but not ion transfer. The kinetic parameters are then extracted by fitting the data with an appropriate model. They showed that their measurements were not compatible with a model describing an heterogeneous mechanism. They explained that the disadvantage of a homogeneous reaction — the need to bring the reagents in the other phase and then transfer the products — was counterbalanced by a larger reaction volume. Nevertheless, their conclusions could be moderated by recalling that they worked with high concentrations of ferrocene that had been shown to significantly partition in the aqueous phase, particularly with nitrobenzene. One year latter, Osakai *et al.* [77], using the same method, published another article where they reported the observation of a "true" electron transfer, that is an heterogeneous transfer. This time they worked with the more hydrophobic cadmium tetraphenylporphyrin, still at the nitrobenzene-water interface.

Scope of the present thesis:

Significant progress has been made over the past decades in the understanding of electrochemistry at the ITIES. These developments opened the way to several applications of charge transfer phenomena at the polarised LLI. Nevertheless, our representations of these reactions remain imperfect. The reason for this is that we still lack a complete knowledge of the ionic structure of the polarised ITIES. Thus, ion transfer and electron transfer reactions can only be studied by indirect methods, which explains why their mechanisms are still debated. In the case of electron transfer, the main question remains that of its dependence on the potential difference at the interface. In the case of ion transfer, the kinetic aspects and the role played by the supporting electrolytes continues to be controversial. Molecular mechanics simulations have been shown to be a valuable tool to understand the ITIES at the molecular level but, unfortunately, previously published results using this method did not take account of the whole complexity of these systems, which somehow limits the range of their conclusions. Thus, here, we propose to carry out large scale atomistic simulations of the polarised ITIES in order to shed a new light on the potential dependent charge transfer phenomena that are observed at these interfaces. Also,

with the help of surface sensitive time-resolved spectroscopic techniques – TRSHG – we will show that chemical reactions can take place not only at the LLI but also in the place of the LLI, *i.e.* in a formally two-dimensional medium. The conclusions presented in this work should bring a new vision on charge transfer reactions at soft interfaces, a subject that has already puzzled several generations of researchers.

Chapter 1

Experimental methods

1.1 Time-resolved second harmonic generation

Spectroscopic setup

SHG data were acquired with the setup presented in Figure 1.1. The pump and probe pulses (∼30 ps, 50 Hz) were generated each by a parametric generator Ekspla PG400 series, pumped by a laser Ekspla PL2230 series. The delay between the pump and probe beams was controlled by a pulse/delay generator BNC model 575. The time resolution of the setup is limited to ∼11.4 ns by the impossibility of synchronise the master oscillators of the lasers. Indeed, the oscillators have a frequency of 87 MHz. Nevertheless, only the opening of the oscillator cavity can be synchronised, not the oscillations. Therefore, the delay between two pulses (one pulse per lasers) can vary between 0 and 1/(87 MHz), *i.e.* 11.4 ns.

The two beams were collinearly aligned with the help of a non-polarising cubic beam splitter that reflected the probe beam but transmitted the pump. In practice, the pump and the probe beams were not exactly collinear: there was a small angle between them in order to compensate for the dispersion at the glass-solvent interface, ensuring that they were collinear in the cell. Then, the beams were focused on the interface, in total internal reflection, by a 100 mm lens (spot size ∼100 μm). The second harmonic of the probe beam, the signal, was then collected by a 100 mm lens and sent to a Triax 320 spectrophotometre. A short-pass

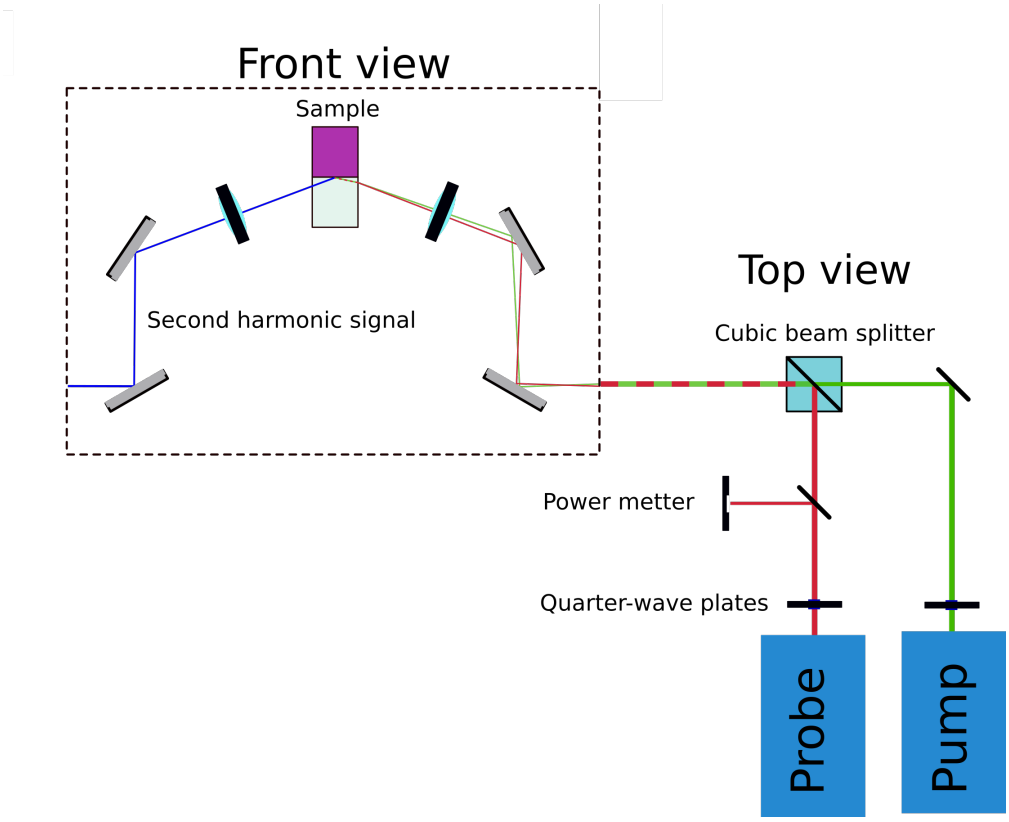

Figure 1.1: *Schematic representation of the time-resolved second harmonic generation setup.*

interference filter cutting the wavelengths longer than 500 nm was placed at the entrance of the spectrophotometre to cut the residuals of the pump beam (565 nm). The signal was then detected by a photomultiplier tube Hamamatsu R928, sent to a boxcar averager and recorded in a computer. The polarisation of the pump and probe pulses were made circular with the help of a quarter-wave plate. The typical pump and pulse energy lied between 0.1 µJ and 2 µJ, the probe energy ranged from 2 µJ to 10 µJ depending on the concentration.

Precautions for sample preparation

The strength of SHG is that it is only sensitive to molecules adsorbed at the LLI. However, this is also a weakness in the sense that small perturbations of

the interface can disturb the measurements. For instance, in the case of Zinc-5,10,15,20-(tetra-N-methyl-4-pyridyl)porphyrin (ZnTMPyP), which is used in Chapter 5, at a bulk concentration of 500 nM, the surface concentration is $4.7{\cdot}10^{-8}{\cdot}\text{mol}{\cdot}\text{m}^{-2}$. Thus, assuming that SHG is generated in the whole fundamental beam spot (diameter of 100 µM) it can be concluded that only $\sim 2{\cdot}10^{8}$ molecules are probed on few molecular layers. Furthermore, taking into account that LLI are fluid – therefore subject to vibrations and capillary waves – makes SHG a very delicate method. Therefore, the following paragraphs aim at listing some advices on the preparation and manipulation of the spectroscopic cells for SHG measurements at the LLI.

Solvent equilibration

LLI are formed by definition between immiscible liquids. However, they are not strictly immiscible and there is necessarily a small quantity of water dissolved in the organic phase and *vice versa*. Thus, when the aqueous and organic phases are put in contact, it is necessary to wait a certain time until the phases are saturated. Nevertheless, it turns out that during equilibration, spontaneous emulsification of water in organic solvent occurs, leading to formation of a light white "veil" on the interface. Such a veil will usually make SHG measurements impossible. More precisely, SHG signal can still be detected but its amplitude varies of ±50% on time scales of few tens of seconds. These fluctuations are very characteristic and help identify the cause of the problem. Unfortunately, these emulsions are stable and the only solution is to prepare a new cell with pre-equilibrated aqueous and organic phases.

Temperature stability

Another problem that can arise is caused by temperature variations. Indeed, it was said in the previous paragraph that the liquid phases are partly miscible. Since the solvents are in large excess, the phases are saturated with each others. However, thermodynamic equilibria – and therefore solubility – depend on the temperature. Thus, once both phases are equilibrated, temperature should be kept constant in order to avoid changes of solubility that would unavoidably lead to formation of the interfacial emulsions described above. This phenomenon is particularly difficult to manage when the cells are prepared in a glove box, where temperature is usually higher

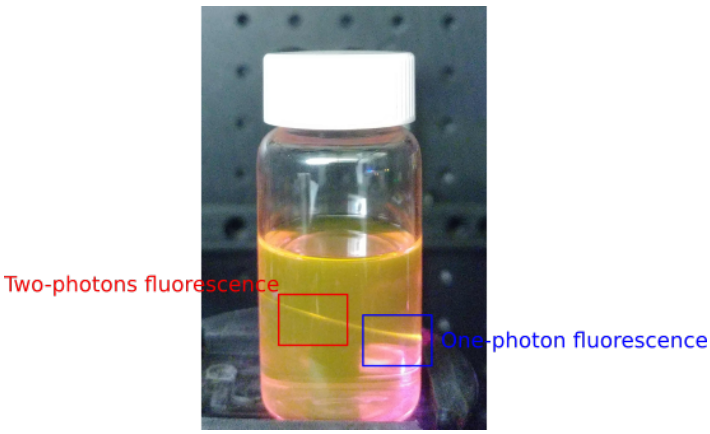

Figure 1.2: *One-photon (wavelength: 565 nm) and two-photons (wavelength: 900 nm) fluorescence of a Rhodamine B solution. The two-photon fluorescence is visible in the focal point of the fundamental beam while the one-photon fluorescence vanishes as the beam penetrates into the solution.*

than room temperature. As a rule of thumb, a temperature decrease of 5°C leads of "precipitation" of water in α,α,α-trifluorotoluene (TFT).

The issue of the variations of the solubility of the solvents with the temperature also arises with gases. However, in this case, it is a temperature increase that triggers the lowering of the solubility of the dissolved gasses and formation of bubbles trapped at the interface. Here, again, this problem can be avoided by keeping the temperature as constant as possible during the measurements and working with pre-equilibrated solvents. Furthermore, when working in a glove box, letting the cell in a light vacuum (0.5 atm) after preparation for few tens of second purges the solvents of excess gases and avoid bubbles formation. The presence of bubbles at the interface does not prevent SHG measurements, but considerably increases the signal noise.

Pump and probe beams alignment

When doing time-resolved experiments, it is of course necessary that the pump and probe beams are aligned at the interface. Such alignment is however difficult to obtain with the setup presented in Figure 1.1 for several reasons. First, the probe (fundamental) beam is not visible and secondly, both beams cross non-perpendicularly several solid/air interfaces (glass/air,

cuvette/organic phase) before being reflected on the liquid-liquid interface. Thus, since the refractive index of a medium is wavelength dependent, the beams will diverge after having passed through these interfaces. In order to overcome this problem, pump and probe beams where aligned visually by filling the optical cell with a solution of rhodamine B in TFT. Indeed, rhodamine B has a strong fluorescence that is visible after both one and two-photon absorption. Therefore, the optical path of the pump and probe beams could be seen by eyes (in the dark). Furthermore, since two-photon absorption is a non-linear process, it occurs only where the light intensity is high *i.e.* where the fundamental beam is focussed. Conversely, the intensity of the one-photon fluorescence decreases as the beam penetrates through the rhodamine B solution. Thus, it is still possible to distinguish the beams even if the fluorescences that they create have the same wavelength. This is illustrated in Figure 1.2

1.2 Molecular mechanics simulations

Short introduction to molecular mechanics simulations

Molecular mechanics simulations consist in simulating molecular systems, assuming that they can be described as simple objects obeying the laws of classical mechanics. Despite this crude approximation, molecular mechanics simulations can, on average and with the appropriate set of parameters, reproduce the physical properties of a system.

Force field

In molecular mechanics, two types of interactions between particules are considered: bonded and non-bonded interactions.

Bonded interactions describe the intra-molecular dynamics, they are of four types: bond stretching, angle bending, improper and proper dihedral deformations. The first three are usually approximated by an harmonic potential, while the proper dihedral are described with periodic functions. All the parameters of these potentials are derived prior to the simulation and are tuned to reproduce some experimental results. For instance, the Optimized Potentials for Liquid Simulations (OPLS) force

field, used throughout the present work, has been derived to reproduce the density and heat of vaporisation of various organic solvents[78]. Other common force fields include, for instance the "GROMOS" force field [79] (parametrised to reproduce solvation enthalpies of small organic molecules), or the "CHARMM" force field (parametrised to reproduce the binding energies and crystallographic structures of proteins and nucleic acids)[80]. Thus, the set of parameters of bonded interactions depends on the type of system that one wants to study.

Non-bonded interactions account for intermolecular forces: the Coulomb force, the Pauli repulsion and the dispersion forces. The Coulomb force is obviously described from the Coulomb potential, while Pauli repulsion and dispersion forces are both modelled with one single function: the Lennard-Jones potential. Lennard-Jones potential is strongly repulsive at short range (Pauli repulsion) and slightly attractive at long range (dispersion forces). Mathematically, the Lennard-Jones potential is the sum of a r^{-12} term and a r^{-6} term:

$$V_{LJ}(r) = \epsilon \left(\frac{\sigma}{r^{12}} - \frac{\sigma}{r^{6}} \right) \tag{1.1}$$

where ϵ is the depth of the attractive well, while σ is the minimum of the well. Interestingly, the r^{-12} term is not based on physical principles but has been chosen for computational efficiency. Indeed, it is faster to compute the r^{-6} term and then square it than to compute two independent terms.

There are actually many more ways to model bonded and non-bonded interactions but it is beyond the scope of the present report to list them all. This, however, does not impede the general understanding of molecular mechanics simulations.

Equation of motion algorithms

Once the system is constructed and its physics described by the appropriate interaction potentials, the dynamics of the system can be simulated by applying Newton's equation of motion *i.e.*:

$$r(t) = r_0 + v_0 \cdot t + \frac{F \cdot t^2}{2m} \tag{1.2}$$

where $r(t)$ is the time-dependent position, r_0 is the position at t_0, v_0 the velocity at t_0, F the force applied on the particle and m its mass. Nevertheless, Equation 1.2 cannot be used directly to compute the trajectory

of the system because v_0 and F are not constants but actually depend on r, which in turn, depends on time. Therefore, Equation 1.2 must be propagated step by step, assuming that the step size is small enough that the true physics of the system is conserved. Thus, Equation 1.2 becomes:

$$r\left(t+\Delta t\right)=r\left(t\right)+v\left(t\right)\Delta t+\frac{F\left(t\right)}{2m}\Delta t^{2} \tag{1.3}$$

One could have also written Equation 1.2 for past times:

$$r\left(t-\Delta t\right)=r\left(t\right)-v\left(t\right)\Delta t+\frac{F\left(t\right)}{2m}\Delta t^{2} \tag{1.4}$$

Then, summing Equation 1.3 and Equation 1.4 gives:

$$r\left(t+\Delta t\right)=2r\left(t\right)-r\left(t-\Delta t\right)+\frac{F\left(t\right)}{m}\Delta t^{2} \tag{1.5}$$

Thus, since $r\left(t\right)$ and $F\left(t\right)$ are known, the next position can be computed. Equation 1.5 is called the "Verlet algorithm" and is an efficient way to propagate Newton's equation of motion. However, Verlet algorithm does not explicitly compute particle velocity (though it can be computed afterwards). This quantity is however important to control the kinetic energy – therefore the temperature – of the system. Consequently, another version of the Verlet algorithm, that explicitly calculates the velocity and the position at the same step has been derived. The update of the particle position is done as follows. First, one calculates the velocity of the next half-step:

$$v\left(t+\frac{1}{2}\Delta t\right)=v\left(t\right)+\frac{\Delta t}{2m}F\left(t\right) \tag{1.6}$$

then the next position:

$$r\left(t+\Delta t\right)=r\left(t\right)+v\left(t+\frac{1}{2}\Delta t\right)\Delta t \tag{1.7}$$

and finally the velocity of the full step:

$$v\left(t+\Delta t\right)=v\left(t+\frac{1}{2}\Delta t\right)+\frac{\Delta t}{2m}F\left(t+\Delta t\right) \tag{1.8}$$

Since this algorithm is based on the Verlet algorithm and computes the velocity, it is called "velocity Verlet" [81]. Another common scheme it the "Leapfrog algorithm" it is however equivalent to the velocity Verlet.

Simulations in NVT and NPT ensembles

Simulating an ensemble with only the equations of motion would produce a system whose energy, number of particles and volume are constant *i.e.* a microcanonical or "NVE" ensemble. Nevertheless, one rarely works in such conditions in "real" experiments and it would be interesting to have a way to simulate systems with constant temperature or pressure. Thus, thermostats and barostats have been implemented in molecular mechanics to allow simulations in the canonical (NVT) or the isothermal-isobaric (NPT) ensembles.

A very naive way – but still efficient – to control the temperature of a simulation is to rescale the velocities of the particle after each steps (or n steps). This can be done by computing the temperature from the kinetic energy of the system, using the equipartition theorem – that states that every quadratic degree of freedom contribute to $1/kT$ of the energy – and the definition of the kinetic energy:

$$E_{kin} = \frac{m \cdot v^2}{2} = \frac{1}{2kT} \tag{1.9}$$

Then, the velocities of the next step are rescaled by a factor proportional to the deviation of temperature from that of the thermostat:

$$\frac{dT}{dt} = \frac{T_0 - T}{\tau} \tag{1.10}$$

where T_0 is the temperature of the thermostat and τ a coupling constant that controls the strength of the damping at each step. This algorithm is called "Berendsen thermostat" and is one of the most basic approach to simulate a NVT ensemble[82]. However, since the velocities are rescaled every step, the fluctuations of the kinetic energy over time are not physical and therefore this thermostat does not sample a true canonical ensemble and using this thermostat is actually not recommended[83]. Nevertheless, a true sampling of the canonical ensemble can be recovered with a slight modification of the Berendsen thermostat. This approach is called "velocity-rescaling" algorithm[84]. Here, the kinetic energy of the system is coupled to that of the thermostat according to the following equation:

$$dK = (K_0 - K)\,\frac{dt}{\tau} + 2\sqrt{\left(\frac{KK_0}{N_f}\right)}\frac{dW}{\sqrt{\tau}} \tag{1.11}$$

where τ is the coupling constant, K_0 the kinetic energy at the desired temperature, N_f the number of degrees of freedom and dW a Wiener process, *i.e.* a stochastic process with zero mean and whose steps are independent. The key modification of Equation 1.11, compared to Equation 1.10, is the addition of the stochastic Wiener process that guarantee realistic fluctuations of the velocities.

System pressure can be controlled similarly to the temperature using the Berendsen barostat. However, in this case, it is not the velocities that are rescaled at each steps but the simulation box dimensions. Indeed, the instantaneous pressure of the system is given by:

$$P = \rho T + \frac{1}{3V} \sum_{i>j} F\left(r_{ij}\right) \cdot r_{ij} \tag{1.12}$$

where ρ is the system density, V the box volume, T its temperature and the last term is the virial. Therefore, the pressure depends on the distance r_{ij} between the particles i and j and on the box volume. Thus, P can be controlled by rescaling both particle position and box length.

$$r' = \mu \cdot r \tag{1.13}$$

$$L' = \mu \cdot L \tag{1.14}$$

where r_i is the position of the particle i and L a dimension of the box. The scaling factor μ is given by:

$$\mu = \left[1 + \frac{\Delta t}{\tau_P} \left(P - P_0\right)\right]^{1/3} \tag{1.15}$$

where τ_P, alike Berendsen thermostat, controls the strength of the coupling of the system to the barostat.

Umbrella sampling

In molecular mechanics simulations, one is usually interested in measuring the most probable configurations of a system, that is, low energy configurations. This is the reason why simulated systems are energy minimized prior to any experiments. However, it might be interesting in some cases to study higher energy configurations *i.e.* less probable configurations. In principle, if a simulation is carried out during a sufficiently long time, all

the accessible configurations will be sampled with a frequency proportional to their Boltzmann weight. It it then possible to simply wait long enough to observe these rare configurations. Nevertheless, computational time is expensive and some configurations might be extremely rare. Thus, it could be convenient to "help" the simulation go in the configurations one is interested by. However, the "help" must be brought in such a way that it does not affect the true properties of the system or, at least, that its effect on the experiments can be cancelled out after the simulations. There are several options to solve this problem, one of them is "umbrella sampling".

Umbrella sampling consists in biasing the true potential energy profile of a simulation, $U(x)$ with an external and artificial potential, $w(x)$, that will push the system in the desired configuration. Doing so, the biased probability distribution of finding the system in the configuration x is:

$$P_b(x) = \frac{\exp\left(-\beta\left(U(x) + w(x)\right)\right)}{\int \exp\left(-\beta\left(U(x) + w(x)\right)\right) dx} = \frac{\exp\left(-\beta\left(U(x) + w(x)\right)\right)}{Z} \tag{1.16}$$

where Z is the partition function of the system. Thus, the true, *i.e* unbiased, distribution $P(x)$ is connected to the biased one by the following relations:

$$P(x) \propto P_b(x) \exp\left(\beta w(x)\right) \tag{1.17}$$

Since the biased distribution is simulated and the external potential is known, the real distribution can be recovered. In practice, however, more than one biasing function is used. Indeed, the system is divided in small regions and each region has its own biasing function. In this case, the probability distribution $P_i(x)$ of finding the system in the configuration x in the region i is:

$$P_i(x) = \frac{\exp\left(-\beta\left(U(x) + w_i(x)\right)\right)}{Z_i} \tag{1.18}$$

and the probability distributions in two regions are related by:

$$P_i(x) = P_j(x) \frac{\exp\left[-w_i(x)\right] Z_j}{\exp\left[-w_j(x)\right] Z_i} \tag{1.19}$$

Here, again, as the probability distributions in every regions are simulated and the biasing functions are known, the whole probability distribution can be reconstructed.

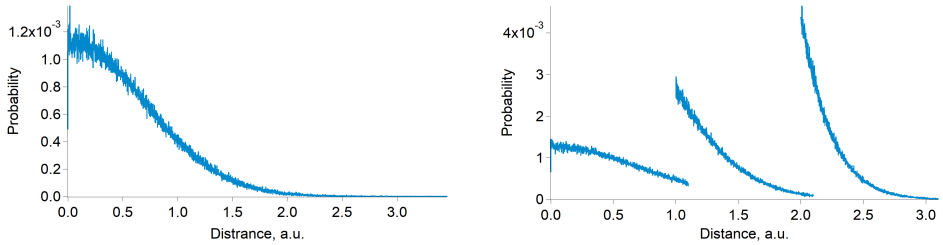

***Figure 1.3: Left**: Position probability distribution function of a particle in a quadratic potential well simulated by Monte-Carlo sampling. **Right**: Probability distribution function of a particle in three biased potential wells simulated by Monte-Carlo sampling. Note that the intervals slightly overlap.*

Example with a quadratic potential

Let's consider a particle moving in a quadratic potential centred in x_0:

$$U(x) = k(x - x_0)^2 \tag{1.20}$$

Since this potential is non-bounded, the configurations at large x will be hard to sample. Indeed, as the Boltzmann weight of the position $x = x_0$ is 1 it can be easily concluded that the probability of finding the particle at position x will be:

$$P(x) = \exp\left[-\beta k(x - x_0)^2\right] \tag{1.21}$$

i.e. it decreases exponentially fast with the distance from the minimum. Figure 1.3 (left) shows $P(x)$ computed by Monte-Carlo simulation for an arbitrary value of k. As expected, the distribution is a Gaussian function and the high energy regions are rarely sampled. Consequently, the uncertainty of $P(x)$ in these regions is high. The umbrella sampling solution to this problem is to divide the x-axis in three intervals $[0, x_1]$,$[x_1, x_2]$ and $[x_2, x_3]$ and to modify the potential in these regions with the following biasing function:

$$w_i(x) = \begin{cases} \infty & x < x_i \\ 0 & x_i \leq x \leq x_{i+1} \\ \infty & x > x_{i+1} \end{cases} \tag{1.22}$$

that is, an infinite potential wall at the intervals boundaries. Figure 1.3 (right) shows the probabilities in each intervals defined as in Equation 1.22, again computed by Monte-Carlo sampling.

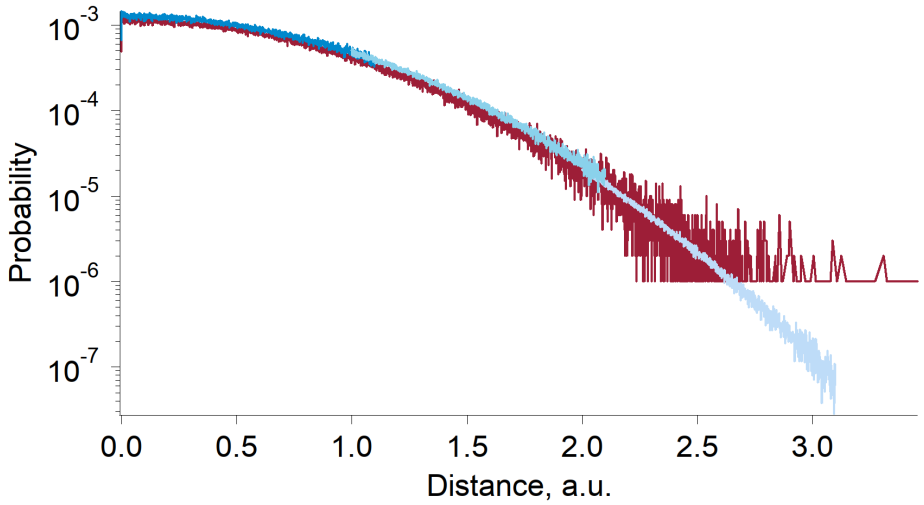

Figure 1.4: *Probability distribution functions computed by Monte-Carlo simulations with (blue) and without (brown) biased potential.*

Finally, using Equation 1.19 the total distribution can be reconstructed. The result is presented in Figure 1.4 on a logarithmic scale. The advantage of umbrella sampling clearly appears at large values of x, when the potential is large. Indeed, for such values the precision of the distribution is much better than with the simple Monte-Carlo scheme. Furthermore, some high energy configurations have even never been sampled with the classical scheme while they appear in the umbrella sampling.

1.3 Fractional derivatives

Fractional derivatives are an extension of the theory of integer-order derivations to derivations of any real order. This section does not aim at providing a mathematically rigorous introduction to fractional calculus but rather to show how non-locality arises from fractional derivation.

By definition, the first derivative of a function $f(x)$ is:

$$\frac{df(x)}{dx} = \lim_{\epsilon \to 0} \frac{f(x) - f(x-\epsilon)}{\epsilon} \tag{1.23}$$

Thus, the first derivative of $f(x)$ in a particular point x_0 only depends on

$f(x_0)$ and its immediate neighbourhood. In this respect, this derivation is local.

The derivation scheme of Equation 1.23 can be extended to higher order integer derivatives. For instance, the second-order derivative of $f(x)$ can be found iteratively from Equation 1.23 and yields:

$$\frac{d^2 f(x)}{dx^2} = \lim_{\epsilon \to 0} \frac{f(x) - 2f(x-\epsilon) + f(x-2\epsilon)}{\epsilon^2} \tag{1.24}$$

Similarly to Equation 1.23, Equation 1.24 shows that the second derivative of $f(x)$ is also local. From Equation 1.24 it is possible to deduce the general pattern of arbitrary integer-order derivation. Indeed, the numerator of the n-order derivative of $f(x)$ will contain $n+1$ terms representing $f(x)$ shifted by increasing numbers of ϵ, while the denominator will be ϵ^n. The coefficients of the terms in the numerator will be the binomial coefficients. This yields:

$$\frac{d^n f(x)}{dx^n} = \lim_{\epsilon \to 0} \frac{1}{\epsilon^n} \sum_{i=0}^{n} (-1)^i \binom{n}{i} f\left(x - i\epsilon\right) \tag{1.25}$$

where the binomial coefficients are given by:

$$\binom{n}{i} = \frac{n!}{i!\,(n-i)!} \tag{1.26}$$

It is possible to define non-integer order derivatives from Equation 1.25. However, in order to do so, this equation has to be slightly modified. Firstly, if n in not an integer, the binomial coefficients can no longer be given by Equation 1.26 since the factorial function is defined only on $\mathbb{N}$. Therefore, the factorial function must be replaced by the gamma function $\Gamma(n)$, *i.e.* its extension on $\mathbb{R}_+^*$. $\Gamma(n)$ has the following property:

$$\Gamma(n) = (n-1)! \qquad\qquad \forall n \in \mathbb{N} \tag{1.27}$$

Thus, Equation 1.26 becomes:

$$\binom{n}{i} = \frac{\Gamma(n+1)}{i!\Gamma(n+1-i)} \tag{1.28}$$

Similarly, the summation in Equation 1.25 is no longer valid if n in not an integer number. In order to solve this issue, one has to realise that in

Equation 1.25, the summation did not necessarily had to stop at n but could have been extended to infinity. If one had done so, the result would have been the same since the binomial coefficients would have been zero for all i larger that n. However, since now the binomial coefficients are defined with $\Gamma(n)$, this is no longer true, and the summation must contain an infinite number of terms instead of being stopped at n. Thus, Equation 1.25 becomes:

$$\frac{d^n f(x)}{dx^n} = \lim_{\epsilon \to 0} \frac{1}{\epsilon^n} \sum_{i=0}^{\infty} (-1)^i \frac{\Gamma(n+1)}{i!\Gamma(n+1-i)} f\left(x - i\epsilon\right) \tag{1.29}$$

Equation 1.29 is still not totally valid. Indeed, since now the summation contains an infinite number of terms, the interval over which the summation is done must be specified. Thus, on the interval $[x, x_0]$, the n-order derivative of the function $f(x)$ is:

$$\frac{d^n f(x)}{dx^n} = \lim_{\epsilon \to 0} \frac{1}{\epsilon^n} \sum_{i=0}^{\frac{(x-x_0)}{\epsilon}} (-1)^i \frac{\Gamma(n+1)}{i!\Gamma(n+1-i)} f\left(x - i\epsilon\right) \tag{1.30}$$

Equation 1.30 is a generalisation of the derivation to any real order. This scheme is non-local, compared to classical integer-order derivation. Indeed, now, the value of the derivative of $f(x)$ in a particular point x_0 depends on *all* the values of $f(x)$ on the interval $[x, x_0]$, and not only on its neighbourhood. This also emphasises that fractional derivatives, alike integrals, depend on an interval. The interest of fractional derivatives in the description of physical phenomena is that since they are non-local, they are convenient to describe correlated systems, hysteresis[85] or memory effects[86, 87]. As an illustration Figure 1.5 shows some fractional derivatives of the function $f(x) = x$ for various values of the fractional order.

1.4 Electrochemistry at the liquid-liquid interface

Interface polarisation

The LLI can be polarised if electrolytes are present in both phases. The influence of electrolytes on the system can be rationalised using a thermo-

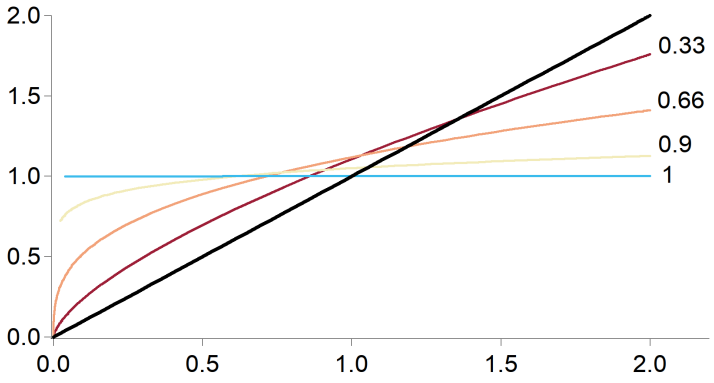

Figure 1.5: *Some fractional derivatives of the function $f(x) = x$ on the interval $[0, 2]$. The fractional orders are 0.33, 0.66, 0.9 and 1.*

dynamic implication that, at equilibrium, the electrochemical potential of an ion i is the same in both phases. The electrochemical potential is the sum of the standard chemical potential and two correction terms:

$$\tilde{\mu}_{i_\alpha} = \mu^{\ominus}_{i_\alpha} + RT \ln(a_{i_\alpha}) + z_i F \phi_\alpha \tag{1.31}$$

where $\mu^{\ominus}_{i_\alpha}$ is the standard chemical potential of the ion i in the phase α, a_i is the activity of the ion i, ϕ_α is the inner potential of the phase α and z_i is the net charge of the ion i. The first correction accounts for the solute-solute short-range interactions and depends therefore on the concentration, while the second term takes into account that the species that we are considering are charged and will therefore feel the inner, or Galvani, potential of the phase α. The equality of the electrochemical potential in both sides of the interface leads to the Nernst equation of ITIES :

$$\Delta\phi^\alpha_\beta = \phi^\alpha - \phi^\beta = \frac{\mu^{\ominus}_{i_\beta} - \mu^{\ominus}_{i_\alpha}}{z_i\, F} + \frac{RT}{z_i F} \ln\left(\frac{a_{i_\beta}}{a_{i_\alpha}}\right) \tag{1.32}$$

where a_{i_α} and a_{i_β} respectively stand for the activities of the ion i in the phase α and β. This expression can be further simplified by introducing the standard transfer potential which is the Gibbs free energy of transfer of an ion i divided by the Faraday constant and the charge of the ion:

$$\underset{\alpha\to\beta}{\Delta}\, \phi^{\ominus}_i = \frac{\underset{\alpha\to\beta}{\Delta}\, G^{\ominus}_i}{z_i F} = \frac{\mu^{\ominus}_{i_\beta} - \mu^{\ominus}_{i_\alpha}}{z_i F} \tag{1.33}$$

Finally one gets:

$$\Delta\phi_{\beta}^{\alpha} = \underset{\alpha\to\beta}{\Delta}\phi_i^{\ominus} + \frac{RT}{z_i F}\ln\left(\frac{a_{i_\beta}}{a_{i_\alpha}}\right) \tag{1.34}$$

The variation of the inner potentials arises from the intrinsically different chemical composition of the phases. The absolute value of the inner potential of one phase is not an experimentally accessible observable and only a difference of potential can be measured. Now that we have defined the Nernst equation of ITIES we can continue further and rewrite it differently by using the decomposition $a_{i_\alpha} = \gamma_{i_\alpha} c_{i_\alpha}$ and by taking into account firstly the conservation of mass:

$$V_\alpha\, c_{i_\alpha} + V_\beta\, c_{i_\beta} = m_i \tag{1.35}$$

where V_α and V_β are the volumes of the phases α and β and m_i is the total amount of the ion i, and secondly the electroneutrality of both phases:

$$\sum_{i\in\alpha} z_i\, c_i = \sum_{i\in\beta} z_i\, c_i = \sum_{i\in(\alpha+\beta)} z_i\, m_i = 0 \tag{1.36}$$

Indeed, using the equation 1.35 one can rewrite and rearrange the equation 1.34 like that:

$$c_{i_\alpha} = \frac{m_i}{V_\alpha + V_\beta \frac{\gamma_{i_\alpha}}{\gamma_{i_\beta}} \exp\left(z_i F \frac{\Delta\phi_{\beta}^{\alpha} - \underset{\alpha\to\beta}{\Delta}\phi_i^{\ominus}}{RT}\right)} \tag{1.37}$$

Finally, using the equations 1.36 one gets:

$$\sum_{i\in(\alpha+\beta)} \frac{z_i\, m_i}{V_\alpha + V_\beta \frac{\gamma_{i_\alpha}}{\gamma_{i_\beta}} \exp\left(z_i F \frac{\Delta\phi_{\beta}^{\alpha} - \underset{\alpha\to\beta}{\Delta}\phi_i^{\ominus}}{RT}\right)} = 0 \tag{1.38}$$

The equation 1.38 is true for all the systems of ions distributed among immiscible solvents [88]. Taking the example of the salt C^+A^- dissolved in both phases, the equation 1.38, with the help of the equations 1.36, gives:

$$\Delta\phi_w^o = \frac{\underset{w\to o}{\Delta}\phi_{C_i^+}^{\ominus} + \underset{w\to o}{\Delta}\phi_{A_i^-}^{\ominus}}{2} + \frac{RT}{2F}\ln\left(\frac{\gamma_{A_w^-}\,\gamma_{C_o^+}}{\gamma_{A_o^-}\,\gamma_{C_w^+}}\right) \tag{1.39}$$

Thus, the inner potential difference is independent of the ion concentration in each phase: the interface cannot be polarised. More precisely, modifying the potential difference implies to change the transfer potential and the activity coefficient of one of the ions, *i.e.* to change the chemical composition of the system.

Now consider a system where the phases are composed of a common ion, C^+, and different counter-ions, W^- in the water phase and O^- in the organic phase. Following the same argument than for the previous case, we simply obtain the Nernst equation of the ITIES for the common ion:

$$\Delta\phi_o^w = \underset{w\to o}{\Delta}\phi_{C^+}^{\ominus} + \frac{RT}{z_{C^+}F}\ln\left(\frac{a_{C^+{}_o}}{a_{C^+{}_w}}\right) \tag{1.40}$$

The interface of such a system is still not actively polarisable. Nevertheless this time the inner potential difference is controlled by the activity of the cation C^+.

The last example consists of a system in which two different salts are dissolved in the aqueous and organic phases. Let's call S^+T^- the hydrophilic salt and U^+V^- the hydrophobic salt. Once again, using the equation 1.38 and translating the hydrophilicity and hydrophobicity of the salts into assumptions on the transfer potentials of the ions, *i.e.*:

$$\underset{w\to o}{\Delta}\phi_{S^+}^{\ominus} \gg 0,\ \underset{w\to o}{\Delta}\phi_{T^-}^{\ominus} \ll 0,\ \underset{w\to o}{\Delta}\phi_{U^+}^{\ominus} \ll 0,\ \underset{w\to o}{\Delta}\phi_{V^-}^{\ominus} \gg 0 \tag{1.41}$$

one gets the following equation:

$$\Delta\phi_o^w = \frac{RT}{2F}\ln\left(\frac{c_w\exp\left(F\frac{\underset{w\to o}{\Delta}\phi_{T^-}^{\ominus}}{RT}\right) + c_o\exp\left(F\frac{\underset{w\to o}{\Delta}\phi_{U^+}^{\ominus}}{RT}\right)}{c_w\exp\left(-F\frac{\underset{w\to o}{\Delta}\phi_{S^+}^{\ominus}}{RT}\right) + c_o\exp\left(-F\frac{\underset{w\to o}{\Delta}\phi_{V^-}^{\ominus}}{RT}\right)}\right) \tag{1.42}$$

The equation 1.42 shows that the potential difference across the interface is a function of the standard transfer potentials of all the species as well as their concentrations. The assumptions of the equations 1.41 imply that over a certain potential range only a small fraction of the hydrophilic electrolytes will be present in the organic phase, and vice versa for the hydrophobic salt. Thus, the applied potential only induces a polarisation of the interface, without modifying the chemical composition of the organic and aqueous phases. Therefore, this system is said to be an ideally polarisable interface [89].

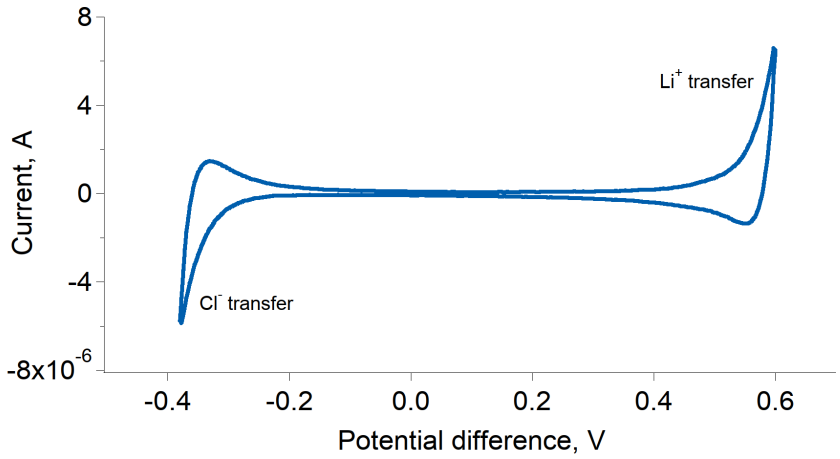

Figure 1.6: *Cyclic voltammogram at the water/TFT interface. Supporting electrolytes: LiCl 10 mM, BATB: 10 mM, scan rate: 10 mV/s.*

Potential window

As demonstrated in the previous paragraph, given a proper choice of supporting electrolytes, the ITIES can be polarised by applying an external potential difference. Throughout this thesis, except otherwise stated, the supporting electrolytes are lithium chloride (LiCl) in the aqueous phase, and BATB (Bis (triphenylphosphoranylidene) ammonium tetrakis (pentafluorophenyl) borate). At the water/TFT interface, these electrolytes give a potential window of roughly 1 V, limited at positive potentials by the transfer of Li^+ from the aqueous phase to the organic phase, and at negative potentials by the transfer of Cl^-. A typical cyclic voltammetry is presented in Figure 1.6:

Four-electrode potentiostat

Interface polarisation and current measurement are realised by a four-electrode potentiostat. This device was used for the first time in the study of ion transfer at the ITIES by Samec *et al.* in 1977 [90]. It has then been improved by the same authors to automatically compensate the IR drop between the Luggin capillaries [91]. It is now commonly used in experiments requiring polarisation of ITIES.

Figure 1.7 shows a simplified version of a four-electrode potentiostat

[92] that aims at applying the voltage V_{in} between the reference electrodes. This device relies on Operational Amplifier (OA). An OA is an electric component that produces an output potential proportional the voltage applied on its inputs, the proportionality constant being the gain of the amplifier. Thus, on the figure 1.7, OA1 will induce a tension on R1 and OA2 until the output tension of OA3 is V_{in}, *i.e.* until the potential difference between the reference electrodes is V_{in}. This retroactive feedback allows to precisely tune the potential difference between the reference electrodes and set it to the desired tension V_{in}. OA2 has one of its input connected to the ground and ensures that the potential applied on CE2 is the opposite of that applied on CE1. Finally, the resistance R1 is used to measure the current inside the circuit.

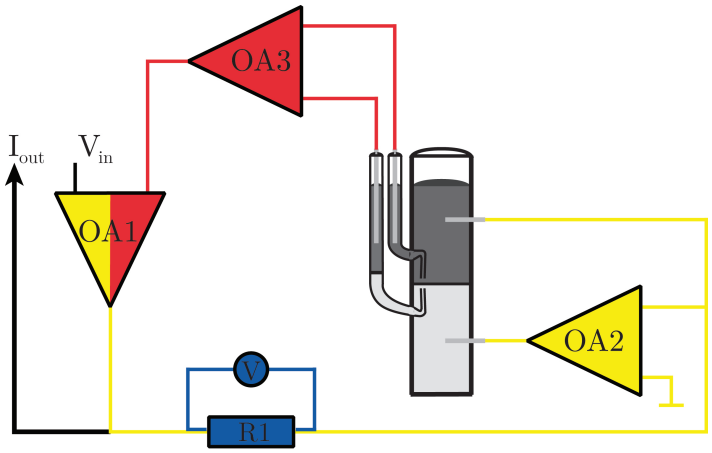

Figure 1.7: *Simplified electronic circuit of a four-electrode potentiostat. Feedback circuit (red), current measurement circuit (blue), potential applying circuit (yellow).*

Capacitance measurements

The capacitance of an electronic component is defined as the ratio between the charge carried by the component over the voltage applied on the component, *i.e.*:

$$C = \frac{Q}{V} \tag{1.43}$$

where Q is the charge, V the voltage and C the capacitance. If the response of the component to the voltage is not linear, the capacitance is defined as

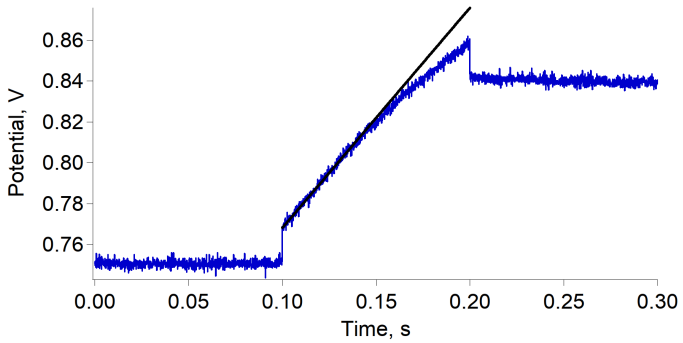

Figure 1.8: *Example of a current step chronopotentiometry recorded at the water-TFT interface. Aqueous phase supporting electrolyte: LiCl 100 mM, organic phase supporting electrolyte: BATB 10 mM, current step: 1 µA, potential: 0.75 V. The potential step at 0.1 s is proportional to the resistance of the interface.*

the variation of stored charge over the variation of polarisation, *i.e*:

$$C = \frac{dQ}{dV} \tag{1.44}$$

Equations 1.43 and 1.44 are however equivalent if the electronic component behaves as a linear capacitor.

Capacitance at the ITIES is usually measured by impedance spectroscopy, assuming that the interface can be modelled with an equivalent circuit, usually a Randles circuit. However, the capacitance can also be measured more conveniently by current step chronopotentiometry. This method relies in polarising the interface at a certain potential and, when equilibrium is reached, apply a fast current step of few micro-amperes per centimetre squared. Because of the current step, the interfacial potential difference immediately rises. The slope at the origin gives the capacitance. Indeed:

$$I = \frac{dQ}{dt} = C\frac{dV}{dt} \tag{1.45}$$

where I is the imposed current, V the potential difference between the reference electrodes and C the capacitance. The capacitance curves presented in Chapter 3 have been obtained as follows. The interface was polarised at a given potential by chrono-amperometry for 60 s. Then, immediately after the end of the chrono-amperometry, a current step of 16 $\mu A \cdot cm^{-2}$ was applied during 100 ms. The capacitance was obtained from slope of

the potential *vs.* time plot as presented above. The procedure was then directly repeated for the next potential step in order to keep the interface always polarised. The whole potential range was measured with increasing steps of 25 mV. When the positive end of the polarisation window was reached, the procedure was continued with steps of -25 mV, down to the negative end of the potential window. A typical capacitance curve was obtained by averaging five such measurements series (five times increasing potentials and five times decreasing potentials).

Electron Conductor Separating Oil-Water (ECSOW)

ECSOW is an electrochemical setup designed to observe biphasic electron transfer reactions without the effects of ion transfer reactions[77]. The principle is the same than for a regular ITIES. Nevertheless, the phases are physically separated and only connected by an electron conductor, typically glassy carbon electrodes.

Figure 1.9 shows a scheme of a typical ECSOW setup. Similarly to a ITIES, the Galvani potential difference between the aqueous and organic phases is varied with the counter electrodes while the potential difference is measured by the reference electrodes. In this respect, the glassy carbon electrodes where placed as close as possible to the reference electrodes in order to lower the IR drop, which can be non-negligible in the organic phase, particularly at low supporting electrolyte concentrations.

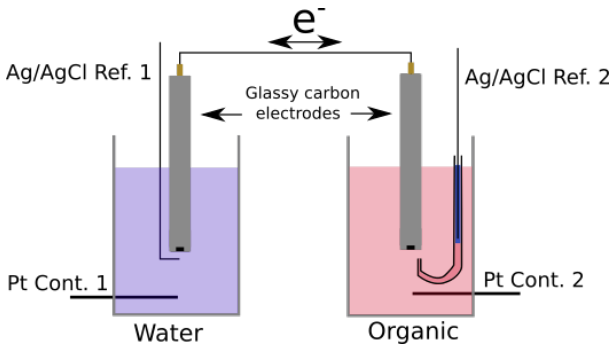

Figure 1.9: *Schematic representation of an ECSOW setup.*

1.5 Chemicals

Anhydrous lithium chloride (LiCl, >99 %) and α,α,α-trilfuorotoluene >99 % were purchased from Sigma. Lithium tetrakis – (pentafluorophenyl) borate ethyl etherate (LiTB) was purchased from Boulder Scientific. Bis (triphenylphosphoranylidene) ammonium chloride (BACl, 98%) was purchased from Fluka. Dry acetonitrile (99,9%), 1-chloro-2,4-dinitrobenzene (99%) and sulfanilic acid (99%) were purchased from Acros. 4,4'-bipyridine (98%) and bis(η_5 pentamethylcyclopentadienyl)iron (DMFc, 99%) were purchased from AB. All porphyrins were purchased from Porphychem. The compound 5,15-(di-4-sulfonatophenyl) -10,20- (di-N-methyl-4-pyridyl) porphyrin (Zinc II) was a custom synthesis of Porphychem. All chemicals were used as received except DMFc that was purified by vacuum sublimation (150°C, 5 Pa) and then stored in a glove box under N_2.

Synthesis

BATB:

Bis (triphenyl-phosphoranylidene) ammonium tetrakis (pentafluorophenyl) borate) (BATB) was synthesised by methathesis of LiTB and BACl as follows. A solution of 1.4 g of LiTB dissolved in 30 mL of a 30% ethanol and a solution of 920 mg of BACl in 30 mL of 30% ethanol where prepared. Then, the solution of BACl was slowly added to the solution of LiTB, under stirring. The precipitation of BATB is immediate. The thus-obtained solution was left under stirring for ten minutes and filtered on Büchner. The organic salt was then dried one hour in an oven at 80°C. Finally, BATB was purified by recrystallisation as follows. Dry BATB is dissolved in a minimum amount of acetone. Then, water is added drop-wise under stirring to the acetone solution until complete precipitation of BATB. The salt is then recovered by filtration on Büchner and washed with water. This procedure is repeated twice.

Viologen derivatives

1,1'-bis(4-sulfophenyl)-[4,4'-bipyridine]-1,1'-diium (1,1'-bis(4-sulfophenyl)-[4,4'-bipyridine]-1,1'-diium (BSPBPy)) was synthesised in two steps from bipyridine according to the procedure presented in Figure 1.10. The

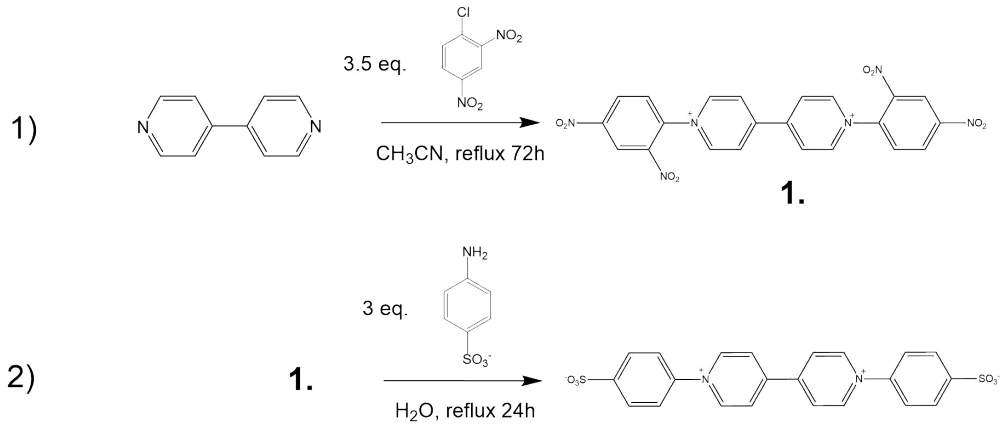

Figure 1.10: *Synthesis scheme of 1,1'-bis(4-sulfophenyl)-[4,4'-bipyridine]-1,1'-diium BSPBPy.*

intermediate **1** 1,1'-bis(2,4-dinitrophenyl)-4,4'-bipyridiinium dichloride was synthesised according to a published procedure [93]. Then, BSPBPy was synthesized as follows. In a round bottom falsk, 750 mg (1,34 mmol) of **1**, 694 mg (4 mmol) of sulfanilic acid and 168 mg (4 mmol) of LiOH monohydrate were added to 100 mL of water and refluxed for 24h. After the reaction, 90% of the solvent were evaporated and 50 mL of acetone were added to the solution. The precipitate was filtered and washed with acetone. The filtrate was then recovered, added to 80 mL of water and the mixture was warmed at 80°C, until complete dissolution of the compound. The solution was then acidified to a pH of 2 with hydrochloric acid, let to cool down to room temperature and finally cooled to 4°C for two hours. The precipitate was filtered on Büchner, washed with water and dried at 80°C in an oven. 1H NMR (D2O): δ 9.36 (d, 4H), δ 8.72 (d, 4H), δ 8.05 (d, 4H), δ (d, 4H).

Chapter 2

Theory

Theory of surface second harmonic generation

The polarization induced in a medium as a response to an external electric field can be described, to first order, by the following equation:

$$P_i = \frac{1}{\epsilon_0}\chi E_i \tag{2.1}$$

where P is the induced polarization vector, E the external electric field, ϵ_0 the vacuum relative permittivity and the index i runs over the Cartesian coordinates. The constant χ is called "polarisability" and is a proportionality constant between the induced polarisation and the electric field. The equation 2.1 is only an approximation and, for lack of exact relation between the polarisation and the electric field, assuming that the polarisation is analytic, one can expand it as a Taylor series of the electric field. Because the equation 2.1 links vectors, the polarisability needs to be a tensor, whose order increases with the powers of the series. Thus, to the n^{th} order, the equation 2.1 becomes:

$$P_i = \frac{1}{\epsilon_0}\left(\chi_i^j E_j + \chi_i^{jk} E_j E_k + \ldots + \chi_i^{j\ldots n} E_j \ldots E_n\right) \tag{2.2}$$

Where we have used the Einstein summation (implicit summation over repeated indices). As the SHG is a second order process, we will only work with the equation 2.2 developed to the second order, that is:

$$P_i = \frac{1}{\epsilon_0}\left(\chi_i^j E_j + \chi_i^{jk} E_j E_k\right) \tag{2.3}$$

The equation 2.3 shows that by expanding the induced polarisation as a function of the field, we have also increased the number of parameters defining χ. Indeed, now χ_i^{jk} is a rank three tensor on $\mathbb{R}^3$ (χ_i^{jk} is real for parametric non-linear processes, it can however be complex for non-parametric processes) and possesses therefore 27 components. Each of these components describes how the polarisation in one Cartesian direction depends on the intensity of the fields in other directions. Nevertheless, when doing SHG at the LLI, this tensor can be greatly simplified by taking account of the symmetries of the interface. Doing so yields only three independent tensor elements, namely:

$$\chi_x^{zx} = \chi_y^{zy} \qquad \chi_z^{xx} = \chi_z^{yy} \qquad \chi_z^{zz} \tag{2.4}$$

The process of SHG can be highlighted by using the equation 2.3 with an explicit expression of the field. Indeed, taking a general form of a time-dependent oscillating electric field as:

$$E(t) = E\exp(\imath\omega t) + E^*\exp(-\imath\omega t) = E\exp(\imath\omega t) + c.c. \tag{2.5}$$

and putting it in the equation 2.3 (taking only the purely second order contribution) one gets:

$$P_i^{(2)} = \chi_i^{jk}\left(E_jE_k^* + E_jE_k\exp(2\imath\omega t) + c.c.\right) \tag{2.6}$$

Thus, it appears that the total induced polarisation (first and second order) contains three components: a time-independent contribution, a contribution depending on the frequency of the incoming field ω (the first order response), and a contribution depending on twice the frequency of the electric field 2ω. Therefore, if the intensity of the incoming field is high enough, it is possible to generate a new electric field oscillating at twice the frequency. This process is what is called "second harmonic generation".

As said previously, the possibility to generate the second harmonic of an incoming beam depends on the geometry of the medium. Indeed, for a system with an inversion symmetry, the following identity holds for all vector quantities $\mathbf{V}$, and in particular for the polarisation:

$$\mathbf{V}(x_i) = -\mathbf{V}(-x_i) \tag{2.7}$$

The equation 2.7 implies that the Taylor series of a vector function in a system possessing an inversion symmetry cannot contain even powers

contributions. This means that the SHG is not possible in such systems. Thus, if an oscillating electric field interacts with an interface and that afterwards a second harmonic signal is detected, it can be said that this signal originates only from the interface. This is this property that makes the SHG interesting in the study of interfaces and interface phenomena.

The theory briefly introduced above also holds at the molecular level. Indeed, as macroscopic media, molecules can be polarised and posses a polarisability. The convention is to call the second order molecular polarisability "first hyperpolarisability" and to write it "β". This quantity has however the same properties as the macroscopic polarisability. If molecules are present at an interface where an oscillating electric field interacts, some molecular properties can be obtained by measuring the generated second harmonic signal. Indeed, the signal can be enhanced by resonance with a transition dipole of the molecules. In this case, the second order polarisability can be expressed from the molecular first hyperpolarisability as:

$$\chi = \frac{N\langle T\rangle\beta}{\epsilon_0} \tag{2.8}$$

where N is the number of molecules present at the interface and T a tensor transforming the coordinates of the molecules to those of the laboratory. Thus, since the second harmonic intensity is proportional to the square of the second order polarisation, the SHG signal is proportional to the square of the molecule number, *i.e* to the square of the concentration:

$$I_{shg} \propto \left|P^{(2)}\right|^2 \propto \left|\chi^{(2)} : E_1E_2\right|^2 \propto \left|\frac{N\langle T\rangle\beta : E_1E_2}{\epsilon_0}^{(2)}\right|^2 \tag{2.9}$$

Since a second harmonic signal can be generated by resonance with the transition dipole of a molecule, the SHG spectrum is similar to a UV-vis spectrum. Furthermore, by changing the polarisation of the incoming and outgoing beams, it is possible to measure the components of the first hyperpolarisability tensor listed in Equation2.6. For instance, the element χ_x^{zz} describes the dependence of the induced polarisation in the x direction as a response to the field in the z direction. This tensor element could therefore be measured by polarizing the incoming field in the z direction — let's say perpendicular to the interface — and recording the SHG signal that has a perpendicular polarization.

The technique of SHG can be extended to the study of time-dependent systems. Indeed, as other spectroscopic approaches like transient absorption it can be used to probe photo-excited molecules. Nevertheless, while transient absorption probes the electronic transitions, SHG probes the polarisability. This is an important difference because an electronic transition is bleached by excitation, while the polarisability changes in both intensity and direction. Thus, TRSHG provides information on the ground state population recovery as well as on the reorientation of the transition dipole upon excitation. Therefore care must be taken in the interpretation of the kinetic traces of TRSHG because their time constant do not only reflect a change of excited state population but also a change of orientation population.

2.1 Review of surface second harmonic generation at the LLI

The development of non-linear optical spectroscopy has enriched the experimental approaches available to the study of chemical systems. Among them, SHG offers both an intrinsic sensitivity to interfaces as well as the possibility to measure the magnitude *and* the direction of dipoles present at these interfaces. This later aspect is critical because in comparison to linear optical spectroscopy SHG provides information on the orientation of the system under study.

SHG as been observed for the first time at the liquid-air interface by Wang in 1969 [94]. Following the work of Bloombergen&Pershan [95], Wang established the theoretical framework of non-linear optics at interfaces, and in particular the theory of SHG of such systems. Since then, the evolution of SHG at soft interfaces has followed the technical development of optical spectroscopy — particularly in time-resolved spectroscopy — where resolutions of few tens of femtoseconds became accessible.

Time-independent second harmonic generation

After the work of Wang[94] at the bare air-liquid interface that were Eisenthal and co-workers, who for the first time, studied the adsorption of

molecular species — phenol and cresol — at the air-water interface [96]. They could measure the average orientation of the adsorbed molecules as well as estimate the Gibbs energy of adsorption, assuming a Langmuir isotherm. In the same group, Castro *et al.*[97] reported in 1989 the measurement of adsorption kinetics of p-nitrophenol in water droplets and showed that the orientation equilibrium of the adsorbates was reached faster than the adsorption equilibrium. Similar studies about the orientation and adsorption of molecules were reported but only at the air-liquid interface[98]. That was in 1988 that the first SHG measurement at the liquid-liquid interface was published by Grubb *et al.* [99]. Nevertheless, the liquid-liquid interface was only one of the systems that they analysed and the first real systematic studies were reported in the early 90's by Higgins *et al.* [100, 101]. They actually worked at the ITIES and reported for the first time the measurement of the potential dependent adsorption of charged species at the liquid-liquid interface. Furthermore, is was successfully shown that, as the molecules were charged, the Frumkin isotherm was more relevant than the Langmuir isotherm in the description of the adsorption process. Furthermore, they showed that the phase of the second harmonic field was dependent on the the orientation of the dipoles at the interface. Thus, by creating monolayers of molecules whose dipoles tend to orient in opposite senses at the interface, and changing the adsorbed ratio of these molecules, they could generate – with an excess of one molecule – or cancel – using equimolar amount – the signal. Obviously, this required the two molecules to have similar resonances at the same wavelengths.

An interesting aspect of SHG in the study of ITIES is that it is sensitive to electric fields at interfaces. Thus, if one usually looks for a resonant enhancement of SHG signal in the case of molecular species, this is actually not necessary and some adsorbed organic ions, because of their intrinsic dipoles, can be detected at the liquid-liquid interface. In this respect, Conboy&Richmond showed in two publications in 1995 [102] and 1997[103] that the polarised ITIES could generate a second harmonic response, and that this response was directly proportional to the polarisability of the electrolytes. Similarly, Petersen *et al.*[104] studied the behaviour of small ions at the air-water interface and showed that, according to their polarisability, ions were preferentially present at the interface or slightly below it. Thus, it was shown that "soft" anions had a stronger affinity for the interface than "hard" anions. Using the same approach, they also

demonstrated that the concentration of hydronium cations was larger at the interface than in the bulk, supporting the hypothesis that the water surface is acidic [105]. Nevertheless, contrary to Conboy&Richmond[102, 103], the SHG signal that they measured in their experiments was resonant with an ion-to-solvent charge transfer band. The conclusions of Petersen *et al.*[105] concerning the acidity of the interface are somewhat in opposition of the observations of Tamburello-Luca *et al.*[106] on the pH equilibrium of "eosin B" at the air-water interface. Indeed, Tamburello-Luca *et al.*[106] showed that the protonated form of the dye was favoured at the interface compared to the bulk. If this seems to agree with Petersen *et al.*[105] – a larger concentration of hydronium favouring the protonation of "eosin B" – it must be recalled that the oxonium ion is more stable at the interface than in the bulk. Thus, its ability to protonate "eosin B" is in principle lower. Nevertheless, the acid form of the dye being also more stable at the interface, the overall equilibrium might be pushed towards the protonation of "eosin B".

In addition to orientation or adsorption at soft interfaces, SHG has been used to record spectra — actual SHG spectra but comparable to absorption spectra — of molecular species. Such studies usually used the observed red or blue shifts of the spectra to show a particular property of the interface with respect to the bulk. Using this approach, Wang *et al.*[107] in 1997 measured the polarity of the air-water interface with the help of a solvatochromic dye. They showed that the spectrum of the dye at the interface was in between that of its vapour phase and that of its bulk phase. Overall, they concluded that the polarity of the air-water interface was comparable to the polarity of tetrachloromethane or butyl-ether; *i.e.* non polar. Soon after this first publication, Wang *et al.*[108] published a second article where the study of soft interfaces polarity was extended to the liquid-liquid interface. Using the same experimental approach than that of their first publication, they found that the polarity of a soft interface was simply the average of the polarity of the two phases, suggesting that the solute-solvent interactions responsible of the solvatochromism were probably long-range interactions. Following the work of Wang *et al.*[108], Steel&Walker[109] published in 2003 the conclusions of their attempt to measure the liquid-liquid interface thickness by varying the distance between the acceptor and donor groups of a solvatochromic dye. They showed that for poorly miscible solvents, the interface polarity changed over less than

one nanometre, suggesting that the thickness of the interface was of the same order. Nevertheless, they also emphasised that there could be specific organizations of the solvents at the interface leading to sharp changes of the polarity.

Shifts of absorption spectra can be caused by solute-solvent but also by solute-solute interactions. In this respect, studies by SHG on the formation of molecular aggregates at the liquid-liquid interface have been reported. In two publications, in 2002 [110] and 2003[111], Nagatani *et al.* showed that excitonic transitions in porphyrin aggregates explained the strong SHG signals of these molecules that, in principle, should not exhibit second order non-linear properties because of their inversion symmetry. By varying the Galvani potential difference between the two phases they could change the concentration of the porphyrins at the interface – the porphyrins were charged – and subsequently record SHG spectra. Thus, they observed that when the molecules were "pushed" towards the interface the spectrum shifted to the red suggesting the formation of "J" aggregates. These findings were confirmed in 2004 by Fujiwara *et al.*[112] who also observed the formation of "J" aggregates at the liquid-liquid interface. Furthermore, by analysing the light polarisation dependence of the second harmonic response they could conclude that the aggregates were chiral and actually had a "helical" structure. In 2012, Olaya *et al.*[113, 114] took advantage of the ability of porphyrins to form aggregates to catalyse the oxygen reduction at the liquid-liquid interface. Here, similarly, they used SHG to show that the active species in the catalytic reaction were the "J" aggregates and that the aggregation could be controlled by tuning the Galvani potential difference.

Time-resolved second harmonic generation

The experimental approaches available to time-independent SHG can be extended to time-dependent systems. What is meant here by "time-dependent" is that it is the evolution of a system after a light induced perturbation that is followed. Indeed, measuring the adsorption of a molecule at an interface over time is already formally "time-resolved" second harmonic generation. The TRSHG is actually a sub-set of the larger domain of pump-probe spectroscopy.

One of the first TRSHG measurement was reported by Sitzmann&Eisenthal

in 1988[115]. They measured the change of excited state lifetime of "rhodamine 6G" by energy transfer to an acceptor at the air-water interface. It was found that "rhodamine 6G" was deactivated faster at the interface than in the bulk. This observation was explained by a shorter donor-acceptor distance at the interface due to adsorption of "rhodamine 6G". The excited state lifetime and deactivation pathways of dyes adsorbed at liquid-liquid interfaces were then further explored by Shi *et al.* who studied the dynamics of malachite green at various interfaces. They showed that the mechanism of the barrierless isomerisation of this dye mainly involved a twist of the aminophenyl groups more than the phenyl groups. This could be concluded because no influence of the viscosity of the organic phase on the excited state lifetime was observed, while the phenyl ring is supposed to be projected in this phase. Following the same approach Fita *et al.*[116] moderate these conclusions by showing that all rings were involved in the deactivation pathway. Nevertheless, their observations agreed with those of Shi *et al.*[117] in that, in very viscous aqueous environments, the twisting of the aminophenyl ring becomes the rate limiting step of the decay. It is interesting to note that these publications did not aim at studying the liquid-liquid interface but actually used it to measure a general property of a molecule. Such experiments would not have been possible without TRSHG and showed that this technique could be used beyond the study of purely interfacial phenomena.

In their article, Fita *et al.*[116] reported the observation of a biexponential decay and explained it by the formation of molecular aggregates at the interface. This particular effect was explored by Punzi *et al.*[118] who studied the effect of salts addition in a solution of malachite green. They found that this lengthened the excited state lifetime of the dye molecules adsorbed at the interface. This effect was explained by an increase of the interfacial concentration with larger ionic strength that lead to formation of "H" aggregates. Interestingly, the influence of several salts was tested and it was found that the order of the most active salts was almost the opposite of that of the Hofmeister series (see [119] for a detailed review of on the Hofmeister series and its effects) of "salting-in" "salting-out" agents. The authors had however no explanations to these observations.

The ability of SHG to measure the orientation of dipoles at interfaces was used to study the reorientation dynamics of molecular species adsorbed at air-liquid or liquid-liquid interfaces. One of the first observations of

such phenomena was reported in a short communication by Castro *et al.* in 1991 with the dye "rhodamine 6G" [120]. By varying the polarisation of the fundamental and second-harmonic beam they could show that the different second-order polarisability tensor elements had different kinetics after excitation. This observation was critical because it proved that the population evolution that was probed was that of oriented molecules and not that of excited molecules. It is therefore the *motion* of the molecules that is seen and not their de-excitation, although their motion is the consequence of the excitation. Because in such experiment it is the orientation of the molecules that is followed, the polarization of the pump beam must be carefully selected. Indeed, by choosing a linearly polarized pump light only a subset of an oriented population will be excited, therefore biasing – on purpose or not – the experiment. In their publication, Castro *et al.*[120] varied the polarisation of the pump but did not observe any difference on the resulting kinetics. In 1998, Antoine *et al.*[121] reported similar observations but with the dicationic form of the dye "eosin B". They however observed a faster kinetic than what was observed with "rhodamine 6G" and explained it by a lower friction at the interface. A polarisation-dependent kinetic was reported the same year by Zimdars *et al.* with the dye "coumarin 314" [122]. They showed that using a circularly polarized pump pulses – perpendicularly hitting the interface – evenly excited the dye molecules with respect to their in-plane orientation, creating therefore an excited population only dependent on the out-of-plane orientation of the ground state molecules. On the opposite, using linearly polarized pulses created an excited population dependent on the in-plane orientation of the ground state. Overall, these studies showed that TRSHG could be used to measure the time dependent orientation of molecules at an interface, and that the reorientation kinetics were relatively fast processes, taking place in time scales of the order of tens to few hundreds of picoseconds.

TRSHG was used to study the solvation dynamics of molecules at soft interfaces. The first observation of such phenomena was reported by in 1999 by Zimdars *et al.* [123] who measured a solvation dynamics of the order of few hundreds of femtoseconds for the dye "coumarin 314" at the air-water interface. Their experiment consisted in exciting the dye and then record the evolution of the second harmonic signal resonant with the $S_0 \leftarrow S_1$ transition, the wavelength of this transition being red-shifted as the excited state solvation reaches equilibrium. The same year, they showed that the

time taken by the solvent molecules to rearrange after excitation was also dependent on the pump pulse polarization, that is on the orientation of the dye dipole at the interface [124]. This observation was consistent with was had been previously reported concerning the interfacial reorientation dynamics, *i.e.* the solvation environment of molecules adsorbed at an interface significantly changes with their orientation.

In conclusion, SHG and TRSHG offers similar possibility than conventional spectroscopy techniques in probing empty or occupied electronic states of molecules. Nevertheless, it has the advantage of the sensitivity to interfaces and dipole orientations. Furthermore, as it is only *resonant*with a transition the molecules are not excited by the probe pulses. The tradeoff is that, as many properties of the molecules are measured, a greater attention must be taken to experimental conditions and data interpretation. Furthermore, because of the interface specificity of SHG only a small number of molecules is probed, implying therefore weak signals. Finally, SHG is only limited to species having significant Non-Linear Optical (NLO) properties.

2.2 Diffusion in solution

Microscopic picture

This section presents an overview of the fundamental description of the motion of particles in the perfect gas model. In this model, the particles are considered as non-interacting hard spheres whose kinematics is described by classical mechanics. These particles are freely moving in an imaginary box with hard walls. The collisions between the particles or between the particles and the walls are assumed to be elastic.

The most simple form of this model is that where there is only one particle in an infinitely large box. In this case, position $r(t)$ of the particle at time t is precisely known and is given by:

$$r(t) = r_0 + vt \tag{2.10}$$

where r_0 is the initial position and v the velocity of the particle. Thus, the squared displacement, with respect to r_0, at time t is given by:

$$(r(t) - r_0)^2 = (vt)^2 \tag{2.11}$$

this quantity obviously scales like the square of the time.

A more interesting case is that where the box contains N particles. However, it is still assumed that the box is large enough – or the particle density low enough – to neglect collisions between the particles. In this case, Equation 2.11 is still valid but, as the particles can have different velocities, the squared displacement must be averaged over all the particles. This quantity is thus called Mean Squared Displacement (MSD) and is given by:

$$\sum_{i=0}^{i=N} \frac{(r_i(t) - r_{0i})^2}{N} = \langle r_i(t) - r_{0i})^2 \rangle = \sum_{i=0}^{i=N} \frac{(v_i t)^2}{N} = \langle v_i \rangle^2 t^2 \tag{2.12}$$

where the square brackets $\langle\rangle$ indicate the average value of the considered variable.

If the number of particle increases – or if the box size decreases – collisions become unavoidable and the displacement of a particle is no longer a linearly increasing function of time. Its trajectory will thus consist in rectilinear motions interspersed by collisions with the other particles, forming an overall *zigzag* pattern. If the number of collisions is large and the trajectory is long, it can be assumed that the rectilinear parts are short and of the same (short) length. Thus, the particle motion can be described using *random walks*. In this model, the particle is assumed to move in small steps of equal length l but random direction. Thus, the average position of a particle after N steps of the walk is:

$$\langle r_N \rangle = \sqrt{N} l \tag{2.13}$$

The equation 2.13 can be related to real time by making physical assumptions on l and N. Indeed, lets call τ the total time of the walk, and t the time between two collisions, then:

$$N = \frac{\tau}{t} \tag{2.14}$$

and

$$l = \langle v \rangle t \tag{2.15}$$

thus, equation 2.13 becomes:

$$\langle r_N \rangle = \langle v \rangle \sqrt{\tau t} \tag{2.16}$$

Equation 2.16 implies that the MSD of a particle scales linearly with the time when account is taken of the collisions with the other particles. This is a remarkable difference with the free motion described in Equation 2.11. It is explained by the stochastic nature of the process. Indeed, in deriving equation 2.13, it is assumed that the direction of each steps is independent of the other ones and that the number of steps is large. Thus, this result is a direct consequence of the central limit theorem. However, these supporting hypothesis are not necessarily verified in real physical systems and this can lead to different scaling of the MSD with time.

Langevin has proposed an equation that shows that classical mechanics can be used to describe the motion of colliding particles. This approach has the advantage of unifying the two formalisms presented above. The Langevin equation describes the motion of a particle undergoing random collisions in a viscous medium. It has the following form (in one dimension):

$$m\frac{d^2x(t)}{dt^2} = a\frac{dx(t)}{dt} + F(t) \tag{2.17}$$

where the first term of the right hand side describes the damping of the particle motion in a fluid of viscosity a and the second term is the random force accounting for the collisions. This equation can be solved to yield the following result for the MSD:

$$\langle x^2 \rangle = \frac{2kT}{a}\left(t - \frac{1}{\gamma}\left(1 - e^{\gamma t}\right)\right) \tag{2.18}$$

where γ is the ratio of the mass over the damping parameter. Equation 2.18 shows that for large values of t, the exponential term becomes negligible and the MSD scales linearly with the time, as expected from the random walk approach. On the opposite, for small values of t, the exponential cancels the factor t in the parenthesis (expanding the exponential to the second order) and the remaining leading term is of second order in t, in agreement with the free moving particle. However, like the random walk approach, the resolution of equation 2.17 relies on the hypothesis that the random force acting on the particle follows a normal law. It can therefore only be applied to uncorrelated particles. In order to go beyond this limitation the Langevin equation can be modified to include time-correlation of the particle. The resulting equation is the Fractional Langevin Equation (FLE)[125]:

$$m\frac{d^2x_\alpha(t)}{dt^2} = a\int_0^t dt'|t-t'|^{-\alpha}\frac{dx_\alpha}{dt'} + \eta\xi(t) \tag{2.19}$$

Alike Equation 2.17, Equation 2.19 describes the motion of a particle undergoing two forces, friction with the surrounding fluid and random collisions. However, the friction in the FLE is replaced by the Boussinesq-Basset force, while the random collisions are accounted for with a fractional Gaussian noise. On one side, the Boussinesq-Basset force includes the retardation of the fluid adaptation to the particle displacement and therefore brings memory effects in the diffusion of the particles. On the other side, the fractional Gaussian noise includes correlation between the collisions undergone by the particle. Thus, the FLE allows a more subtle description of the diffusion, to the cost of a substantial complication of the theory. The MSD associated to the FLE is[125]:

$$\langle x_\alpha^2(t)\rangle = \frac{2t^2}{\beta m} E_{2-\alpha,3}\left[\Gamma(1-\alpha)\frac{\gamma}{m}t^{2-\alpha}\right] \tag{2.20}$$

where $E_{a,b}$ is the Mittag-Leffler function and $\Gamma(x)$ the usual gamma function. The interesting result of equation 2.20 is that now, compared to equation 2.18, the MSD of the particle can have a continuous range of scaling with time, depending on the value of the parameter α. Thus, at long times, FLE can describe the so-called *anomalous diffusion* regime.

Normal and anomalous diffusion

As seen in the previous paragraphs, the MSD is an important value that characterises the diffusion regime of a system. Formally, MSD is the variance of the position of a system of N particles with time:

$$MSD(t) = \frac{1}{N}\sum_i^N (r_i(t) - r_i(t_0))^2 \tag{2.21}$$

In principle, MSD scales linearly with time, except for very short times – between collisions – where it scales quadratically, according to Newtonian mechanics. This diffusion regime is called "ballistic diffusion". However, MSD can present deviations from this behaviour which are characteristic of anomalous diffusion regimes.

Anomalous diffusion is formally any deviations of MSD from linearity.

$$\langle (r_i(t) - r_i(t_0))^2\rangle \propto t^\alpha \qquad\qquad \alpha \neq 1 \tag{2.22}$$

super-linear trends ($\alpha > 1$) are called "super-diffusive", while sub-linear trends ($\alpha < 1$) are called "sub-diffusive".

In addition to the anomalous trends with time, MSD can also be dependent on the way the averaging is done. Thus, there are three type of MSD: time-averaged MSD (tMSD), ensemble-averaged MSD (eMSD) and time-averaged ensemble-average MSD (teMSD). For discrete time steps Δt, the various MSD are calculated as follows[126]

$$tMSD(t = m\Delta t) = \frac{1}{N-m} \sum_{i=1}^{N-m} \left[x_j\left(t_i + m\Delta t\right) - x_j\left(t_i\right)\right]^2 \tag{2.23}$$

$$eMSD\left(t = m\Delta t\right) = \frac{1}{J} \sum_{j=1}^{J} \left[x_j\left(t_i + m\Delta t\right) - x_j\left(t_i\right)\right]^2 \tag{2.24}$$

$$teMSD\left(t, T\right) = \frac{1}{J} \frac{1}{\frac{T}{\Delta t} - m} \sum_{i=1}^{(T/\Delta t)-m} \sum_{j=1}^{J} \left[x_j\left(t_i + m\Delta t\right) - x_j\left(t_i\right)\right]^2 \tag{2.25}$$

where N is the total number of time steps in the trajectories, and J the number of particles. It has to be emphasized that the time variable of MSD is not the real time of the experiment but the lag time at which the MSD is computed. For instance, with a 100 ns trajectory where the positions of the particles are saved every 1 ns, tMSD(20 ns) would be the average value of the MSD between 0 ns and 20 ns, 1 ns and 21 ns, and so on until 80 ns and 100 ns.

In well behaved systems, these three quantities are equal and consequently teMSD is preferred because it is calculated from a larger set of data and consequently more accurate. However, some cases of sub-diffusive media present a weak ergodicity breaking, *i.e.* the time-averaged and ensemble-averaged thermodynamic quantities are different [126–128].

Macroscopic picture

The previous section has shown how diffusion was modelled at the molecular level, that is, considering the motion of particles in an homogeneous environment. However, it is sometimes more convenient to describe diffusion at a larger scale, assuming a continuous picture of matter. In this respect,

the basic equation of diffusion is Fick's second law given by:

$$\frac{\partial C(x,t)}{\partial t} = D\Delta C \tag{2.26}$$

This equation simply states that the concentration of a compound changes over time according to its second space derivative. It has to be noted that compared to the molecular picture of diffusion, Equation 2.26 predicts that there will be no diffusion in absence of concentration gradient, in other words, diffusion stops when the system is at equilibrium. The Fick's second law is thus applied to non-equilibrated environment, while a stochastic approach usually assumes thermodynamic equilibrium. Indeed, in the cases where particles diffuse as a consequence of a concentration gradient, a preferred diffusion direction appears – the direction that tends to decrease the gradient – this is therefore in contradiction with the assumption of equiprobability of the steps direction in the random walk description, or with the assumption of a normal probability distribution.

The macroscopic Fick's second law can also be extended to allow description of anomalously diffusing particles. This, similarly to the microscopic description, involves fractional derivatives that include non-locality and correlation in the motion of the particles. Doing so results in the space-time fractional Cattaneo equation[129]:

$$\frac{\partial^\gamma C(x,t)}{\partial t^\gamma} + \tau^\gamma \frac{\partial^{2\gamma} C(x,t)}{\partial t^{2\gamma}} = D\frac{\partial^\mu C(x,t)}{\partial |x|^\mu} \tag{2.27}$$

Equation 2.27 is similar to Equation 2.26, except that it allows fractional order space and time derivatives. Furthermore, the second term of the left hand side aims at avoiding the infinite diffusion speed of the concentration by introducing a "relaxation" of the concentration flux. Indeed, the solution of 2.26 is a gaussian function whose width spread with time. Thus, this solution allows in principle a non-zero concentration at large distances after short times, which implies an infinite diffusion velocity.

Here, alike FLE, taking account of the correlation between the diffusing particle introduces complication in the models. However, it can be shown that the MSD predicted by equation 2.27 indeed present a quadratic dependence at short times and a linear dependence at large times in the case of normal diffusion ($\gamma = 1$), and a power law dependence for $\gamma > 0$[129].

$$\langle |x^2| \rangle = \frac{2Dt^{2\gamma}}{\tau^\gamma} \left[\frac{t^\gamma}{\tau^\gamma} E_{\gamma,1+2\gamma}\left(-\frac{t^\gamma}{\tau^\gamma}\right) + E_{\gamma,1+\gamma}\left(-\frac{t^\gamma}{\tau^\gamma}\right) \right] \tag{2.28}$$

Reaction - diffusion equation

In unstirred media, diffusion of the chemical reagents towards each others plays a critical role. Therefore, diffusion equations can be coupled to reaction kinetic equations to describe the time and space evolution of the reagents and products. Coupling Fick's second law (Equation 2.26) to chemical kinetics gives the well-known Smoluchovki equation for diffusion-limited reactions. In this equation, it is assumed that the reaction probability is one when the reagents are close enough. Therefore, the apparent rate constant of the reaction is simply given by the flux of reagents towards a target molecule. This flux can be directly obtained from Equation 2.26 in spherical coordinates:

$$\frac{\partial C(r,t)}{\partial t} = D\frac{1}{r^2}\frac{\partial}{\partial r}\left(r^2\frac{\partial C(r,t)}{\partial r}\right) \tag{2.29}$$

Solving Equation 2.29 with the boundary conditions:

$$\lim_{r\to\infty} C(r,t) = C_{bulk} \tag{2.30}$$

$$C(r,t)|_{r=r_0} = 0 \tag{2.31}$$

gives the diffusion limited rate constant of the Smoluchovski theory:

$$k = 4\pi D r_0 \tag{2.32}$$

where r_0 is the radius of the particle.

The same approach can be used to describe diffusion limited reaction in two-dimensional media as proposed independently by Razi-Naqvi and Owen [130, 131]. In principle Equation 2.29 has to be solved in cylindrical coordinates:

$$\frac{\partial C(r,t)}{\partial t} = D\left(\frac{\partial^2 C(r,t)}{\partial r^2} + \frac{1}{r}\frac{\partial C(r,t)}{\partial r}\right) \tag{2.33}$$

The solution of equation 2.33 is however more involved than its three-dimensional counterpart. It was proposed by Carslaw and Jaeger in 1939[132] and yields:

$$C(r,t) = \frac{2C_0}{\pi}\int_0^\infty \exp(-Du^2t)\frac{J_0(ur_0)Y_0(ur) - J_0(ur)Y_0(ur_0)du}{u(J_0^2(ur_0) + Y_0^2(ur_0))} \tag{2.34}$$

where C_0 is the bulk concentration, u a dummy integration variable, J_0 and Y_0 the Bessel functions of the first and second kind, and r_0 the radius

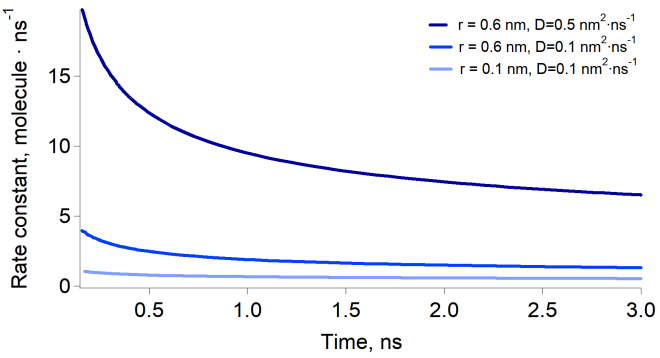

Figure 2.1: *Two-dimensional rate coefficient calculated with Equation 2.35 for different values of the particle radius and diffusion coefficient.*

of the particle. Following the same procedure than the three-dimensional case gives the two-dimensional diffusion-limited rate constant[130, 133].

$$k(t) = \frac{16DC_0}{\pi} \int_0^\infty \frac{\exp(-Du^2t)du}{u\left[J_0^2(ur_0) + Y_0^2(ur_0)\right]} \tag{2.35}$$

The remarkable difference between the two-dimentional and three-dimensional results is that the rate constant is actually time-dependent – and therefore no longer a constant – in two-dimensional media. Furthermore, Equation 2.35 has no asymptotic value at long times and therefore diffusion limited reactions in plans never formally reach a steady state[130, 134]. Several example of the the rate constants calculated with equation 2.35 are presented in Figure 2.1

Chapter 3

Structure of the ITIES

This chapter first presents an overview of the actual theories of the ionic structure of the polarised ITIES, from the Goüy-Chapman model (GCM) to the PB-PMF. The hypothesis and assumptions from which they are derived are introduced and their limitations are discussed. Then, a new model of the ITIES based on our experimental results is presented. This model is called the Double Ionic Monolayer Model (DIMM) and its particularity is that it is based on a molecular representation of the polarised interface, from which macroscopic properties are derived. Thus, it assumes that the interface can be represented as a plan capacitor and that the dependence of the capacitance on the potential difference actually reflects the variation of the distance between the ion layers at the interface. Thus, inverting the capacitance curves gives insight in the free energy profile of the ions at the interface. The DIMM presents a picture of the ITIES that is in agreement with electrochemical and SHG measurements and provides a theoretical framework in which the mechanisms of charge transfer phenomena at the ITIES can be analysed.

3.1 Introduction: electrified soft interfaces, the Goüy-Chapman model and beyond

One of the most basic approach in the description of ions at soft interfaces consists in transposing the GCM from electrode/electrolyte interfaces to electrolyte/electrolyte interfaces. This model relies in five main assumptions:

- The ions behave as point charges
- The ions interact only through electrostatic interactions
- The solvent can be approximated by a continuous medium of constant permittivity
- The electrode can be seen as a homogeneous distribution of charges.
- The ions follow a Boltzmann distribution

Then, the potential profile at the polarised electrolyte solution can be found by solving the Poisson-Boltzmann equation (in one dimension):

$$\epsilon_0 \epsilon_r \frac{d^2\phi(z)}{dz^2} = -\sum_i z_i e N_i^{\infty} \exp\left[-z_i e \frac{\phi(z) - \phi^{\infty}}{k_B T}\right] \tag{3.1}$$

where N_i^{∞} and ϕ^{∞} are the number of ions and the potential far from the electrode surface. The GCM was successful in explaining some experimental results at the electrode/electrolyte interface like, for instance, the potential dependence of the capacitance of the electrodes or the "electrowetting" effect. Nevertheless, its direct application to ITIES, despite some success, often showed qualitative agreement with the experimental results, but only poor quantitative predictions. Indeed, using impedance spectroscopy, Melo-Pereira *et al.* concluded already in 1994 that their observations could "*hardly be explained by a model consisting of two "back to back" diffuse layers even after the introduction in Goüy-Chapman theory of image forces and ion size*" [16]. Indeed, their results showed a marked dependence of the differential capacitance on the supporting electrolyte, which is not predicted by the GCM. For instance, the differential capacitance curves presented a marked asymmetry between positive and negative polarisations or a shift of the minimum that depended on the salt used as supporting

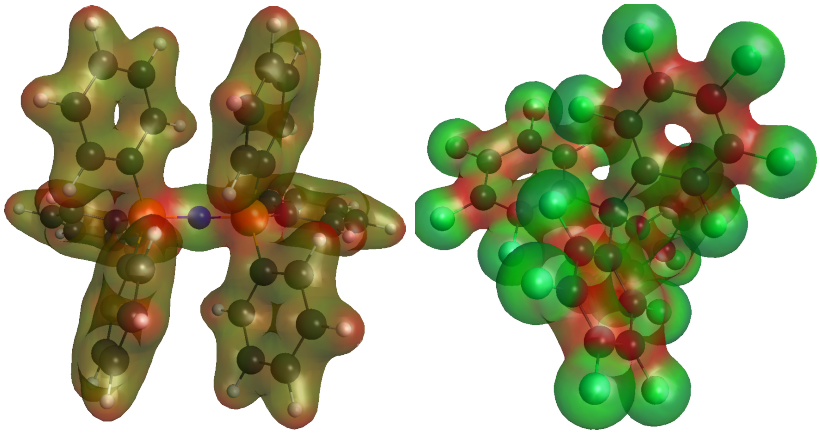

Figure 3.1: *BA^+* ***left*** *and TB^-* ***right*** *electron density computed at the def2-TZVP/ωB97X-D level of theory. Electron rich regions are represented in green. Both pictures show that the formal charge of the ions is distributed over the whole molecule and not carried by only one atom. Consequently, such ions cannot be approximated by point charges.*

electrolyte. More significantly, it was found that the important variable that determined the shape of the potential-capacitance curves was the nature of the ions present in excess at the polarised interface. Indeed, at positive polarisations, it is expected that the surface concentrations of the aqueous cation and organic anions are in excess (and *vice versa* at negative polarisation). Thus, changing the aqueous anion and organic cation should not change the trends of the curves on the positive side of the potential window, since the concentration of these species is reduced at the interface. That was indeed what Melo-Pereira *et al.* found and it was therefore suggested that ion pairs could be formed at the ITIES and that the extend of the apairement depends on the ion size, solvation energy and permittivity of the interface. Somehow surprisingly, they also concluded that the charges of the ions in the pairs would compensate each others and consequently have no impact on the interfacial potential drop, that was assumed to be mainly occurring in the space charge layer[17].

The conclusions of Melo-Pereira *et al.* are however not totally unexpected since two of the hypothesis supporting the GCM are not satisfied at the ITIES. Indeed, large organic ions, unlike alkali and halide ions, cannot be approximated by point charges since the charge is distributed over the whole molecule. Indeed, Figure 3.1 shows the electron density of the BA^+

and TB^- ions calculated by Density Functional Theory (DFT). It clearly appears that for both ions the electric charge is not carried by one atom but rather shared by the different functional groups. Furthermore, unlike EEI, ions do not interact with an homogeneous surface but with localised charges. It is this later point that is less compatible with the model. Indeed, in order to apply the GCM to the ITIES, it must be assumed that one phase is composed of point charges interacting with a plane and, at the same time, that the other phase is also made of point charges interacting with a plane surface. Thus, to satisfy the model, the two immiscible solutions should be both an electrode *and* an electrolyte solution. This paradoxical situation is well illustrated when the GCM equations are applied. Indeed, the potential profiles in each phase are given by the following equations:

$$\phi_{x>0} = \phi_w + \frac{4RT}{F} \arctan\left[\exp\left(F\sqrt{\frac{2C_w}{RT\epsilon_w\epsilon_0}}\right)x\right] \tanh\left[\frac{F}{4RT}\left(\phi_2 - \phi_w\right)\right] \tag{3.2}$$

for the aqueous phase, and

$$\phi_{x<0} = \phi_o + \frac{4RT}{F} \arctan\left[\exp\left(-F\sqrt{\frac{2C_o}{RT\epsilon_o\epsilon_0}}\right)x\right] \tanh\left[\frac{F}{4RT}\left(\phi_2 - \phi_o\right)\right] \tag{3.3}$$

for the organic phase. Here, the indices w and o stands for the water and organic phases, C denotes the electrolyte concentration and ϵ is the solvent permittivity. It appears that both equations depend on a common parameter, ϕ_2, the potential at the interface with respect to the bulk of the aqueous phase. In an electrode/electrolyte system, ϕ_2 would be the electrode potential, *i.e.* one of the important parameters that affects the shape of the profile. However, at the ITIES, ϕ_2 is imposed by the equality of the charge densities in each side of the interface. This leads nevertheless to non-continuous potential profiles and electric fields [135]. This is illustrated in Figure 3.2. This problem originates from the boundary conditions chosen in the solution of the Poisson-Boltzmann equation and could be solved by imposing the continuity of the potential and that of its first derivative at the interface. However, this would not greatly improve the model because, anyway, it inherently lacks a description of the ion-solvent interactions and ion-ion correlations.

The conclusions of Melo Pereira *et al.* where then corroborated by a series of publications from the group of Mark Schlossman. Using X-ray

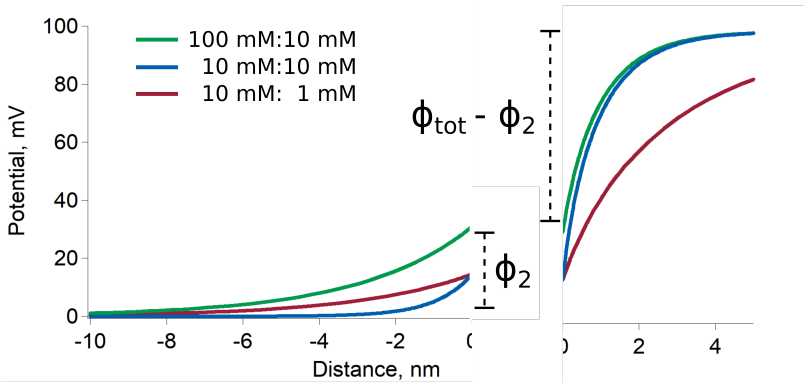

Figure 3.2: *Potential profile at the ITIES calculated with Equations 3.2 and 3.3, for various supporting electrolytes concentrations.*

reflectivity, they measured the electron density at the LLI and compared the results with a modified Poisson-Boltzman equation that accounted for ion-solvent interaction. In this model, called PB-PMF, the electric potential is defined by the following equation [19]:

$$\frac{d}{dz}\epsilon\left(z\right)\frac{d}{dz}\phi\left(z\right)=-\sum_{i}e_{i}c_{i}^{o}\exp\left[-\frac{\Delta E_{i}\left(z\right)}{k_{B}T}\right] \tag{3.4}$$

where $E_i\left(z\right)$ is the sum of the electrostatic potential energy and the free energy profile of the supporting electrolyte in the solvents, approximated by the function $f_i\left(z\right)$.

$$E_{i}\left(z\right)=e\,\phi_{i}\left(z\right)+f_{i}\left(z\right) \tag{3.5}$$

The function $f_i\left(z\right)$ was obtained independently from molecular mechanics simulations. Nevertheless, in the cases where such simulations are not available, $f_i\left(z\right)$ can be approximated by an error function [20]:

$$f_{i}\left(z\right)=\left(f_{i}\left(0\right)-f_{i}^{p}\right)\frac{\operatorname{erfc}\left[\frac{\left(|z|-\delta_{i}^{p}\right)}{L_{i}^{p}}\right)}{\operatorname{erfc}\left(-\frac{\delta_{i}^{p}}{L_{i}^{p}}\right)}+f_{i}^{p} \tag{3.6}$$

Using this approach, a remarkable agreement between the experimental data and the theory was found and only small corrections to this model were necessary to describe more correlated systems [21, 23]. Indeed, Laanait *et*

al. found that the surface density of electrolytes becomes so large at high polarisation that ion-ion repulsion can no longer be ignored, giving rise to a "correlation". The correlation was accounted for by an excess chemical potential dependent on the distance from the interface. Unfortunately, this quantity could not be estimated *a priori* and was let as a free fitting parameter. Nevertheless, alike Melo-Pereira *et al.*, these results suggested that the electrical double layer at the interface was "sharply defined". The conclusions of several authors presented in the previous paragraphs thus show that the structure of the ITIES pictured by the Goüy-Chapman model is not fully consistent with many experimental results.

Interestingly, and somehow surprisingly, the quasi-linear dependence of the capacitance over the interfacial potential difference was often overlooked in the many publications dedicated to the ionic structure at the ITIES. In the early years of electrochemistry at soft interfaces, this could be explained by the experimental limitations of the apparatus, as well as a low number of available solvents or organic supporting electrolytes. However, with the improvement of the experimental methods, the linear trend of the capacitance became more easily noticeable. For instance, Hou *et al.* applied the PB-PMF model to explain the capacitance curves of various alkali halide solutions in contact with DCE [23]. They could reproduce relatively well the linear dependence of the capacitance, but in some cases the capacitance was approximately 20% lower than the measured values, particularly at positive potentials.

The structure of the polarised ITIES is usually studied with two experimental methods: impedance spectroscopy and surface tension measurements. These two techniques are both dependent on the interfacial charge density. Indeed, differential capacitance (measured by impedance spectroscopy) is the derivative of the surface charge density with respect to the potential, while it can be shown that surface tension is the integral of charge density with respect to the potential. In the framework of GCM, Equations 3.7 quite nicely relate C, σ and γ with hyperbolic functions, *i.e.* C and γ depend on V like and hyperbolic cosine while σ depends on the potential like an hyperbolic sine.

$$\gamma(E) \propto \cosh(E) \quad \xrightarrow{\frac{d}{dE}} \sigma(E) \propto \sinh(E) \quad \xrightarrow{\frac{d}{dE}} C(E) \propto \cosh(E) \quad (3.7)$$

This relation is qualitatively followed at low potential differences [136], but discrepancies have been reported at large polarisations. Indeed, Trojánek *et*

al. [137] and Lhotský *et al*[138] showed that surface tension measurements where reliable at high potential differences, but that impedance results where more affected by residual faradaic currents at the edges of the polarisation window, leading to significant overestimations of the differential capacitance. For instance, Daikhin&Urbakh reported values of C as high as several hundreds of microfarad per centimetre squared for the water/2-heptanone interface[139]. Such capacitances correspond to surface charge densities of hundreds of charges per nanometre squared, which is unrealistic. In conclusion, the following points summarise the actual knowledge on the structure of the polarised ITIES:

- The electrical double-layer is sharp, of the order of one nanometre.
- The GCM is qualitatively correct, but lacks ion-solvent and ion-ion correlation.
- Capacitance and surface tension measurements agree at small polarisations.
- Capacitance curves are asymmetric and dependent on the organic phase supporting electrolyte.

3.2 Molecular mechanics simulations of ITIES

As presented in the previous paragraphs, the structure of the polarised ITIES has often been deduced from macroscopic measurements. In this section, we would like to derive a coherent picture of this interface starting from a molecular description. In order to do so, we conducted a series of molecular mechanics simulations of the water/TFT and water/DCE interfaces at different Galvani potential differences. The potential difference was not imposed as an external electric field but by creating an excess of positive (negative) ions in one phase, counterbalanced by the same excess of negative (positive) ions in the other phase. This situation is thermodynamically equivalent to applying an external potential difference (Equation 1.40) and allows a faster equilibration of the ions in the simulation box.

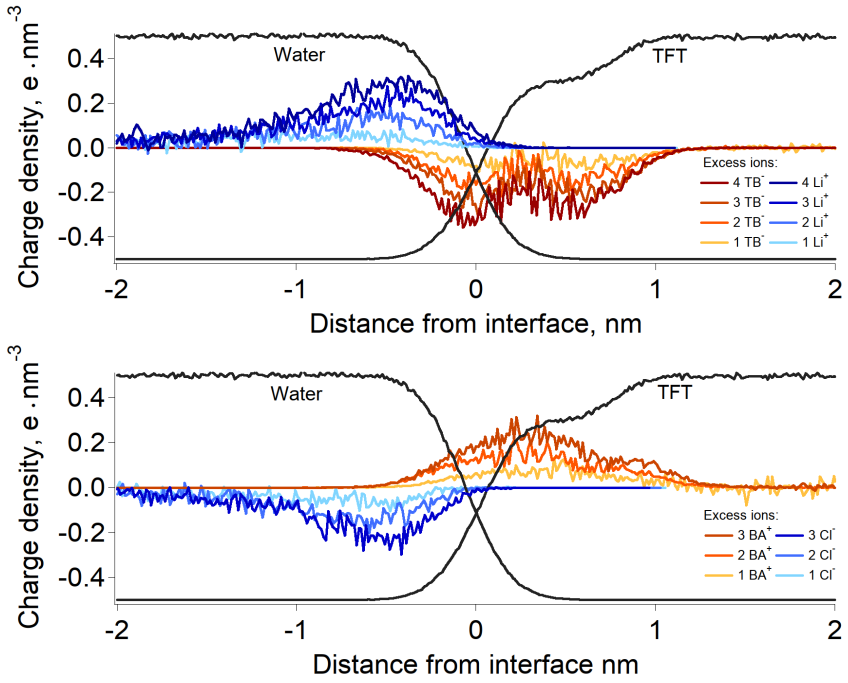

Figure 3.3: *Excess charge density profiles simulated at the water/TFT interface. Aqueous electrolyte: LiCl 200 mM (blue). Organic electrolyte: BATB 20 mM (red).* ***Top****: positive polarisation.* ***Bottom****: negative polarisation. The black curves shows the water and TFT density profiles in arbitrary units.*

Figure 3.3 shows the ion density profiles of a water/TFT interface for various positive (top) and negative (bottom) polarisations. The aqueous phase supporting electrolyte is LiCl, at a concentration of 200 mM, while the organic phase supporting electrolyte is BATB, at a concentration of 20 mM. It has to be noted that this concentration is slightly larger than the saturation concentration of BATB in TFT at room temperature (∼18 mM). However, we think that since the ion concentration is significantly larger at the interface than in the bulk (*vide infra*), a locally supersaturated solution is reasonable. It clearly appears in Figure 3.3 that, as observed by Luo *et al*, the interfacial double layer is sharp, extending over two nanometres. Furthermore, even at high polarisations, no diffuse layer is observed, in contradiction to the GCM. This results is however consistent since the charge density in one phase is exactly compensated in the opposite phase within one ionic layer.

At positive polarisations, the charge density of the excess organic anion presents two peaks. These peaks are each due to the pentafluorophenyl groups of the TB^- anion (two groups directed towards the interface and two directed towards the organic phase), while the well in between corresponds to the boron atom. Thus, the TB^- density is represented by the whole curve. Also, these shows that the negative charge is actually carried by the fluorine atoms rather than by the boron.

The profiles presented in Figure 3.3 show that the organic ions markedly penetrate into the aqueous phase, contrary to the aqueous ions that stay solvated in their respective phase. This trend is more pronounced with BA^+, *i.e.* at negative polarisations, which reflects the lower transfer potential of BA^+ with respect to that of TB^-. Furthermore, it appears that the double layer position with respect to the interface is controlled by the penetration of the organic ions in the aqueous phase. Indeed, at negative polarisations, the excess Cl^- density decreases before that of water, implying that some water molecules are present between Cl^- and TFT. Thus, in principle, Cl^- could penetrate further in the organic phase. Nevertheless, these ions do not go deeper than half the charge density of BA^+, because otherwise this would result in formal transfer of Cl^- into the organic phase. Thus, Cl^- is blocked by the layer of BA^+. For the same reason, Li^+ density stops where that of TB^- begins but, however, since TB^- extends less in the aqueous phase, Li^+ can reach the surface of the aqueous phase.

Interpenetration of the ionic layers was hypothesised by some authors in order to explain capacitance-potential curves at the ITIES[139]. Here, however, the extend of interpenetration appears virtually independent of the surface charge density. This suggests that ion pairs are formed at the interface and that the interpenetration width is actually dependent on the cation-anion equilibrium distance.

Figure 3.4 (top) shows the electric potential profiles corresponding to the charge densities presented in Figure 3.3. The potential is calculated by integrating the charge densities of the ions and solvent molecules with respect to the z-axis, *i.e.*

$$\phi(z) = -\iint_0^{l_z} \frac{\rho(z)}{4\pi\epsilon_0}\, dz \tag{3.8}$$

Here, the permittivity is only that of the vacuum since the permittivity of the solvents is accounted for by partial charges of the solvent molecules.

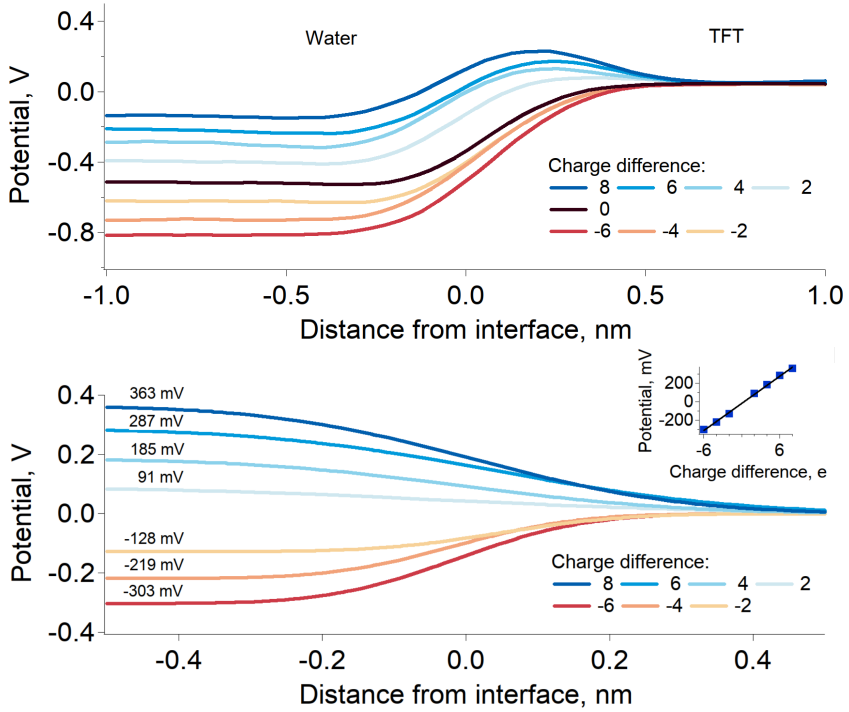

Figure 3.4: ***Top****: electric potential profiles along the simulated water/TFT interface.* ***Bottom****: electric potential profiles along the simulated water/TFT interface corrected for the contribution of the solvent dipoles. The inset shows the potential difference as a function of the charge difference. Aqueous electrolyte: LiCl 200 mM. Organic electrolyte: BATB 20 mM.*

The potential calculated according to Equation 3.8 represents the Galvani potential difference between the two phases. This difference can be separated in two contributions, that of the solvent dipoles and that of the charges[140].

$$\Delta_\alpha^\beta \phi = \phi^\beta - \phi^\alpha = \Delta_\alpha^\beta g(dip) + \Delta_\alpha^\beta g(charge) \tag{3.9}$$

Figure 3.4 (top) shows that the solvent dipolar contributions represents a significant part of the total Galvani potential difference. Indeed, at zero charge density *i.e* at zero polarisation, the potential difference is 450 mV. This value has already been reported at the water/nitrobenzene by Michael&Benjamin[3]. Despite such a large magnitude, these dipoles do not influence ion properties at the ITIES in the simulations. Furthermore,

in a four-electrode cell, since the organic phase reference electrode is also a water-TFT interface, any dipolar contributions cancel out and it is only the Galvani potential difference due to the charges that is measured. Thus, in order to analyse only the potential drop due to the ion double layer, the profiles of Figure 3.4 (top) where fitted with two "error functions", one of which was kept constant, accounting for the surface potential. Figure 3.4 (bottom) shows the ion-only electrostatic potential for each surface density, *i.e.* the error function that was let free in the fittings of Figure 3.4 (top). There are two notable features in this Figure. Firstly, the potentials drop entirely at the interface, over less than one nanometre, which is much sharper that what predicts the GCM. Secondly, their is a quasi-linear dependence between the total Galvani potential difference and the surface charge density.

Working at the water/TFT interface has the inconvenient that the concentration of BATB is limited to few tens of millimolars. Nevertheless, this limitation can be overcome by working at the water/DCE interface, where BATB is soluble up to at least 100 mM. The advantage of this system over the water/TFT interface is that as the ion concentration is larger, a good sampling of their properties can be faster achieved. Furthermore, the ratio between the total number of organic anions and cations is closer to one, which is a more realistic situation. Indeed, since the polarisation is imposed by a neat charge difference between the two phases, at low ion concentrations and large polarisations the organic phase contains almost only one ionic species. Figure 3.5 shows the interfacial ion density simulated at the water/DCE interface. However, here, the charge density is presented for every ion while only the excess charge is shown in Figure 3.3. These results are similar to those observed at the water/TFT interface, *i.e* the potential drops entirely between ions pairs at the interface. Nevertheless, a small excess of counter-ion behind the double layer ion is visible in each phase. The excess of Li^+ behind the Cl^- can be explained by the need to balance the Cl^- that is adsorbed at the interface even when no polarisation is imposed. Indeed, halide ions are known to be present in excess at the liquid liquid interface [141]. The explanation is also supported by the fact that this situation is not observe at positive polarisation, *i.e.* when Li^+ is in excess at the interface. On the other hand, the slight increase of counter-ion concentration in the organic phase can be explained by the electrostatic interaction with the double layer.

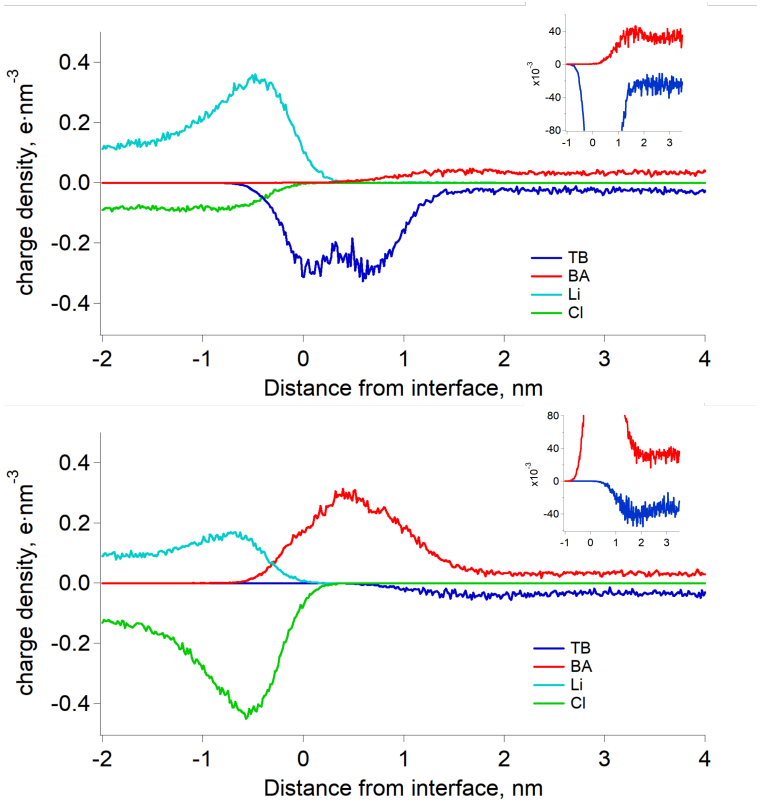

Figure 3.5: *Ion density profiles simulated at the water/DCE interface. Aqueous electrolyte: LiCl 200 mM. Organic electrolyte: BATB 100 mM (red).* ***Top****: positive polarisation (8 charges).* ***Bottom****: negative polarisation (-8 charges). The inset show the slight counter-ion excess.*

3.3 Surface charge density measured by SHG

The dependence of the surface change density on the potential difference can be experimentally measured by SHG. Indeed, as already shown by Conboy&Richmond[102, 103], it is possible to observe a non-resonant second harmonic signal from the organic supporting electrolytes of a polarised ITIES. Since the second harmonic signal intensity is proportional to the square root of the surface dipole concentration (from Equation 2.9), this spectroscopic method offers a direct way to probe the ionic layer.

Figure 3.6 shows the normalised square root of the second harmonic

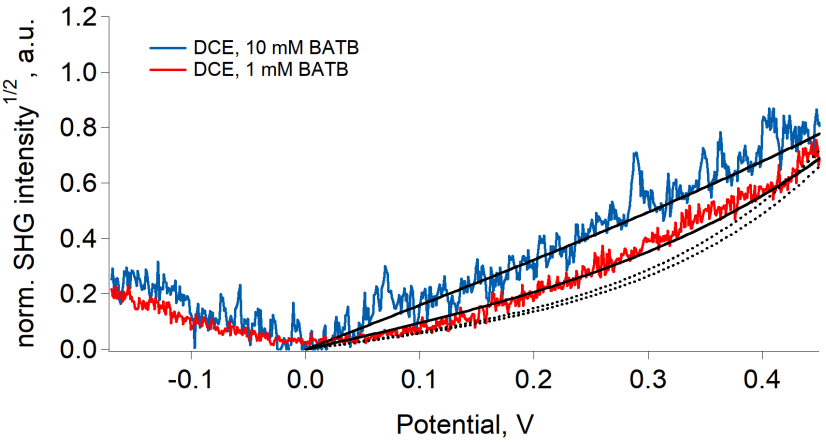

Figure 3.6: *Normalised square root of the non-resonant second harmonic signal of the polarised water/DCE interface. Fundamental wavelength: 910 nm (p polarised). Aqueous electrolyte: LiCl 10 mM. Organic electrolyte: BATB 1 mM (red) and 10 mM (blue). The black plain curves show fitting with Equation 3.10, while the dashed curves show the prediction of Equation 3.10 assuming that 30% of the potential drops in the organic phase.*

signal measured at the water/DCE interface. The supporting electrolytes are 10 mM LiCl and 1 mM BATB or 10 mM BATB. Clearly, at 10 mM, the surface concentrations of TB^- at positive polarisations, and that of BA^+ at negative polarisations increase linearly with the potential difference. These results are similar to those of Conboy&Richmond, on an larger potential window. These authors applied the GCM and the modified Verwey-Niessen model[6] to explain these trends and concluded that less than 10% of the potential difference dropped in the organic side of the interface. Indeed, in the modified Verwey-Niessen model, the interface is divided in three regions, an aqueous side, an organic side and an ion-free layer in between. The potential drop is allowed to vary independently is each phase, while the total potential difference is recovered with the contribution of the solvent dipoles in the ion-free region. In each phases, the GCM applies and predict the following trend of the surface charge density:

$$\sigma\left(\phi\right) = -\sqrt{8RT\epsilon_0\epsilon_r c_\alpha}\sinh\left[\frac{F}{2RT}\left(f_\alpha \cdot \phi\right)\right] \tag{3.10}$$

where f_α is the fraction of the total potential difference in the phase α and c_α the concentration of supporting electrolyte in the same phase. The other

symbols have their usual meaning. Here, fitting the data with Equation 3.10 implies that 8% and 20 % of the total potential difference drops in the organic phase at 10 mM and 1 mM. Such results are nevertheless difficult to explain in light of the simulations presented in the previous section. Indeed, the simulations did not show the existence of the three regions presupposed by the modified Verwey-Niessen model. Consequently, separating the potential profile in an aqueous and organic contributions is no longer relevant. Indeed, since the potential drops only between the ion layers, it is not necessary to distinguish aqueous and organic sides. Thus, we hypothesise that low values of the parameter f are found because the trends actually do not follow an hyperbolic sine, at least at 10 mM. Therefore, in fitting the data, a low value of f is found because then the argument of the hyperbolic sine is small, and this function actually becomes linear. However, at low BATB concentrations and low polarisations, the electrolyte surface concentration significantly deviate from the quasi-linear trend observed in the simulations. This result suggest that at the GCM is valid at low electrolyte concentrations, which is to be expected since in these conditions the hypothesis of the model hold.

3.4 Capacitance of the ITIES

As presented in introduction, the capacitance of the polarised ITIES has been discussed in many publications in the past and several models have been proposed to explain the experimental results. In the following section, we would like to show how the conclusions drawn from the molecular mechanics simulations and SHG can be used to develop a simple qualitative description of the capacitance at the ITIES.

Figure 3.7 shows the capacitance of the water/DCE interface at various organic electrolyte concentrations (left) and the capacitance of the water/DCE, water/TFT and water/nitrobenzene interfaces for the same organic electrolyte concentrations (right). As already reported by many authors, the capacitance curves are asymmetric with respect to the Point of Zero Charge (PZC)[16, 17]. This asymmetry reflects the change of interfacial population with the polarisation. Indeed, since the interface is covered by BA^+ at negative polarisation and by TB^- at positive polarisations, it is reasonable to assume that these ions are responsible for the trends of the capacitance. However, an interesting feature is that,

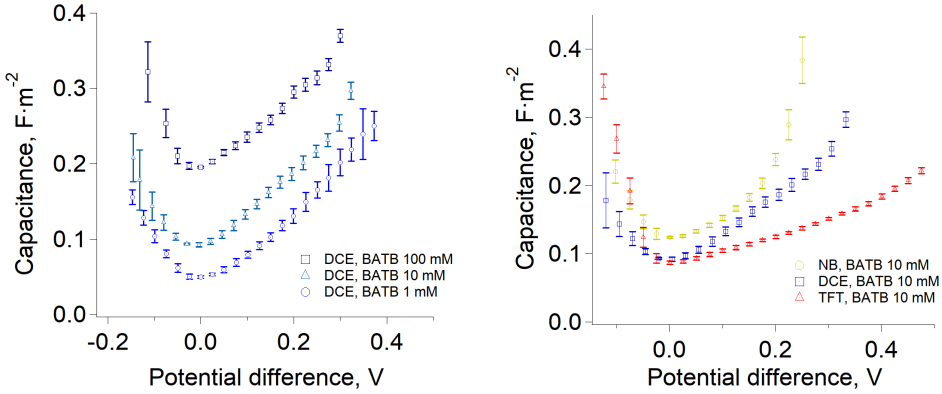

***Figure 3.7: Left**: capacitance of the water/DCE interface at various BATB concentrations. From bottom to top: 1 mM, 10 mM, 100 mM. **Right**: capacitance of the water/TFT, water/DCE and water/nitrobenzene interfaces. BATB concentration: 10 mM. The error bars show the standard deviation over ten measurements.*

at positive polarisations, the asymmetry is more pronounced when the organic solvent is TFT rather than DCE (Figure 3.7, right). Therefore, it is not only the ions in excess that control the slope of the capacitance but rather the solvent-ion interaction. This suggests that the slopes of the capacitance curves are dependent on the standard Gibbs free energies of transfer of the organic supporting electrolytes. In this respect, Figure 3.8 shows cyclic voltammetries measured at the water/DCE and water/TFT micro-interfaces. It appears that the transfer potentials of BA^+ and TB^- are –0.58 V and 0.55 V at the water/DCE interface, and –0.48 V and 0.71 V at the water/TFT interface. Thus, these values are consistent with the more pronounced asymmetry of the capacitance curves at the water/TFT interface (compared to water/DCE) since the standard transfer potentials of the organic supporting electrolytes is also assymetric.

Another remarkable feature in Figure 3.7 (left) is that at same electrolyte concentrations, the capacitance at the PZC increases with the solvent dielectric constant (ϵ_{tft}=9.18, ϵ_{dce}=10.36, ϵ_{nb}=34.82). Nevertheless, the capacitance variations with the organic solvents are not directly proportional to their dielectric constants. Indeed, the capacitance in nitrobenzene is not three times that in TFT or DCE. However, it seems reasonable to assume that the interface dielectric constant is the average of that of the two solvents. Indeed, the polarity of the LLI has already been found

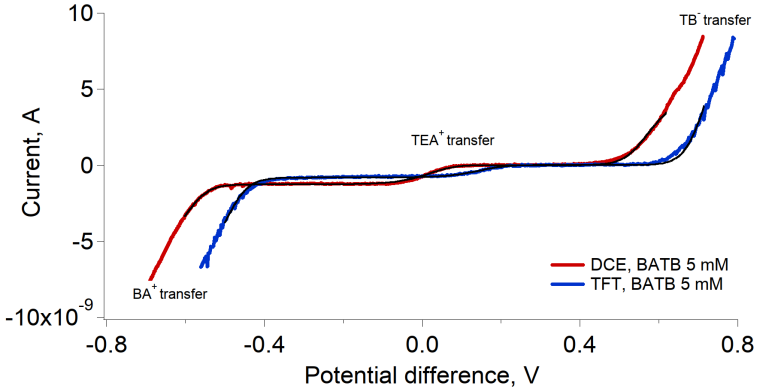

Figure 3.8: *Micro-hole supported cyclic voltammetry at the water/DCE (red) and water/TFT interfaces. No aqueous supporting electrolyte. Organic supporting electrolyte: BATB 5 mM. The zero of the potential window has been determined assuming a half-wave transfer potential of tetraethylammonium ion of 0.05 V of the water/DCE interface and 0.17 V for the water/TFT interface.*

to follow this simple rule [108]. Furthermore, the relative permittivity of miscible solvents mixtures is also proportional to their molar fractions [142]. Consequently, taking the dielectric constant of water equal to 80, one finds for the three interfaces: $\epsilon_{h2o/tft}$=44.6, $\epsilon_{h2o/dce}$=45.2 and $\epsilon_{h2o/nb}$=57.4. With these values, is appears that the capacitance curves, at equal concentrations and low polarisations, are simply proportional to the interface dielectric constant. This observation is indeed valid mainly at low polarisations, where the asymmetry of the curves is not pronounced.

The conclusions of the previous paragraphs and the interface structure pictured by the molecular mechanics simulations suggest that the polarised ITIES could be simply described as a planar capacitor. This simple electronic component is described by the following equations:

$$E_{pc} = \frac{\sigma}{\epsilon_0 \epsilon_r} \qquad V_{pc} = \frac{\sigma d}{\epsilon_0 \epsilon_r} \qquad C_{pc} = \frac{\epsilon_0 \epsilon_r}{d} \tag{3.11}$$

where σ is the charge density on the plates of the capacitor, d is the distance between the plates, ϵ_0 the vacuum permittivity and ϵ_r the relative permittivity of the medium between the plates. E_{pc}, V_{pc} and C_{pc} are the electric field, the potential difference and the capacity of the capacitor. Therefore, Equation 3.11 suggests that the increase of capacitance with

the polarisation visible on Figure 3.7 is due to a shortening of the distance between the ion layers.

A theory of the capacitance at the ITIES must include the features presents on Figure 3.7 in the capacity Equation 3.11. It thus naturally follows that d must be a function of the potential difference, that takes the transfer potential of the supporting electrolytes as parameters; the inverse of the ion transfer free energy profiles fulfil these requirements. In a simple approach, this function can be assumed to be linear, in agreement with Markin *et al.* [143]. Thus, the free energy $U_i(x)$ of an ion crossing the interface is:

$$U_i(x) = \Delta\phi_i \begin{cases} 0 & x < -r_i \\ 0.5 \cdot (1 + \frac{x}{r_i}) & -r_i \leq x \leq r_i \\ 1 & x > r_i \end{cases} \tag{3.12}$$

where $U_i(x)$ is the free energy of the ion i, $\Delta\phi_i$ its transfer potential and r_i its radius. Thus, the inverse of function 3.12 is:

$$x(U_i) = \begin{cases}]-\infty, -r_i[& U_i = 0 \\ 2U\frac{r_i}{\Delta\phi_i} - r_i & 0 \leq U_i \leq \Delta\phi_i \\ ]r_i, \infty[& U_i = \Delta\phi_i \end{cases} \tag{3.13}$$

Inserting Equation 3.13 in Equation 3.11 and identifying the free energy U_i with the potential difference E yields:

$$C_i(E) = \frac{\epsilon_0\epsilon_r}{w + r_i - 2E\frac{r_i}{\Delta\phi_i}} \tag{3.14}$$

where $C_i(E)$ is the capacitance at polarisations where the organic ion i is in excess at the interface and w is a constant such that $C_i(E)$ does not diverge when the distance is zero. By construction, Equation 3.14 possesses the features observed on the experimental capacitance curves, *i.e.* the slope of the capacitance is asymmetric and depends inversely on the standard transfer potential. Then, a plot of $1/C$ *vs.* E should give approximately two linear functions whose slopes are proportional to the ionic diameter divided by their transfer potentials. Figure 3.9 shows $\epsilon_0\epsilon_r/C_i$ for the water/TFT, water/DCE and water/nitrobenzene interface (results are given in caption). It can be seen that at high concentrations and large

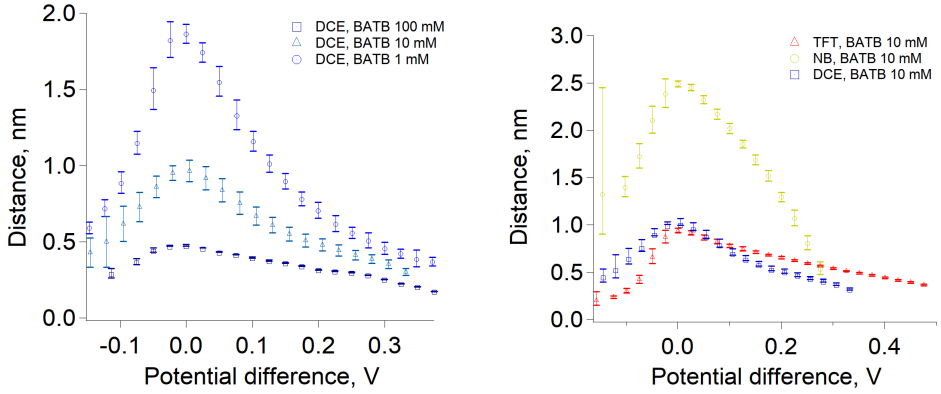

Figure 3.9: *Distance (according to the capacitor model) between the ion layers as function of the potential difference. Data are the same than in Figure 3.7. Fitting these results with Equation 3.14 gives the following radii for BA^+: 1.9 nm (TFT), 1.1 nm (DCE) 3.9 nm (NB), and for TB^-: 0.9 nm (TFT), 1.1 nm (DCE), 0.9 nm (NB).*

polarisations the inverse of the capacitance actually behaves as expected from equation 3.14. Nevertheless, there is only a relative agreement at low concentrations. Here, however, the GCM gives satisfactory results.

3.5 Summary and conclusions

The results presented here are encouraging, kipping in mind the simple model used to derive Equation 3.14. There is no doubts that a more sophisticated description of the free energy profiles would produce better results. In this respect, the model of equation 3.14 is mainly valid at short distances (large polarisations), when the free energy profile is dominated by the contribution of the aqueous phase and thus almost linear. Thus, at low concentrations and polarisations, the free energy is dominated by electrostatic repulsion from the interface, which explains why the capacitance curves are similar for all solvents. Furthermore, the aqueous supporting electrolyte is not taken into account in this simple model while it must necessarily contribute to the capacitance, even for a smaller part. Finally, another limitation of this model arises from the difficulty to estimate the relative permittivity to be used in Equation 3.14. Indeed, the distances calculated from equation 3.14 are directly proportional to the dielectric constant of the medium between the plates of the capacitor. However, this

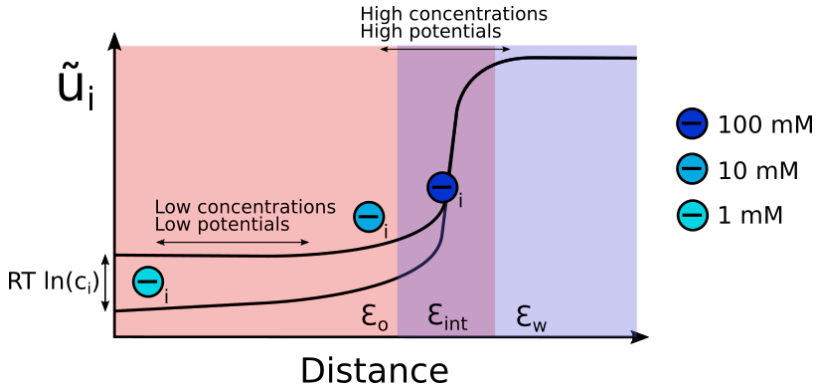

Figure 3.10: *Schematic representation of the organic ion energy profile at the ITIES.*

value varies significantly whether one assumes water, the interface or the organic solvent as the relevant medium. It has been shown that these could have a significant impact on the capacitance curves at the ITIES [144].

The important contribution of this model is to show that the capacitance of the ITIES mainly reflects the free energy profile of the organic supporting electrolytes, which explains the asymmetry, the solvent dependence and the concentration dependence. This is illustrated in Figure 3.10. At low concentrations and low polarisations, since the ions are in the flat part of the free energy profile, it is energetically easy to decrease the distance between the ion layers. This is what is seen in Figure 3.9 where the distance sharply decreases over the first hundreds of millivolts, and in Figure 3.6, where the surface charge density increases slowly. In this conditions, the relevant dielectric constant is that of the organic solvent since the charges are far from the interface. Oppositely, at large polarisations and large concentrations, since the ions are close to the interface – therefore in the sharp part of the energy profile – the polarisation has little impact on the distance. This is what is seen in Figure 3.9 where the distance is almost constant and in Figure 3.6, where the surface charge density increases linearly with the potential. Here, the relevant dielectric constant is that of the interface, *i.e.* the average of those of the water and the solvent. The role of the concentration is to shift up the ion electrochemical potential since it is given by Equation 1.31. Thus, as the concentration increases, the ions are closer to the interface, and therefore already in the sharp part of the free energy profile. This is translated in Figure 3.9 by curves shifted towards the PZC. Finally, the distance *vs.* potential curves do

not exactly converge at large polarisations because the dielectric constant of the organic phase is changed by the ion concentration. Indeed, in the case of chlorinated solvent, the permittivity of the solvent is increased by roughly 30% at salt concentrations of 100 mM [145]. To conclude, the free energy profile of the organic ions is obtained, to some extent, by "rotating" Figure 3.9 of 90°, *i.e.* by expressing the potential difference as a function of the distance.

3.6 Computational details

The molecular mechanics simulations were all carried out using GROMACS 2018.1.

Topologies:

The simulations contain six types of chemical species: water, TFT (or DCE), BA^+, TB^-, Li^+ and Cl^-. The water was simulated with the TIP4P model while the TFT molecules used the standard OPLS force field parameters. Li^+ and Cl^- were simulated with the parameters of Jensen&Jorgensen [146]. The geometries and partial charges of the organic ions were calculated from DFT simulations using the GAMESS 2018. The exchange and correlation functional was the ω-B97XD while the basis set was a triple zeta plus polarisation of Ahlrichs *et al.* [147] for both the geometries and charges. The charges were obtained by fitting the electrostatic potential using the CHELPG algorithm under the constraint that the sum of the partial charges should reproduce the total molecular charge. The thus obtained values were then averaged over all symmetry equivalent atoms in order to have an homogeneous distribution.

Electrostatic potential profile simulations:

The dimensions of the simulations boxes were 5x5x40 nm, with 20 nm dedicated to each phase (aqueous and organic). The aqueous phase contained p_A positive ions (Li^+) and n_A negative ions (Cl^-) such that $p_A+n_A=120$ and $p_A-n_A=c$, where c is the desired charge difference. This gives a LiCl concentration of $\sim$200 mM. Similarly, the organic phase contained p_O positive ions (BA^+) and n_O negative ions (TB^-) such that $p_O+n_O=12$ and $p_O-n_O=c$. This gives a BATB concentration of $\sim$ 20 mM. The electrostatic interactions were calculated using PME summation. However, in order to avoid artefacts due to the three dimensional periodic boundary conditions, the simulations were periodic only the x and y directions. Consequently, a

pseudo two-dimensional Ewald summation was used. Walls where therefore placed at z=0 nm and z=40 nm to contain the system. The system energy was then minimized until a force threshold of 100 $kJ \cdot mol^{-1} \cdot nm^{-1}$ was reached. Then, the box was quickly equilibrated for 1 ns in the NVT ensemble at 293 K using the "V-rescale" thermostat with a time constant coupling of 0.5 ps and a time step of 2 fs. Finally, the simulations were run in the NPT ensemble for 60 ns, with a time step of 2 fs, at 293 K and 1 bar using the "V-rescale thermostat" (time constant coupling of 0.5 ps) and Berendsen barostat (time constant coupling of 1ps). The semi-isotropic pressure coupling was used with a compressibility of 0 bar^{-1} in the x and y directions and of $4.5 \cdot 10^{-5}$ bar^{-1} in the z direction. The last 20 ns of each simulations where used for analyses.

Chapter 4

Electron transfer reactions at the liquid-liquid interface

This chapter first presents a summary of the study of electron transfer reactions at the polarised ITIES over the past decades. Then, a truly potential-dependent heterogeneous electron transfer reaction is presented. The reaction is studied by cyclic voltammetry at the ITIES and in an ECSOW configuration. Thus, it is shown that the mechanism of the reaction at the ITIES is different than that at the EEI, which supports the conclusions of the previous chapter, i.e the ITIES cannot be described as an EEI. In particular, the separation of the forward and reverse electron transfer peaks is larger at the ITIES. This observation is tentatively explained by preliminary results of molecular mechanics simulations of ion energy profiles at the ITIES.

4.1 Introduction

The evolution of the understanding of the electron transfer at the polarised ITIES has followed, to some extend, the same path than that of the ion transfer. Indeed, the first publication dedicated to this subject attempted to apply the theories of the EEI to the ITIES in order to understand the potential dependence of the kinetics of the reaction [33, 46, 47, 51]. Nevertheless, the lack of understanding of the ITIES at the molecular level

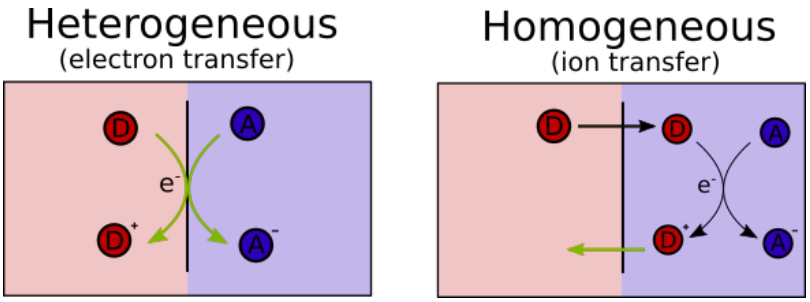

Figure 4.1: *Schematic representation of the homogeneous vs. heterogeneous current mechanisms. The phenomena responsible for the interfacial current are represented with green arrows. In the homogeneous mechanism, the low solubility of the donor in the acceptor phase is compensated by a larger reaction volume.*

brought several questions regarding the mechanism of the electron transfer. In particular, the role of the potential difference on the kinetics was debated. Indeed, some authors reported that the rise of the interfacial current with the polarisation was due to an increase of the reaction driving force [48, 50], while other claimed that this could be explained by a concentration change of the reagents [52, 67].

An interesting aspect of electron transfer reactions, compared to ion transfer reactions, is that the former can be studied with a larger range of experimental tools. Thus, the question of the role played by the polarisation on the kinetics of the electron transfer reaction could be tackled by SECM [55], *in situ* UV-vis spectroscopy [61], fluorescence spectroscopy [62] or time-resolved UV-vis spectroscopy [63]. Nevertheless, despite this larger range of experimental approaches, contradictory results concerning the dependence of the current on the polarisation were published with claims of a potential dependent [58, 59] and potential independent [65, 66] electron transfer.

In addition to the question raised by the potential dependence of the electron transfer, the mechanism of the current generation was also debated. Thus, comparing experimental results to finite elements simulations [148], some authors suggested that the observed charge transfer was not a true electron transfer but actually an interfacial ion transfer following a redox reaction in one of the phases [76, 149]. This mechanism was called "homogeneous" electron transfer as opposed to the "heterogeneous" electron transfer, *i.e.* a truly interfacial electron transfer (see Figure 4.1. The

possibility of a homogeneous mechanism was actually envisaged earlier [56] but without a dedicated study.

The necessitiy of carefully defining the experimental conditions to study electron transfer reactions is illustrated in the publications of Hotta *et al.*[76] and Osakai *et al.*[150]. Indeed, using identical experimental methods, they draw different conclusions on the electron transfer mechanism, at the ITIES, because they worked with different reagents [76, 150], whose partial solubility in the opposite phase varied. In this respect, as a recommendation to avoid confusion, authors should always specify whether they measured an interfacial current, which can be homogeneous or heterogeneous, or directly an electron transfer, which by definition can only be heterogeneous at the ITIES.

4.2 Heterogeneous electron transfer reaction at the ITIES

System characterisation

As presented in the introduction, electron transfer reactions at the ITIES can be parasitised by several factors. One of these factors is the use of charged donors and acceptors. Indeed, such compounds are not ideal, firstly because their concentration at the interface depends on the polarisation and secondly because they can transfer with the polarisation, limiting therefore the potential window. In order to avoid these limitations, we will work with BSPBPy as electron acceptor (see Section 1.5) and Decamethylferrocene (DMFc) as electron donor. Indeed, these two molecules are neutral.

Another frequent problem encountered in the literature dedicated to the electron transfer at the ITIES is the use of donor/acceptor couples whose reactivity was thermodynamically spontaneous, *i.e* that, in principle, did not require an over-potential to react. This problem is that prensented by Hotta *et al.*[76], Osakai *et al.*[77] and Peljo *et al.*[149] where $Fe(CN)_6^{3-}$ can homogeneously oxidise the electron donor. In these cases, it becomes difficult to rule out whether the observed current presents a significant contribution from homogeneous redox reactions followed by ion transfer.

Figure 4.2 shows cyclic voltammograms of BSPBPy recorded in water. It appears that BSPBPy presents three reduction peaks located at -170

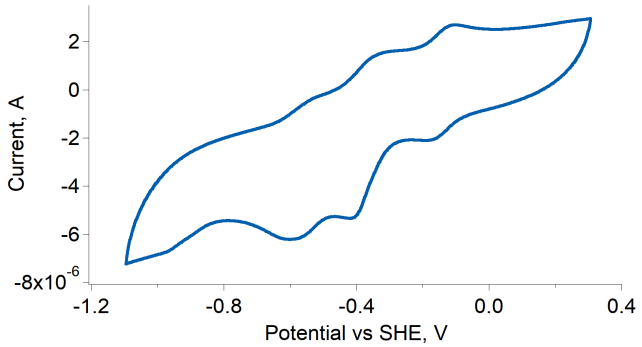

Figure 4.2: *Cyclic voltammetry of BSPBPy 100 µM in water (LiCl 100 mM, glassy carbon electrode).*

mV_{she}, -380 mV_{she} and -570 mV_{she}. Such results are unusual for a viologen derivative that in principle present only two reduction peaks [151]. We think that the extra peak is due to dimerisation of BSPBPy which is commonly encountered with viologens. On the other side, the redox potential of DMFc was found to be +118 mV in TFT [152] and +101 mV in water [153]. Therefore, the interfacial oxidation of DMFc by BSPBPy requires an over-potential of at least 288 mV (27.8 $kJ{\cdot}mol^{-1}$ while the homogeneous oxidation requires 271 mV (26.1 $kJ{\cdot}mol^{-1}$). For such Gibbs energy differences, the corresponding equilibrium constant is of the order of $1{\cdot}10^{-5}$. Thus, because of the strict insolubility of the donor/acceptor couple in the their opposite phase, their large redox potential difference and their neutrality, we expect to see a faradaic current only due to heterogeneous charge transfer.

Results

Figure 4.3 shows cyclic voltammetries recorded at the water/TFT interface with, and without the above-mentioned redox couples under N_2 atmosphere. The supporting electrolytes are LiCl 10 mM in water and BATB 5mM in TFT. In can be seen on Figure 4.3 (top) that the blank experiments, *i.e.* cyclic voltammetries in presence of only the electron donor or electron acceptor, do not feature any faradaic currents, except the transfer of the supporting electrolytes at the edges of the potential window. However, Figure 4.3 (bottom) shows that when both donor and acceptor are present,

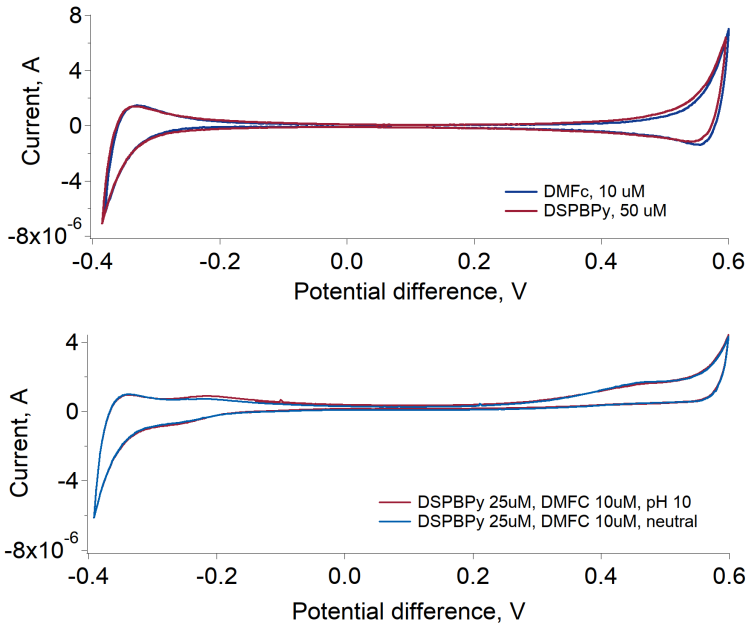

Figure 4.3: *Cyclic voltammetry of BSPBPy and DMFc at the water/TFT interface (LiCl 10 mM, BATB 5 mM).* ***Top****: blank experiments with only the donor or only the acceptor in their respective phases.* ***Bottom****: experiments with both donor and acceptor at neutral and basic pH.*

a clear current response is visible at positive and negative polarisations. The current at negative polarisations can be explained by the transfer of $DMFc^+$ from the organic to the aqueous phase, indeed, the standard transfer potential of $DMFc^+$ from TFT to water is -260 mV[154], while the peak at positive polarisation is attributed to interfacial electron transfer reaction. Indeed, the experimental precautions presented in the previous section makes the homogeneous mechanism unlikely.

DMFc has been reported to reduce protons and oxygen at the LLI [152]. In the present experiment, oxygen reduction can be excluded as a possible explanation of the current response at positive polarisations since the experiments are conducted under N_2 atmosphere. Concerning the hydrogen evolution, Figure 4.3 (bottom) shows that the cyclic voltammetries recorded at a pH of 10 are similar to those at neutral pH, within experimental variations. Consequently, we also exclude hydrogen evolution as a possible side-reaction. Whatsoever, as previously emphasised, blank experiments

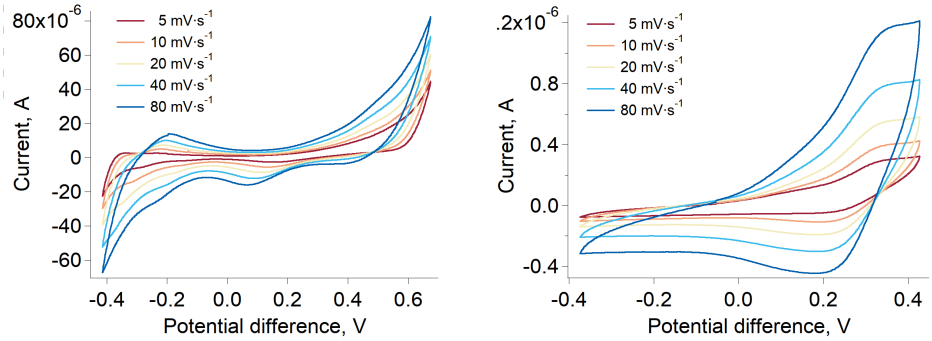

Figure 4.4: *Cylcic voltammetries of BSPBPy 250 µM in water, pH 10, LiCl 10 mM and DMFc in TFT, BATB 10 mM.* ***Left****: Liquid-liquid interface* ***Right****: ECSOW (glassy carbon electrodes).*

did not show any faradaic current within the polarisation window. Thus, we conclude that this current is indeed an heterogeneous electron transfer.

The absence of electron back transfer peak in Figures 4.3 (bottom) and the transfer of $DMFc^+$ suggests that BSPBPy reduction is irreversible either chemically or electrochemically. The chemical irreversibility could be explained by $BSPBPy^-$ disproportionation, as suggested by the bulk cyclic voltammetry presented in Figure 4.2. On the other hand, an electrochemical irreversibility indicates a sluggish kinetic of the back electron transfer. In order to get insight into the electron transfer mechanisms between BSPBPy and DMFc, we conducted a series of ECSOW experiments with the same system. The fact that in ECSOW no ion transfer currents can take place has a twofold interest: firstly only electron transfer is seen and secondly the potential window is only limited by the solvents oxidation/reduction. Figure 4.4 compares cyclic voltammetries of BSPBPy in water and DMFc in TFT when the phases are in direct contact (left) or connected by glassy carbon electrodes (right). The electron transfer peak visible in the ECSOW corresponds to the first reduction of BSPBPy. The peak separation is 150 mV, in relative concordance with the 123 mV predicted for a reaction involving two redox couples in equimolar concentrations, located in separated phases [155]. Furthermore, the forward and backward peak currents depends linearly on the square root of the scan rate. Thus, in agreement with Stewart *et al.*, the midpeak potential as been set to the formal potential of the reaction: 288 mV.

Comparing the cyclic voltammetries at the LLI and those of the ECSOW

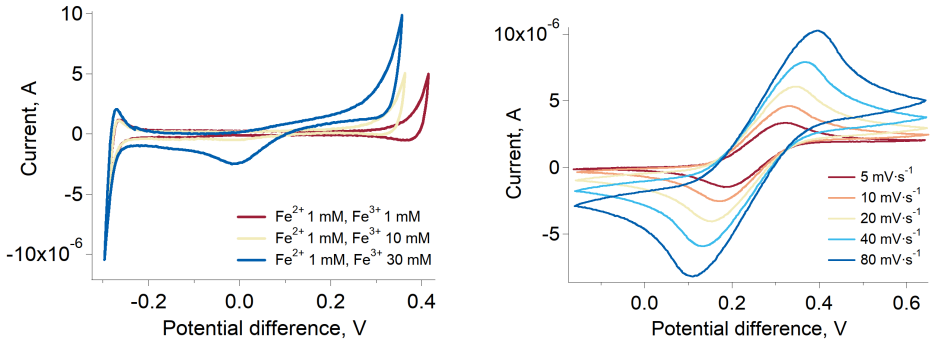

Figure 4.5: *Cyclic voltammetries of* $Fe(CN)_6^{3-}$ *30 µM/*$Fe(CN)_6^{4-}$ *1mM in water, LiOH 10 mM and Decamethylruthenocene (DMRc) in DCE, BATB 10 mM.* ***Left****: Liquid-liquid interface* ***Right****: ECSOW (glassy carbon electrodes).*

system, it appears that the reduction peak is shifted to more positive values at the liquid interface (480 mV at the ITIES *vs* 370 mV with ECSOW. This is consistent with the simulated potential profiles presented in Figure 3.4. Indeed, in the case of a species adsorbed at the interface, like BSPBPy, the effective part of the potential applied between the reagents is smaller than the total potential difference. Thus, a polarisation larger than the formal potential is necessary to observe an neat electron transfer. Another remarkable difference between the two systems is the much larger peak separation at the LLI. Indeed, the back electron transfer is only visible between 100 mV and 200 mV, depending on the scan rate. This observation suggests that the back transfer is impeded at positive polarisations. This can be explained by the the interface structure presented in Chapter 3. Indeed, Figure 3.5 shows that at large polarisations, only one type of ion is present at the interface, *i.e.* the counter-ions concentration is very low. Thus, when transposed to the electron transfer between BSPBPy and DMFc, since TB^- is in excess at positive polarisations, one can conclude that $DMFc^+$ is repealed from the interface, preventing therefore any recombination with $BSPBPy^-$. Thus, the back transfer is only possible when the excess ion surface concentration is low, *i.e.* at low polarisations.

The prevention of the back electron transfer can be emphasized by working with a more reversible donor/acceptor couple: $Fe(CN)_6^{3-}$/DMRc. This system is not ideal for an ITIES since the electron acceptor is charged and is therefore subject to polarisation dependent concentrations. Nevertheless, these two couples are standard in electrochemistry and reversible

compared to the more versatile BSPBPy. Figure 4.5 shows cyclic voltammetries of $Fe(CN)_6^{3-}/Fe(CN)_6^{4-}$ in water at various concentration ratio, and DMRc in DCE, in direct contact or in ECSOW configuration. The aqueous supporting electrolyte in both cases is LiOH 10 mM in order to avoid hydrogen evolution from DMRc[156, 157]. The redox potential of the couple $Fe(CN)_6^{3-}/Fe(CN)_6^{4-}$ in these conditions is 412 mV_{she} while that of DMRc in DCE has been reported to be 750 mV_{she}[156]. Thus, the oxidation of DMRc by $Fe(CN)_6^{3-}$ requires an over-potential of at least 338 mV to proceed, *i.e.* the reaction is not spontaneous and needs a positive polarisation. Consequently, as expected, only a small faradaic current is observed in Figure 4.5 at the positive side of the polarisation window with only an equimolar ratio of $Fe(CN)_6^{3-}$ and $Fe(CN)_6^{4-}$. However, when the concentration of oxidant is increased by one decade – which, according to Nernst equation, implies that the redox potential is 59 mV more positive – a clear current is visible at positive polarisation and a small back transfer peak is visible in the middle of the potential window. If the oxidant concentration is further increased, the electron transfer current clearly dominates the ion transfer current. Here, alike the BSPBPy/DMFc couple, the peak separation at the ITIES is large compared to that of the ECSOW, roughly 350 mV *vs.* 150 mV. However, since the two redox couples are reversible, the shift of the electron back-transfer peak cannot be ascribed to a slow kinetics. This observation thus supports the hypothesis that the excess ions prevent the reverse electron transfer reaction. This point is discussed in the next section.

4.3 Ions energy profile at the ITIES

This section introduces a simple model explaining the depletion of the non-polarising ions at the interface and presents preliminary results of molecular mechanics simulations that supports this model.

A important difference between a polarised electrode and a polarised ITIES is that, in the later case, the polarisation is carried by the ions and not by electrons in a solid conductor. Thus, in potentiostatic conditions, the ionic population of the interface must remain constant. This necessarily leads to counter-ion exclusion at the interface. This situation is schematically presented in Scheme 4.6. The mechanism is divided in three steps, for clarity, but the overall process is continuous. The situation

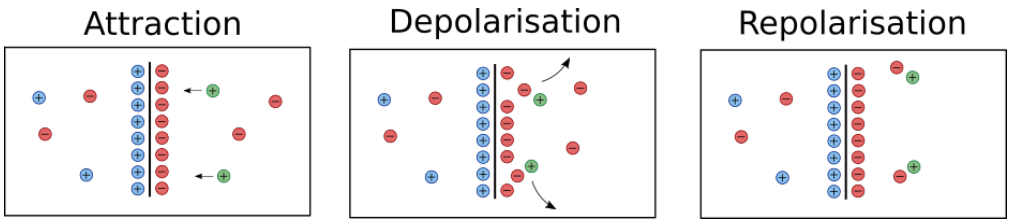

Figure 4.6: *Schematic representation of the mechanism of ion repulsion at the ITIES. The supporting electrolyte ions are represented in red and blue while the redox active ion is represented in green.*

at the left of Figure 4.6 shows the electrostatic interaction between the ion layer and the counter-ions in solution. Here, the polarised interface can be seen as a dipole layer, therefore, the corresponding electrostatic potential has a shorter range than that of a point charge. If a counter-ion comes close enough to the interface, it is possible that it forms an ion pair with one of the polarising ions. Then, either the pair is unstable and the counter-ion returns in the bulk phase, either it is stable and the pair leaves the interface. In the former case, nothing changed from the initial situation. However, in the later case, the interface polarisation is changed by the departure of a polarising ion. Nevertheless, since the system operates in potentiostatic conditions, the ion that left the interface will be replaced by a anion from the bulk. This process however has an energy cost since an interfacacial pair is broken. Overall, the equilibrium situation is a balance between the attraction from the dipole layer and the necessity to maintain the interface polarisation. Therefore, we suggest that this leads to the slight counter-ion concentration bump visible in Figure 3.5 behind the polarising ion layer. Furthermore, this phenomenon also explains the lack of electron back transfer presented in the previous section. Indeed, in Figure 4.6, the positive ion appears as "repelled" from the interface.

In order to confirm the theory presented above, we simulated by umbrella sampling the free energy profile of the transfer of tetraethylammonium (TEA) at polarised the water/DCE interface. The results are presented in Figure 4.7. The supporting electrolytes are LiCl ∼200 mM in water and BATB ∼100 mM in the organic phase. The polarisation was imposed by a charge difference of 2 charges. In Figure 4.7, it appears that the energy profile of TEA is not monotonic. Starting from the bulk of the aqueous phase, the ion first faces an energy barrier of $\sim$ 5 kJ·mol^{-1} due to the

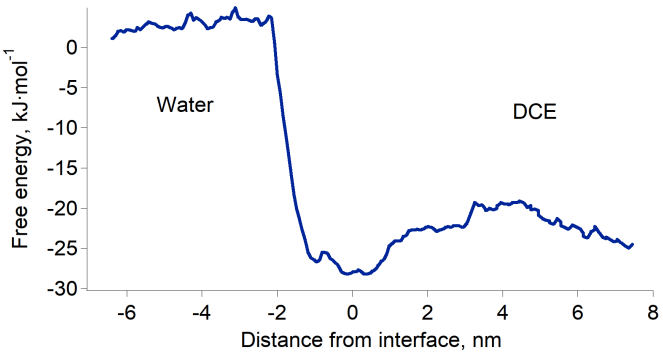

Figure 4.7: *Potential of mean force of the tetramethylammonium ion at the polarised waterDCE interface. Supporting electrolytes: LiCl 200 mM, BATB 100 mM. Charge difference: 2.*

repulsion of the Li^+ ion layer. Then, the ion energy is significantly lowered by formation of a pair with TB^-. This configuration is the global minimum of the simulation and reflects the favourable electrostatic interaction as well as the greater stability of the TEATB pair with respect to LiTB. Interestingly, as already reported in Chapter 3, since the organic ions protrude in the aqueous phase, the minimum of the interaction is located before the organic phase. Finally, as the TEA cation progresses deeper in the organic phase, it faces a second energy barrier corresponding to the breaking of the TEATB pair and solvation of TEA in the bulk.

The simulations results presented in Figure 4.7 are preliminary and requires confirmation with other potential differences, ions and supporting electrolyte concentrations. Unfortunately, such simulations, especially at low electrolytes concentrations, are time consuming, if not technically impossible. Nevertheless, similar energy profiles have already been proposed by Schmickler [39, 67], with however a much simpler description. This, nevertheless, supports the results presented here. However, this model, was only concerned with the energy profile of an ion crossing the interface and did not describe the equilibrium configuration of the polarised ITIES.

4.4 Conclusion

This chapter discussed experimentally and with simulations the consequences of the ITIES structure presented in Chapter 3 on charge transfer

phenomenon at soft interfaces. Thus, it was shown that intermolecular potential dependent electron transfer could be indeed measured at the LLI. An interesting implication of this observation – often overlooked in dedicated publication – is that this is formally a novel approach to control the reactivity of molecular species. Indeed, on the two paradigms controlling a chemical reactions – kinetics and thermodynamics – chemists can only act on the kinetics by helping the reagent passing activation energy barriers by, for instance, thermal activation, photo-excitation, ultra-sonication, etc. Nevertheless, in electrochemistry, the thermodynamic equilibrium and the kinetics of a reaction can be controlled. This, however, requires the intermediation of a solid electrode between the reagents. Thus, the results presented here demonstrate that the polarised ITIES can be used to observe a direct intermolecular electron transfer and to control the thermodynamic and kinetic of the reaction.

Chapter 5

Anomalous reaction kinetics at the liquid-liquid interface

This chapter presents a reaction that takes place in the plan of the interface and not at the interface, as was the case in the previous chapter. Here, we study the kinetics of a diffusion-controlled Triplet-Triplet Annihilation (TTA) reaction between zinc porphyrins adsorbed at the LLI by TRSHG. The decays show that the excited triplet population half-life at the interface is four orders of magnitude shorter than in the bulk at similar concentrations. This behaviour is due to the adsorption of the molecules at the interface that locally increases their density. The close packing of the molecules has two opposing effects: it favours the TTA pathway between neighbour molecules, but at the same time, hinders the diffusion of the molecules and consequently lowers the reaction kinetics. The reaction is then further studied by molecular mechanics simulations on similar time-scales. We thus observe that at low surface concentrations, the two-dimensional diffusion is normal and the kinetics can be described with the Smoluchowksi diffusion-reaction equation adapted to two-dimensional systems. However, at high surface concentrations, because the viscoelasticity of the interface changes, the kinetics becomes anomalous and the motion of the reagents is described by the FLE.

5.1 Introduction

Following the very early work of Benjamin Franklin, studying the spreading of a spoon of oil on water, Lord Rayleigh was able to show that this spreading forms a molecular film and from simple geometric considerations was able to measure the thickness of a molecule. Pockels[158] and later Langmuir[159] improved the methodology to study molecules on a planar soft interface. So, if purely two dimensional monolayer molecular films have been observed for more than a century, very few studies have been concerned with reaction kinetics within these monolayers, and were often limited to unimolecular reactions [160, 161].

As seen in Chapters3 and 4, the LLI is a medium with physical properties that significantly differ from that of the two bulk phases. It has been shown, for instance, that in such systems the polarity of the interface is the average of that of the two liquids [107, 108, 162] and that it changes on a subnanometer length scale across the interface[109]. Likewise, the viscosity of the interface is different from that of the contacting solvents, which leads, for example, to peculiar non radiative de-excitation pathways of adsorbed malachite green molecules [116]. The reduced dimensionality of the interface is another difference when compared to the bulk solutions. The consequences of the dimensionality on the way a particle trapped at an interface can explore its surrounding space are commonly treated using random walks (see 2.2). One of the well-known results of this approach is that two-dimensional walks are recurrent while higher dimensional walks are transient. Such models, applied to simulated chemical reactions, have shown surprising dimension-dependent kinetics, with consequences on the survival probability over time of the reacting particles[163, 164], as well as segregation effects of the reagents [165–167]. Consequently, the experimental study of diffusion-influenced chemical reactions occuring within the plane of soft surfaces requires a dedicated approach. Section 2.2 presented some specific models designed to treat such systems. It was shown that compared to three-dimensional cases, two-dimensional rate constants – or coefficient, as they are no longer constant[168] – never reach an asymptotic value, implying that the reactions do not formally attain a steady state [130, 133, 168, 169]. As demonstrated by Bénichou *et al.*, many diffusion schemes actually belong to a same universality class[170], and an important parameter to classify the diffusion processes is the compact

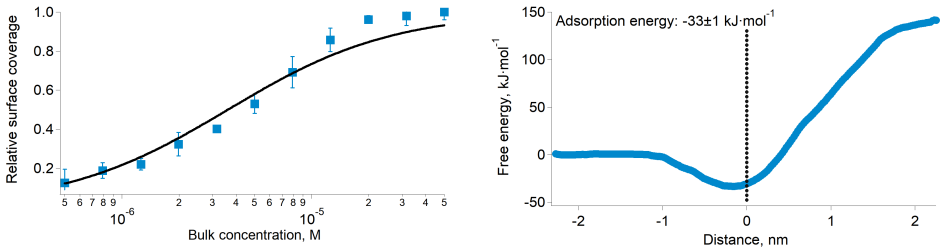

***Figure 5.1: Left**: ZnTMPyP surface coverage measured by TRSHG as function of bulk concentration. The data have been fitted assuming a Langmuir isotherm. Adsorption energy: -31 ± 0.3 kJ·mol^{-1} **Right:** Free energy profile of the transfer of ZnTMPyP from the aqueous phase to the organic phase simulated by molecular mechanics. Adsorption energy: -33 ± 1 kJ·mol^{-1}*

versus non-compact exploration schemes. These schemes depend on the dimensions of the walk and of that of the surrounding medium. Such peculiar reactions are not only interesting at the fundamental level but have also practical applications for chemical reactions taking place in biological membranes[171–173]. However, there are only a few examples where this formalism has been applied to two-dimensional media[174–176], and these examples measured reaction kinetics in modified lipid films which, although more similar to biological systems, are not truly two-dimensional as the motion of the probes are, to some extent, independent of the lipid motion.

5.2 System characterisation

Surface concentration

Relative surface coverage

Figure 5.1 shows the surface concentration of ZnTMPyP as a function of the bulk concentration measured by surface second harmonic generation. The concentration was determined as follows. A custom cell of ~ 20 cm^3 was filled with 6.5 cm^3 of TFT and 6.5 cm^3 of water. Then, the concentration of ZnTMPyP was varied by addition of the appropriate volume of a 100 µM solution of ZnTMPyP. For each concentration, the intensity of the second harmonic signal of an incoming 880 nm pulse, resonant with the Soret band of ZnTMPyP, was measured during 20 minutes (average over

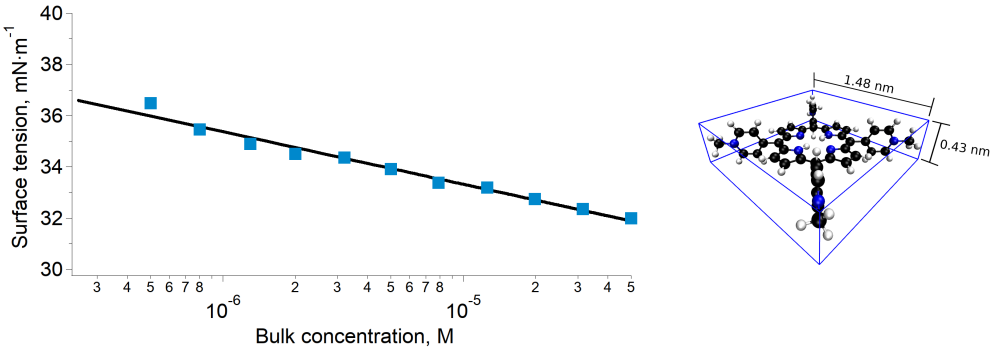

***Figure 5.2: Left**: water/TFT surface tension measured by the pendant drop method as function of the ZnTMPyP bulk concentration. The data have been fitted assuming a Langmuir isotherm. Area per molecule at full surface covergage: 4.6 nm^2. **Right:** dimensions of a box containing ZnTMPyP. The box edges stop exactly at the atomic positions, therefore, taking account of the van der Waals radii, the molecule is slightly larger.*

$6{\cdot}10^4$ pulses) after $\sim$ 1 h of equilibration, increasing the concentration from 500 nM to 50 µM. This procedure was repeated five times. The data where then fitted assuming a Langmuir isotherm:

$$\frac{\Gamma(c)}{\Gamma_{max}} = \frac{c\beta}{1 + c\beta} \tag{5.1}$$

where $\Gamma(c)$ is the surface concentration of ZnTMPyP, Γ_{max} the maximum surface concentration, c the bulk concentration and β the Langmuir parameter. Fitting the data with a Frumkin isotherm did not improve the quality of the fit and the interfaction paremtre was close to zero, which implies that the interaction between the adsorbed molecules is weak. The value found for the adsorption Gibbs free energy is $-31.0{\pm}0.3$ kJ·mol^{-1}, which indicates a strong affinity of the porphyrin for the interface. This value is in concordance with that obtained by molecular dynamics, $-33{\pm}1$ kJ·mol^{-1}, as well as with previously published values [110]. Using the experimental results, the surface coverage of ZnTMPyP at bulk concentrations used in this chapter, 500 nM, 5 µM and 50 µM, is estimated to be 12±1%, 58±1% and 93±1%.

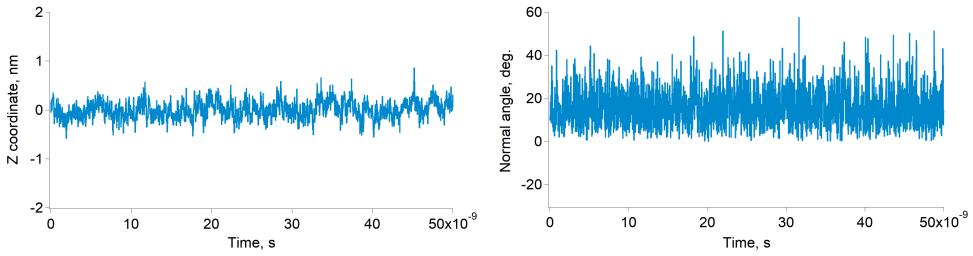

Figure 5.3: ***Left****: Z-coordinate of ZnTMPyP over time and* ***Right****: tilt angle of ZnTMPyP over time simulated by molecular mechanics*

Maximum surface concentration

The data presented in Figure5.1 only allow determination of the relative surface coverage, but not the absolute surface concentration. Thus, the maximum surface concentration was obtained by measuring the surface tension of the water/TFT interface as a function of the bulk concentration of ZnTMPyP by the pendant drop method [177]. As in the case of the isotherms, the concentration of ZnTMPyP was varied by addition of the appropriate volume of a 100 μM solution of ZnTMPyP. The values were reported after $\sim$ 1 h of equilibration. The data have been fitted using the Gibbs adsorption equation, assuming again a Langmuir isotherm. The results are presented in Figure 5.2. Thus, the maximum surface coverage was found to be $3.6{\cdot}10^{-7}$ mol·m^{-2}, which implies a molecular surface of $\sim$4.6 nm^2, in good concordance with the approximate size of ZnTMPyP, *i.e.* a square of 1.5 nm sides (Figure 5.2 right). Consequently, at full surface coverage, the adsorbed molecules form a closely packed film.

Porphyrin orientation at the LLI

Molecular mechanics simulations allow to easily measure the position and orientation of the simulated molecules over time. Figure 5.3 left shows the coordinate perpendicular to the interface (z-axis) of the centres of mass of the pophyrins over time. The standard deviation is 180 pm, meaning that the molecules are indeed segregated in a two dimensional environment, altough the interfacial capillary waves tends to roughen the surface on a larger scale [19]. Figure 5.3 right shows that the molecules are slightly tilted at the interface, with an average normal angle of $16° \pm 8°$, in agreement with the previously reported value [110]. Assuming an extreme value of 24°

and a length of 1.5 nm for the porphyrin, the z-coordinates of the highest and lowest atoms is 0.6 nm. Thus, adding the fluctuations of the centre of mass and that due to the tilting, the total variation of the z-coordinates is of the order of 0.8 nm.

Photophysical properties of ZnTMPyP

Ground state properties

Figure 5.4 (top left) shows the visible absorption spectrum of ZnTMPyP. This spectrum is typical of that of metaloporphyrins, with a strong absorption band – the Soret band – situated around 450 nm, and two lower intensity absorption band – the Q bands – around 650 nm. The presence of two well separated absorption regions simplify the TRSHG studies of these molecules. Indeed, their concentration can be probed using the Soret, while the Q bands can be used for excitation. Thus, their is a large wavelength difference between the pump and the probe beams, which avoid detector saturation. Figure 5.4 (top right) shows the SHG spectrum of ZnTMPyP. As expected, since the SHG signal is resonant with the Soret transition, the SHG spectrum is similar to the visible absorption spectrum.

Triplet state properties

Figure 5.4 (bottom left) shows the time evolution of the optical density at 440 nm of a 2.5μM solution of ZnTMPyP after excitation at 565 nm, under N_2 atmosphere. The ground state recovery can be well fitted by a simple exponential whose time-constant is 261.0±0.3 s^{-1}, thus the first triplet lifetime is 3.831±0.004 ms. Figure 5.4 (bottom right) shows the transient absorption spectrum of ZnTMPyP 100 ns after excitation at 565 nm. This spectrum shows a bleaching of the Soret band and the apparition of a distinct, weaker, absorption band at 476 nm. Thus, in principle, it is possible to separately follow the time evolution of the triplet and ground states.

5.3 Triplet states lifetimes at the LLI

The left column of Figure 5.5 shows the second harmonic intensity of a 880 nm pulse – resonant with the Soret band of ZnTMPyP – as a

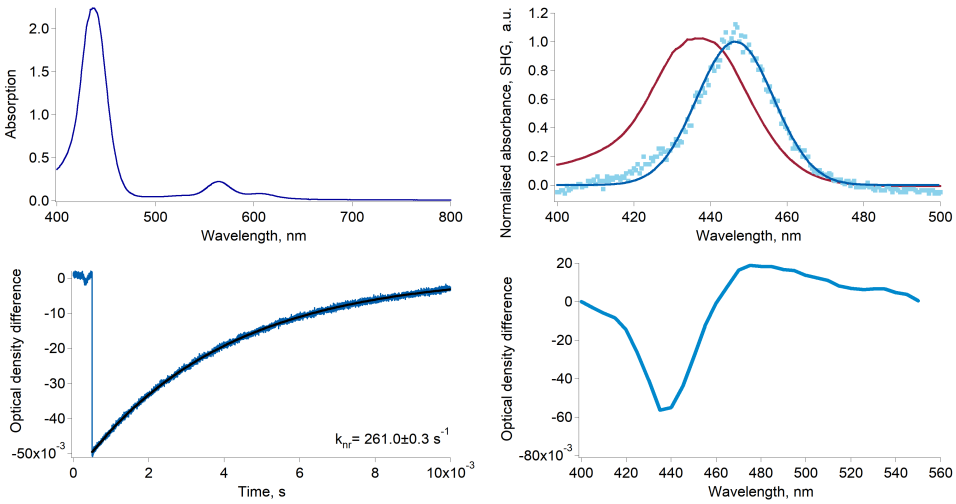

Figure 5.4: Top left: *UV-vis absorption spectrum of ZnTMPyP, 20 µM in water.* ***Top right:*** *normalised SHG spectrum of ZnTMPyP at the water/TFT interface compared to the UV-vis spectrum.* ***Bottom left:*** *Transient absorption at 440 nm of ZnTMPyP 2.5 µM in water, after excitation at 565 nm.* ***Bottom right:*** *Transient absorption spectrum of ZnTMPyP 100 ns after excitation at 565 nm, 2.5 µM in water.*

function of the time delay with the excitation pulse at 565 nm, at various surface concentrations and excitation intensities. No second harmonic signal specific to the triplet state of ZnTMPyP was observed in the experimental conditions by varying the probe wavelength from 400 nm to 500 nm. Thus, the decays presented in Figure 5.5 correspond to the repopulation of the ground state and therefore, the depletion is directly proportional to the concentration of the triplet excited state. The triplet concentration was controlled by varying the excitation intensity. It has to be noted that the excitation pulse actually populates the first excited singlet, however, due to the high intersystem crossing quantum yield of this porphyrin (90%)[178], and because this phenomenon is fast, only the lowest triplet can be detected in the time scale of this experiment.

The traces presented in Figure 5.5 show that the half-life of ZnTMPyP* (triplet state of ZnTMPyP) at the liquid-liquid interface is of the order of hundreds of nanoseconds to few microseconds. These half-lives are short compared to values in the bulk at similar concentrations (see Figure5.4 bottom left), indicating that the interface is remarkably different. Experiments conducted at the water/DCE or water/dichloromethane interfaces

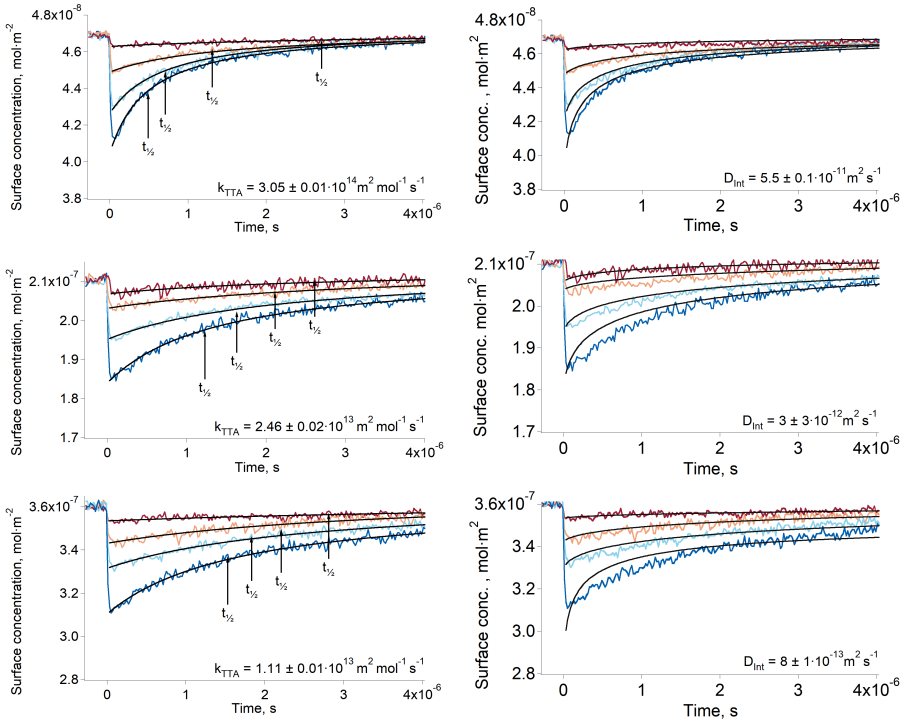

Figure 5.5: *Ground state recovery of ZnTMPyP after excitation at 565 nm at various intensities (from brown to blue: ∼125 nJ, ∼250 nJ, ∼500 nJ, ∼1µJ) under N_2 atmosphere. The bulk concentrations are, from top to bottom : 500 nM, 5 µM and 50 µM. The left column data were fitted using equation 5.2 in order to obtain the rate constant, while the right column data where fitted using the model of Razi-Naqvi [130] and Owen [131] in order to obtain the diffusion coefficients.*

produced identical results, meaning that the solvent is not responsible for the fast decay. Another explanation of a shorter half-life could be aggregation of the porphyrin. Indeed, if dimerisation of ZnTMPyP occured at the interface, one could observe the decay of a supramolecular assembly instead of that of ZnTMPyP*. For instance, Nagatani *et al.* observed a red shift of the second harmonic spectrum of ZnTMPyP, which was tentatively explained as J-aggregation[110]. However, the spectra that we measured could be fitted with only one Gaussian peak, implying that there is no aggregation.

The arrows on the traces presented in the left column of Figure 5.5 show the actual half-lives of the excited porphyrin populations. It can be seen that these times are inversely proportional to the initial triplet

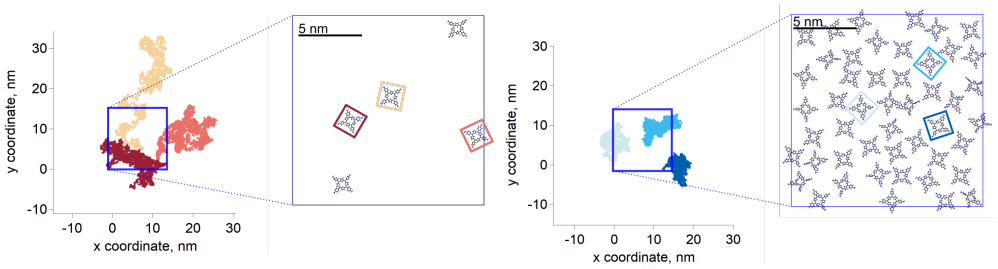

Figure 5.6: Illustration of the interface population and dynamics. *Examples of trajectories and corresponding interfacial population from the molecular mechanics simulations at 10 percent* ***left*** *and 100 percent* ***right*** *surface coverage. At high concentration the molecules explore a smaller part of the interface. The blue squares show the limits of the simulation box, solvent molecules and counter ions have been removed for clarity. The trajectories are plotted without periodic boundary conditions.*

concentrations, which were controlled by varying the excitation intensities. Such a behaviour is typical of a second order reaction. Indeed, the kinetics of the TTA can be described by the following equation:

$$\frac{dT^*}{dt} = -k \cdot T^{*2} \Rightarrow T^*(t) = \frac{T_0^*}{1 + k \cdot T_0^* \cdot t} \tag{5.2}$$

where $T^*(t)$ is the concentration of porphyrins in the triplet state at time t, T_0^* the triplet concentration at $t = 0$ and k is the TTA rate constant. Thus, the half-life is: $t_{1/2} = (k \cdot T_0^*)^{-1}$. The fact that the kinetics traces presented in Figure 5.5 follow this trend further support the conclusion that the phenomenon responsible for the shorter lifetime at the interface is indeed TTA. Because of the time resolution of our setup (∼20 ns), any events taking place on and below this time scale cannot be probed. However, it is consistent with the TTA mechanism to suppose that all the excited porphyrins in close contact annihilate in the first tens of nanoseconds, leaving only a population of triplets too separated to react and whose reactivity is therefore limited by mass transport. Figure 5.6 presents pictures of the simulated systems at 10 percent (left) and 100 percent (right) surface coverages, as well as typical trajectories of the adsorbed molecules. These graphs illustrate the change of surface compactness with the bulk concentration and its influence on the diffusion. Indeed, at full coverage the trajectories are more hindered and compact, implying a less

efficient exploration of the interface. By contrast, at low surface coverage, the molecules explore a larger portion of the interface.

5.4 Fitting of the spectroscopic results

In a first approach, the rate constant of the TTA at the liquid-liquid interface can be obtained by fitting the results presented in Figure 5.5 with equation 5.2. The first-order decay can be neglected as its time scale is four orders of magnitude longer than that of the experiment. The rate constants thus obtained are presented in Table 5.1. It appears that the TTA rate constant is smaller at higher porphyrin concentrations, when the interface coverage increases. This observation suggests that the surface compactness changes the kinetics of the reaction. Such an effect of the compactness of the reaction medium on the kinetics has already been observed in the bulk, both experimentally and theoretically for biologically relevant systems [179, 180], introducing the concept of geometry-controlled kinetics[170]. In such systems, the large concentration of macromolecules or the presence of obstacles are thought to impede the diffusion of the reacting species, leading to anomalous diffusion and impacting therefore on the kinetics of the reactions. The hypothesis made in the present report is that at high surface coverages the adsorbed molecules in their ground state act as obstacles to the diffusion of the excited triplets, limiting their diffusion and therefore the triplet-triplet annihilation. We propose to rationalise the change of kinetics with the crowding of the interface by extracting the

Table 5.1: Triplet-triplet annihilation rate constant and diffusion coefficient. *The TTA rate constants have been obtained by fitting of the data with the equation 5.2, while for the diffusion coefficients the equations 5.2 and 5.3 were used. At high surface coverage the experimental diffusion coefficients are no longer in agreement with the simulated values. k_{TTA} (10^{13} $m^2 \cdot mol^{-1} \cdot s^{-1}$), D ($10^{-11}$ $m^2 \cdot s^{-1}$)*

C_{Int}	500 nM	5 µM	50µM
k_{TTA}	30.5±0.1	2.46±0.02	1.11±0.01
D_{Int}	5.5±0.1	0.3±0.3	0.08±0.01
D_{Sim}	24±6	23±2	18±2

lateral diffusion coefficients of ZnTMPyP from the kinetic traces and by simulating the diffusion of the porphyrin at the liquid-liquid interface by molecular dynamics.

As independently demonstrated by Razi-Naqvi[130] and Owen[131], due to the two-dimensional nature of the interface between the organic and aqueous phases, conventional diffusion-influenced quenching equations like that of Smoluchowski cannot be directly applied to the present case, as they are derived in spherical coordinates, that is, for three-dimensional systems. The above-mentioned authors have thus developed a model based on the Smoluchowski approach, but derived in cylindrical coordinates, that yields an expression for the apparent time-dependent rate constant of diffusion-controlled reactions. In this model, the time-dependent rate constant is given by :

$$k\left(t\right) = \frac{16DNc_0}{\pi} \int_0^\infty \frac{\exp\left(-tu^2 \frac{D}{R^2}\right) du}{u\left(J_0\left(u\right)^2 + Y_0\left(u\right)^2\right)} \tag{5.3}$$

where D is the diffusion coefficient, R the reaction radius, c_0 the initial concentration of quencher, $J_0(u)$ and $Y_0(u)$ the zero order Bessel functions of the first and second kind and u a dummy integration variable. Here, we use the same expression for the rate constant, but we insert it in the differential equation 5.2. The resulting equation no longer has an analytical solution and therefore, the differential equation and the integral in equation 5.3 were solved numerically in order to make the fitting. In the case of a triplet-triplet annihilation, the quencher concentration, c_0, is replaced by the time dependent concentration, *i.e.* $T^*(t)$. We use value of 1.5 nm for the reaction radius, which is the approximate size of the core of ZnTMPyP, and is consistent with the mechanism of the TTA that involves the transfer of electrons and therefore orbital overlap of the reacting species. The obtained diffusion coefficients are presented in Table 5.1. At low surface concentrations, these values have orders of magnitude that could be expected for such systems and in concordance with the simulated diffusion coefficients. Nevertheless, the two-dimensional model does not appropriately fit the data at large surface coverage, and the resulting diffusion coefficients are far from the simulated values. As this model essentially relies on the resolution of the Fick diffusion equation in two-dimensions, we conclude that the observed discrepancies between the data and the model imply that in such conditions the diffusion of the

species is no longer Fickian, which support the hypothesis of anomalous diffusion.

5.5 Molecular mechanics simulations

As presented is section 2.2, anomalous diffusion is characterised by a non-unity power law scaling of the mean squared displacement of a particle with time [181, 182]:

$$\langle (x_i(t) - x_i(t_0))^2 \rangle = D_i \cdot t^d \tag{5.4}$$

When the exponent of the time variable is less than one, the diffusion regime is said to be sub-diffusive. Figure 5.7 (left) shows the time-averaged ensemble-averaged mean squared displacements (teMSD) of the porphyrin simulated by molecular dynamics over 150 ns at 10 percent and 100 percent surface coverages. These results show that the diffusion of the porphyrins at full surface coverage scales like $t^{0.8}$ in the first tens of nanoseconds, while at longer times the system recovers a linear scaling. In contrast, the dependence is always linear at low surface coverage. Thus, the transport regime becomes sub-diffusive as the surface concentration of adsorbed porphyrins increases. Although anomalous diffusion is observed only in the time scale of few tens of nanoseconds, this still has consequences at every moments of the reaction because the transient regime is independent of the starting time of the experiment. Indeed, the first tens of nanoseconds of transport are abnormal independently of the absolute starting time of the observation. Thus, the overall reaction and equilibrium properties of a system can be affected by a transient anomalous regime [183]. Furthermore, it can be seen that the mean squared displacement of a porphyrin after $\sim$30 ns is $\sim$20 nm^2, which means a displacement of $\sim$4.5 nm. Such diffusion distances still allow triplets to react even at low surface concentrations, implying that indeed, the sub-diffusion regime impacts on the kinetics of the tails of the traces presented in Figure 5.5.

There are different mechanisms underlying a sub-diffusive regime, like diffusion in fractal environments [168] or in crowded or obstructed media [165]. The latter mechanisms are usually treated using the continuous time random walk (CTRW) or the fractional Brownian motion (FBM) formalisms[167]. One of the main consequences of the CTRW model is the weak ergodicity breaking, that is that the time and ensemble averages of

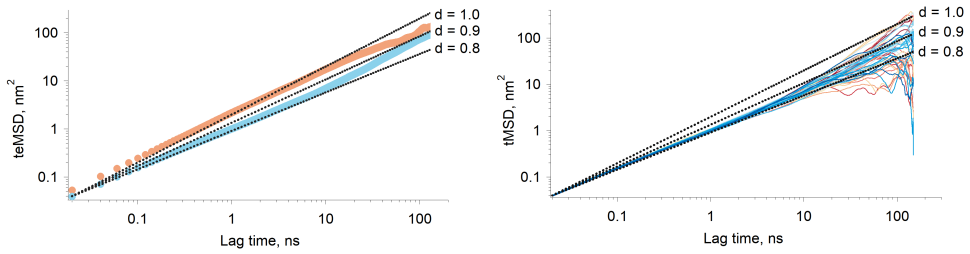

Figure 5.7: Results of simulated interfacial diffusion. Left: *Time-averaged ensemble-average mean square displacement of the porphyrin simulated over 150 ns at 10 percent coverage (brown) and full coverage (blue). The black lines indicate scaling proportional to $t^{0.8}$, $t^{0.9}$ and t.* ***Right:*** *Individual time-averaged mean squared displacement of the porphyrin at full surface coverage. The black lines indicate scaling proportional to $t^{0.8}$, $t^{0.9}$ and t.*

thermodynamic quantities are no longer identical[184]. Simulations of lipid bilayers have shown however that such systems were better described by fractional FLE because these systems were found to be ergodic [125]. Figure 5.7 (right) shows the time-averaged mean squared displacement (tMSD) of the individual porphyrins adsorbed at the liquid-liquid interface at full surface coverage. It appears that the sublinear scaling of the teMSD is also observed with the tMSD. This proves that there is no ergodicity breaking and that alike lipid bilayers, the system is governed by FLE dynamics. This conclusion is also supported by the calculation of the displacement autocorrelation function (Figure 5.8, left) which again corresponds to what can be expected from FLE dynamics [125]. A sub-diffusive motion described by a FLE suggests the presence of a memory effect in the motion of the particles. Thus, it appears that as the interfacial concentration increases, the displacements of the porphyrins become correlated in time, impacting therefore on their reactivity.

5.6 Simple model of anomalous reaction-diffusion

Different models have been derived to analyse the diffusion controlled reactions using the formalism of CTRW or FBM [185–188], giving interesting theoretical insights into these mechanisms. Nevertheless, these models are most of the time too involved to be applied to experimental data. Thus,

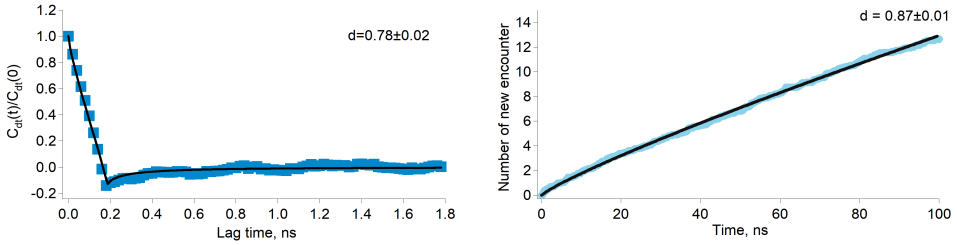

Figure 5.8: Left: *displacement autocorrelation function calculated according to Jeon et al.[125]. The result is consistent with a FLE dynamics as shown by the fitting. The time interval was set to 200 ps.* ***Right:*** *simulated average number of new encounter for a poprhyrin at full surface coverage as a function of time. The black line is a fitting with a power law.*

in order to relate the simulated and experimental results, we decided to estimate the triplet collision frequency from the simulations and to compare it to the experimental data. Then, using the collision theory, we relate this quantity to the reaction rate constant. Indeed, the collision theory states that the rate constant is proportional to the collision frequency:

$$k \propto Z \tag{5.5}$$

where k is the rate constant and Z the collision frequency. Thus, the time dependence of k is directly proportional to that of Z.

Figure 5.8 (right) shows the average number of new molecules that a porphyrin (ground state *and* triplet) encounters over time, for a full surface coverage (the data were truncated at 100 ns in order to limit finite size effects). The number of new molecules was calculated from the trajectories of the simulations. This quantity represents the total number of porphyrins that came in the neighbourhood of one peculiar porphyrin at a time t. However, one molecule cannot be counted two times. The "neighbourhood" being arbitrarily defined by a certain radius. In the present case this radius was set to 1.5 nm, as it is the approximate size of the porphyrin core. The calculation is done as follow. At t_0 and for one porphyrin, the number of neighbours is listed. Then, as the simulation proceeds, the neighbours list is updated each time the porphyrin comes closer than 1.5 nm from the center of mass of another porphyrin that is not already in the list. At the end of the simulation, the number of elements in the list gives the new encounter number. This number is then averaged over all the porphyrins. Once the new encounter number is known, the reaction rate over the first 100 ns can

be estimated by multiplying it by the square of the surface concentration of triplets in the considered time slice. For instance, in the first 100 ns of reaction at full surface coverage, 15 % of the molecules are triplets, the new encounter number will thus be multiplied by 0.0225. The obtained value is the number of reaction events on a surface of 225 nm^2 in 100 ns. It must then be converted to $mol \cdot m^{-2}$ by simple arithmetic operations.

Interestingly, the number of new encounter is proportional to $t^{0.87}$, which is consistent with the sub-diffusion observed in the simulation and experimental results. The time derivative of the new encounter number is the new encounter frequency and is proportional to $t^{-0.13}$. This quantity is the average number of new porphyrins that come in close contact per unit time (here porphyrin means triplet *and* ground state). The probabilities that the contacting molecule and the considered porphyrins are both triplets is also proportional to the triplet relative concentration. Furthermore, two triplets T^* that encounter will react. Thus, if one calls the new encounter frequency f, the number of reaction events per unit time, that is the reaction rate, will be:

$$rate = f \cdot T^{*2} \tag{5.6}$$

Identifying this equation with equation 5.2 shows that there is a direct equivalence between the rate constant and the new encounter frequency. Thus, as this latter quantity scales proportionally to $t^{-0.13}$, the rate coefficient should scale similarly (from equation 5.5). The validity of this approach is confirmed by fitting the full surface coverage decays with the phenomenological reaction rate equation on fractals[167, 168]:

$$\frac{dT^*(t)}{dt} = -k_0 \cdot t^{-h} \cdot T^*(t)^2 \tag{5.7}$$

Doing so gives a value of 0.13 ± 0.01 for the h parameter, in excellent agreement with the simulated value. Thus, we show that the effects of the complex physics underlying anomalous diffusion can be recovered in a more intuitive expression that provides a phenomenological description of a reaction presenting anomalous kinetics.

To conclude, we report the first experimental observation of a diffusion-controlled triplet-triplet annihilation reaction in a soft planar environment, and the appearance of an anomalous diffusion regime at high surface converge. This phenomenon is a unique example of a truly diffusion-controlled two-dimensional bimolecular chemical reaction and presents

the property of having kinetics that depends on the compactness of the adsorbed molecular layer. At low surface concentrations, the diffusion is Brownian and the reaction can be described with a two-dimensional Smoluchowski model. However, as the concentration increases, the diffusion becomes anomalous and follows a fractional Langevin equation motion. Consequently, the Smoluchowski model fails to adequately account for the experimental results. This behaviour shows similarities with the motion of lipids in biological membranes, and suggests that the anomalous diffusion of these species originates from their high density rather than from a motion in a low-dimensional medium. With the help of molecular mechanics simulations, we have shown that, under simple assumptions, the rate of the TTA could be related to the triplet encounter frequency. This work is an experimental realisation of models usually verified by simulations and opens the way to the exploration of others kinetic schemes, involving for instance macromolecular crowding or obstructed diffusion.

5.7 Computational details

The molecular mechanics simulations were all carried out using GROMACS 2018.1. [189–195]

Topologies.

In order to simplify the topology, the porphyrin that was simulated was the free base TMPyP instead of the metallated ZnTMPyP (the one that is used in the experiments). We believe that this has no influence on the diffusion properties of the molecule.

The charges of the porphyrin core were taken from the coresponding atoms of the OPLS force field, while the charges of the four methylpyridinium ligands were taken from Sambasivarao *et al.*[196]. Doing so, the total charge of the molecule is only 3.32. Thus, the missing charge was evenly dispatched on all the atoms of TMPyP (0.008 charge per atom) in order to reach a total charge of 4. Finally, the polarisation effects at the interface were effectively taken into account by rescaling all the charges of the porphyrin by 0.75 (and counter ions, *i.e.* chloride ion), as suggested by Leontyev and Stuchebrukhov [197, 198]. This method provides reliable adsorption behaviour of charged species at liquid-liquid interfaces [141]. All the bonded parameters were those of the OPLS force field.

The water was simulated using the TIP4P model. The TFT molecules and

chloride ions were simulated with the parameters of the OPLS force field.

Box construction and simulation.

The simulated systems consisted in a 15 nm by 15 nm by 7 nm boxes divided in two phases of equal volumes. Periodic boundary conditions were used in all directions. The porphyrins molecules were directly added at the interface. The total charge of the system was neutralised by addition of four times more chloride atoms than porphyrins molecules. Once constructed, the energy of the boxes was minimised using the steepest descent algorithm until a force threshold of 100 $kJ{\cdot}mol^{-1}{\cdot}nm^{-1}$ was reached. Then, the system was equilibrated for 1 ns, with a time step of 1 fs, in the NVT ensemble using the V-rescale thermostat [84] at 293 K. Finally, the production simulations were carried out in the NPT ensemble, using the V-rescale thermostat and the Berendsen barostat [82] at a temperature of 293 K and pressure of 1 bar, using a time step of 2 fs. During the simulations the LINCS algorithm [199] was used to constrain all the bonds.

Adsorption energy.

The adsorption energy of the porphyrin was simulated by constructing by umbrella sampling the potential of mean force required to transfer the molecule from the aqueous to the organic phase (see SI). The starting configurations were generated by placing the molecule under study at the centre of a 4 nm by 4 nm by 4 nm box. The molecule was then solvated in TIP4P water and the box was placed in contact with a 4 nm by 4 nm by 8 nm box, filled with TFT molecules, forming an overall 4 nm by 4 nm by 12 nm box. The energy of the system was then minimized using the steepest descent algorithm until a force threshold of 100 $\cdot mol^{-1}{\cdot}nm^{-1}$ was reached. The system was subsequently equilibrated for 1 ns in the NPT ensemble. During the equilibration procedure the molecule under study was constrained at its initial position. After the equilibration, the solute was pulled 4.5 nm across the interface, while being constrained in the directions parallel to the interface, still in the NPT ensemble. Finally, the potential of mean force was reconstructed using the umbrella sampling technique (g_wham[200]) on several configurations of the solute with respect to the interface. The spacing between two configurations was roughly 0.15 nm along the perpendicular to the interface. However, when necessary, additional configurations were included in order to get a sufficient overlap of the configurations histograms. Each umbrella sampling run was performed for 2.5 ns in the NPT ensemble at 293K and 1 bar using a harmonic biasing

force, with a force constant of 2000 $mol^{-1} \cdot nm^{-2}$. In the simulation of the transfer the charges of TMPyP were not scaled by 0.75 as in the diffusion simulation, as this is required only to simulate ions at the interface and not in bulk phases.

Sample preparation an measurements

All time-resolved measurements were done in an air-tight optical cell. The cell was prepared in a glove-box under nitrogen atmosphere (concentration of dioxygen ∼4ppm) and was then placed in an air-tight box equipped with optical windows and kept under a constant nitrogen flux during the measurements. A typical cell was made of 1.5 mL of TFT and 1 mL of aqueous phase containing various concentrations of ZnTMPyP. The cells were prepared at least one hour before the measurements in order to let the interfacial concentration reach its equilibrium value. The temperature of the room was kept constant at 20.1°C.

The traces were obtained by averaging 250 to 500 measurements. One measurement consists in scanning the pump-probe delay from -0.3 µs to 4 µs by steps of 20 ns (215 steps). Each step is an average over 50 pulses (1 s). Thus, one measurement last 4 minutes and consequently getting one trace required 15 to 30 hours. As the second-harmonic intensity depends on the square of the surface concentration of adsorbed species, all the traces presented in this work are the square-root of the measured data.

Conclusion and outlook

The results presented in this thesis have shown how atomistic simulations could be coupled to experimental methods to provide a better understanding of electrochemical reactions at LLI and ITIES. Thus, it was shown that when such interfaces are polarised, the supporting electrolytes form a compact ion double-layer, even at moderate concentrations or voltages. Since all the potential difference drops between the ions, the interface is devoid of diffuse layers. This observation is a significant improvement of the classical picture of the ITIES relying on the GCM. This model, however, was already questioned by several authors over the past decades. One of the consequences of the new picture of the interface is that since the ions responsible for the polarisation lies at the interface, polarisation-dependent properties of the system had to be correlated to interfacial properties of the ions. Thus, we derived a simple model explaining the trends of the capacitance curves of different ITIES by relating them to the standard transfer potential of the supporting electrolytes. The model presents the interface as a plan capacitor therefore the distance between the ions is the only variable of the model, and this distance is the penetration depth of the organic ions into the aqueous phase.

The fact that the totality of the potential difference drops over less than one nanometre at the ITIES naturally leads to the idea that the interface could be used to carry out redox reactions. This is, however, an old debate in electrochemsitry and numerous contradictory publications can be found on this subject. Nevertheless, the originality of our contribution to this topic is that our results are based on a molecular description of the interface that was corroborated with different experimental observations presented in Chapter 3. Thus, we have been able to show a clear heterogeneous electron transfer reaction at the ITIES. Our experimental approach was carefully designed to avoid the flaws reported by the authors who already

cleared the question in the past. These results further supported the conclusions of the chapter dedicated to the structure of the ITIES. Also, we presented preliminary evidences that the interfacial ion layers could significantly impact the kinetics of the heterogeneous electron transfer reaction. This leads to significantly different cyclic voltammetries where a same electrochemical reaction is carried out on the solid electrode or at a soft interface. Thus, this observation further highlights the difference between these two types of interfaces. Finally, the possibility to observe and control a direct intermolecular electron transfer was discussed and presented as a novel way to carry out electrochemical reactions without an electrode.

Molecular mechanics simulations were also applied to the study of diffusion-controlled reactions in two-dimensional media. Here, however, the reaction was not a charge transfer but an energy transfer reaction: triplet-triplet annihilation. Using TRSHG in the microsecond domain, we could measure for the first time the triplet-triplet annihilation kinetics of a zinc porphyrin in a two-dimensional environment. In addition to its low dimensionality, this system presented the interesting property of changing of diffusion regime with the concentration. Indeed, at low surface coverage, the motion of the adsorbed reagents is free and the diffusion is therefore normal. However, as the concentration approaches the saturation limit, the diffusion regime becomes anomalous, *i.e.* the mean square displacement of the porphyrins no longer linearly scales with time. Here, again, we could corroborate the experimental results to simulations performed over a similar time-scale. These results are, to the best of our knowledge, a unique example of a complex chemical kinetic studied both experimentally and by simulations on such a long time-scale.

Overall, this thesis aimed at presenting a coherent picture of liquid-liquid interfaces based on molecular simulations, time-resolved spectroscopy and electrochemistry. The primary objective of this work was to apply TRSHG to the study of photoinduced electron transfer reaction kinetics at soft interfaces. Nevertheless, it turned out that many theoretical and technical difficulties had to be solved before tackling this question. These difficulties were, among others, the need for a precise understanding of the nature of the ITIES as well as a theoretical description of reaction kinetic in two-dimensional media. In this respect, we think that the results presented here bring solutions to these difficulties and offer solid

bases to eventually answer the initial question. Furthermore, because of the obvious similitude between glslli and biological membranes, the conclusions presented in this thesis necessarily imply the questioning of our understanding of charge transfer and potential profiles at such interfaces. We think that our findings constitute an interesting basis for future work in the domain a electrochemistry at soft interfaces.

Bibliography

[1] J. Struwolf, A.L. Barker, M. Gonsalves, D.J. Caruana, P.R. Unwin, D.E. Williams, and J.R.P. Webster. Probing liquid-liquid interfaces using neutron reflection measurements and scanning electrochemical microscopy. *Journal of Electroanalytical Chemistry, 483*, pages 163–173, 1999.

[2] L. Guangming, S. Malkova, S.V. Pingali, D.G. Schultz, B. Lin, M. Meron, T.J. Graber, J. Gebhardt, P. Vanýsek, and M.L. Schlossman. X-ray studies of the interface between two polar liquids: neat and with electrolytes. *Faraday Discussions, 129*, pages 23–34, 2004.

[3] David Michael and Ilan Benjamin. Molecular dynamics simulation of the water—nitrobenzene interface. *Journal of Electroanalytical Chemistry*, 450(2):335 – 345, 1998.

[4] Académie des sciences (France). *Comptes rendus hebdomadaires des séances de l'Académie des sciences: Sciences chimiques. Série C*. Gauthier-Villars., 1968.

[5] Z. Samec, V. Mareček, and J. Weber. Detection of an electron transfer across the interface between two immiscible electrolyte solutions by cyclic voltammetry with four-electrode system. *Journal of Electroanalytical Chemistry and Interfacial Electrochemistry*, 96(2):245 – 247, 1979.

[6] Claude Gavach, Patrick Seta, and Bertrand D'epenoux. The double layer and ion adsorption at the interface between two non miscible solutions: Part i. interfacial tension measurements for the water-nitrobenzene tetraalkylammonium bromide systems. *Journal of Electroanalytical Chemistry and Interfacial Electrochemistry*, 83(2):225 – 235, 1977.

[7] M. Gros, S. Gromb, and C. Gavach. The double layer and ion adsorption at the interface between two non-miscible solutions: Part ii. electrocapillary behaviour of some water-nitrobenzene systems. *Journal of Electroanalytical Chemistry and Interfacial Electrochemistry*, 89(1):29 – 36, 1978.

[8] Patrick Seta, Bertrand d'Epenoux, and Claude Gavach. The double layer and ion adsorption at the interface between two immiscible solutions: Part iii. long chain alkyl-trimethylammonium halides at partition equilibrium

between water and nitrobenzene. *Journal of Electroanalytical Chemistry and Interfacial Electrochemistry*, 95(2):191 – 199, 1979.

[9] Takashi Kakiuchi and Mitsugi Senda. Structure of the electrical double layer at the interface between nitrobenzene solution of tetrabutylammonium tetraphenylborate and aqueous solution of lithium chloride. *Bulletin of the Chemical Society of Japan*, 56(6):1753–1760, 1983.

[10] Z. Samec, V. Mareček, and D. Homolka. The double layer at the interface between two immiscible electrolyte solutions: Part i. capacity of the water/nitrobenzene interface. *Journal of Electroanalytical Chemistry and Interfacial Electrochemistry*, 126(1):121 – 129, 1981.

[11] Zdeněk Samec, Vladimír Mareček, and Daniel Homolka. Double layers at liquid/liquid interfaces. *Faraday Discuss. Chem. Soc.*, 77:197–208, 1984.

[12] H.H. Girault and D.J. Schiffrin. Thermodynamic surface excess of water and ionic solvation at the interface between immiscible liquids. *Journal of Electroanalytical Chemistry and Interfacial Electrochemistry*, 150(1):43 – 49, 1983. Electronic and Molecular Structure of Electrode-Electrolyte Interface.

[13] H.H.J. Girault and D.J. Schiffrin. Thermodynamics of a polarised interface between two immiscible electrolyte solutions. *Journal of Electroanalytical Chemistry and Interfacial Electrochemistry*, 170(1):127 – 141, 1984.

[14] Zdenèk Samec, Vladimír Mareček, and Daniel Homolka. The double layer at the interface between two immiscible electrolyte solutions: Part ii. structure of the water/nitrobenzene interface in the presence of 1:1 and 2:2 electrolytes. *Journal of Electroanalytical Chemistry and Interfacial Electrochemistry*, 187(1):31 – 51, 1985.

[15] Z. Samec, V. Mareček, K. Holub, S. Račinský, and P. Hájková. The double layer at the interface between two immiscible electrolyte solutions: Part iii. capacitance of the water/1,2-dichloroethane interface. *Journal of Electroanalytical Chemistry and Interfacial Electrochemistry*, 225(1):65 – 78, 1987.

[16] C. Melo Pereira, A. Martins, M. Rocha, C. J. Silva, and F. Silva. Differential capacitance of liquid/liquid interfaces: effect of electrolytes present in each phase. *J. Chem. Soc., Faraday Trans.*, 90:143–148, 1994.

[17] C. Melo Pereira, W. Schmickler, F. Silva, and M.J. Sousa. Ion association at liquid—liquid interfaces. *Journal of Electroanalytical Chemistry*, 436(1):9 – 15, 1997.

[18] T. Huber, O. Pecina, and W. Schmickler. The influence of the ions on the capacity of liquid—liquid interfaces. *Journal of Electroanalytical Chemistry*, 467(1):203 – 206, 1999.

[19] Guangming Luo, Sarka Malkova, Jaesung Yoon, David G. Schultz, Binhua

Lin, Mati Meron, Ilan Benjamin, Petr Vanýsek, and Mark L. Schlossman. Ion distributions near a liquid-liquid interface. *Science*, 311(5758):216–218, 2006.

[20] Nouamane Laanait, Jaesung Yoon, Binyang Hou, Petr Vanysek, Mati Meron, Binhua Lin, Guangming Luo, Ilan Benjamin, and Mark L. Schlossman. Communications: Monovalent ion condensation at the electrified liquid/liquid interface. *The Journal of Chemical Physics*, 132(17):171101, 2010.

[21] Nouamane Laanait, Miroslav Mihaylov, Binyang Hou, Hao Yu, Petr Vanýsek, Mati Meron, Binhua Lin, Ilan Benjamin, and Mark L. Schlossman. Tuning ion correlations at an electrified soft interface. *Proceedings of the National Academy of Sciences*, 109(50):20326–20331, 2012.

[22] Binyang Hou, Nouamane Laanait, Hao Yu, Wei Bu, Jaesung Yoon, Binhua Lin, Mati Meron, Guangming Luo, Petr Vanysek, and Mark L. Schlossman. Ion distributions at the water/1,2-dichloroethane interface: Potential of mean force approach to analyzing x-ray reflectivity and interfacial tension measurements. *The Journal of Physical Chemistry B*, 117(17):5365–5378, 2013. PMID: 23551255.

[23] Binyang Hou, Wei Bu, Guangming Luo, Petr Vanýsek, and Mark L. Schlossman. Ion distributions at electrified water-organic interfaces: Pb-pmf calculations and impedance spectroscopy measurements. *Journal of The Electrochemical Society*, 162(12):H890–H897, 2015.

[24] Nouamane Laanait. *Ion Correlations at Electrified Soft Matter Interfaces*. Springer Theses, 2013.

[25] H.H.J. Girault and D.J. Schiffrin. Theory of the kinetics of ion transfer across liquid/liquid interfaces. *Journal of Electroanalytical Chemistry and Interfacial Electrochemistry*, 195(2):213 – 227, 1985.

[26] Zdeněk Samec, Yuri I. Kharkats, and Yuri Ya. Gurevich. Stochastic approach to the ion transfer kinetics across the interface between two immiscible electrolyte solutions comparison with the experimental data. *Journal of Electroanalytical Chemistry and Interfacial Electrochemistry*, 204(1):257 – 266, 1986.

[27] H.H. Girault. The potential dependence of the rate of ion transfer reactions across a liquid/liquid interface. *Journal of Electroanalytical Chemistry and Interfacial Electrochemistry*, 257(1):47 – 55, 1988.

[28] Zdenék Samec, Vladimír Mareček, and Daniel Homolka. Charge transfer between two immiscible electrolyte solutions: Part ix. kinetics of the transfer of choline and acetylcholine cations across the water/nitrobenzene interface. *Journal of Electroanalytical Chemistry and Interfacial Electrochemistry*, 158(1):25 – 36, 1983.

[29] Toshiyuki Osakai, Tadaaki Kakutani, and Mitsugi Senda. A.c. polarographic study of ion transfer at the water/nitrobenzene interface. *Bulletin of the Chemical Society of Japan*, 57(2):370–376, 1984.

[30] Toshiyuki Osakai, Tadaaki Kakutani, and Mitsugi Senda. Kinetics of the transfer of picrate ion at the water/nitrobenzene interface. *Bulletin of the Chemical Society of Japan*, 58(9):2626–2633, 1985.

[31] Zdeněk Samec and Vladimír Mareček. Charge transfer between two immiscible electrolyte solutions: Part x. kinetics of tetraalkylammonium ion transfer across the water/nitrobenzene interface. *Journal of Electroanalytical Chemistry and Interfacial Electrochemistry*, 200(1):17 – 33, 1986.

[32] Yu.Ya. Gurevich and Yu.I. Kharkats. Ion transfer through a phase boundary: a stochastic approach. *Journal of Electroanalytical Chemistry and Interfacial Electrochemistry*, 200(1):3 – 16, 1986.

[33] H.H.J. Girault and D.J. Schiffrin. Electron transfer reactions at the interface between two immiscible electrolyte solutions. *Journal of Electroanalytical Chemistry and Interfacial Electrochemistry*, 244(1–2):15 – 26, 1988.

[34] Ilan Benjamin. Mechanism and dynamics of ion transfer across a liquid-liquid interface. *Science*, 261(5128):1558–1560, 1993.

[35] Karl Schweighofer and Ilan Benjamin. Transfer of a tetramethylammonium ion across the water-nitrobenzene interface: Potential of mean force and nonequilibrium dynamics. *The Journal of Physical Chemistry A*, 103(49):10274–10279, 1999.

[36] Pedro Alexandrino Fernandes, M. Natália D. S. Cordeiro, and José A. N. F. Gomes. Influence of ion size and charge in ion transfer processes across a liquid—liquid interface. *The Journal of Physical Chemistry B*, 104(10):2278–2286, 2000.

[37] Liem X. Dang. A mechanism for ion transport across the water/dichloromethane interface: A molecular dynamics study using polarizable potential models. *The Journal of Physical Chemistry B*, 105(4):804–809, 2001.

[38] W. Schmickler. A model for ion transfer through liquid/liquid interfaces. *Journal of Electroanalytical Chemistry*, 426(1):5 – 9, 1997.

[39] Stefan Frank and Wolfgang Schmickler. Ion transfer across liquid/liquid interfaces from transition-state theory and stochastic molecular dynamics simulations. *Journal of Electroanalytical Chemistry*, 590(2):138 – 144, 2006.

[40] Collin Wick and Liem X. Dang. Molecular mechanism of transporting a polarizable iodide anion across the water-ccl4 liquid/liquid interface. *The*

Journal of Chemical Physics, 126(13):134702, 2007.

[41] Nobuaki Kikkawa, Lingjian Wang, and Akihiro Morita. Microscopic barrier mechanism of ion transport through liquid–liquid interface. *Journal of the American Chemical Society*, 137(25):8022–8025, 2015. PMID: 26057005.

[42] Nobuaki Kikkawa, Lingjian Wang, and Akihiro Morita. Computational study of effect of water finger on ion transport through water-oil interface. *The Journal of Chemical Physics*, 145(1):014702, 2016.

[43] Peng Sun, François O. Laforge, and Michael V. Mirkin. Ion transfer at nanointerfaces between water and neat organic solvents. *Journal of the American Chemical Society*, 127(24):8596–8597, 2005. PMID: 15954756.

[44] Francois O. Laforge, Peng Sun, and Michael V. Mirkin. Shuttling mechanism of ion transfer at the interface between two immiscible liquids. *Journal of the American Chemical Society*, 128(46):15019–15025, 2006.

[45] Peng Sun, François O. Laforge, and Michael V. Mirkin. Role of trace amounts of water in transfers of hydrophilic and hydrophobic ions to low-polarity organic solvents. *Journal of the American Chemical Society*, 129(41):12410–12411, 2007. PMID: 17894499.

[46] Zdeněk Samec. Charge transfer between two immiscible electrolyte solutions: Part i. basic equation for the rate of the charge transfer across the interface. *Journal of Electroanalytical Chemistry and Interfacial Electrochemistry*, 99(2):197 – 205, 1979.

[47] R. A. Marcus. Reorganization free energy for electron transfers at liquid-liquid and dielectric semiconductor-liquid interfaces. *The Journal of Physical Chemistry*, 94(3):1050–1055, 1990.

[48] G. Geblewicz and D.J. Schiffrin. Electron transfer between immiscible solutions: The hexacyanoferrate-lutetium biphthalocyanine system. *Journal of Electroanalytical Chemistry and Interfacial Electrochemistry*, 244(1–2):27 – 37, 1988.

[49] R. S. Nicholson. Theory and application of cyclic voltammetry for measurement of electrode reaction kinetics. *Analytical Chemistry*, 37(11):1351–1355, 1965.

[50] Yufei Cheng and David J. Schiffrin. Electron transfer between bis(pyridine)meso-tetraphenylporphyrinato iron(ii) and ruthenium(iii) and the hexacyanof errate couple at the 1,2-dichlor. *Journal of Electroanalytical Chemistry and Interfacial Electrochemistry*, 314(1–2):153 – 163, 1991.

[51] R. A. Marcus. Theory of electron-transfer rates across liquid-liquid interfaces. *The Journal of Physical Chemistry*, 94(10):4152–4155, 1990.

[52] Yufei Cheng and David J. Schiffrin. A.c. impedance study of rate constants for two-phase electron-transfer reactions. *J. Chem. Soc., Faraday Trans.*, 89:199–205, 1993.

[53] Alan R. Brown, Lesley J. Yellowlees, and Hubert H. Girault. Photoinitiated electron-transfer reactions across the interface between two immiscible electrolyte solutions. *J. Chem. Soc., Faraday Trans.*, 89:207–212, 1993.

[54] Yoram Selzer and Daniel Mandler. A novel approach for studying charge transfer across an interface of two immiscible solutions using the scanning electrochemical microscope (secm). *Journal of Electroanalytical Chemistry*, 409(1–2):15 – 17, 1996.

[55] Theodros Solomon and Allen J. Bard. Reverse (uphill) electron transfer at the liquid/liquid interface. *The Journal of Physical Chemistry*, 99(49):17487–17489, 1995.

[56] Chang Wei, Allen J. Bard, and Michael V. Mirkin. Scanning electrochemical microscopy. 31. application of secm to the study of charge transfer processes at the liquid/liquid interface. *The Journal of Physical Chemistry*, 99(43):16033–16042, 1995.

[57] Z. Samec, V. Mareček, J. Weber, and D. Homolka. Charge transfer between two immiscible electrolyte solutions: Part vii. convolution potential sweep voltammetry of cs+ ion transfer and of electron transfer between ferrocene and hexacyanoferrate(iii) ion across the water/nitrobenzene interface. *Journal of Electroanalytical Chemistry and Interfacial Electrochemistry*, 126(1–3):105 – 119, 1981.

[58] Michael Tsionsky, Allen J. Bard, and Michael V. Mirkin. Scanning electrochemical microscopy. 34. potential dependence of the electron-transfer rate and film formation at the liquid/liquid interface. *The Journal of Physical Chemistry*, 100(45):17881–17888, 1996.

[59] Michael Tsionsky, Allen J. Bard, and Michael V. Mirkin. Long-range electron transfer through a lipid monolayer at the liquid/liquid interface. *Journal of the American Chemical Society*, 119(44):10785–10792, 1997.

[60] Hajime Katano, Kohji Maeda, and Mitsugi Senda. Effect of diffuse layer on the rate of electron transfer across an electrolyte vb electrolyte solution interface. *Journal of Electroanalytical Chemistry*, 396(1–2):391 – 396, 1995.

[61] Zhifeng Ding and Pierre F. Brevet. Heterogeneous electron transfer at the polarised water/1,2-dichloroethane interface studied by in situ uv-vis spectroscopy and differential cyclic voltabsorptometry. *Chem. Commun.*, pages 2059–2060, 1997.

[62] Robert A. W. Dryfe, Zhifeng Ding, R. Geoffrey Wellington, Pierre F. Brevet, Alexander M. Kuznetzov, , and Hubert H. Girault. Time-resolved laser-induced fluorescence study of photoinduced electron transfer at the water/1,2-dichloroethane interface. *The Journal of Physical Chemistry A*, 101(14):2519–2524, 1997.

[63] David J. Fermin and H. Dung Duong. Photocurrent responses associated

with heterogeneous electron transfer at liquid/liquid interfaces. *Chem. Commun.*, pages 1125–1126, 1998.

[64] H. Dung Duong, Pierre F. Brevet, and Hubert H. Girault. Heterogeneous electron transfer reactions at liquid/liquid interfaces studied by time-resolved absorption spectroscopy. *Journal of Photochemistry and Photobiology A: Chemistry*, 117(1):27 – 33, 1998.

[65] Biao Liu, , and Michael V. Mirkin. Potential-independent electron transfer rate at the liquid/liquid interface. *Journal of the American Chemical Society*, 121(36):8352–8355, 1999.

[66] Chunnian Shi, , and Fred C. Anson. Electron transfer between reactants located on opposite sides of liquid/liquid interfaces. *The Journal of Physical Chemistry B*, 103(30):6283–6289, 1999.

[67] W. Schmickler. Electron-transfer reactions across liquid/liquid interfaces. *Journal of Electroanalytical Chemistry*, 428(1-2):123–127, 1997.

[68] Jie Zhang and Patrick R. Unwin. Potential dependence of electron-transfer rates at the interface between two immiscible electrolyte solutions: reduction of 7,7,8,8-tetracyanoquinodimethane in 1,2-dichloroethane by aqueous ferrocyanide studied with microelectrochemical techniques. *The Journal of Physical Chemistry B*, 104(10):2341–2347, 2000.

[69] Zhifeng Ding, Bernadette M. Quinn, and Allen J. Bard. Kinetics of heterogeneous electron transfer at liquid/liquid interfaces as studied by secm. *The Journal of Physical Chemistry B*, 105(27):6367–6374, 2001.

[70] Chunnian Shi and Fred C. Anson. Rates of electron-transfer across liquid/liquid interfaces. effects of changes in driving force and reaction reversibility†. *The Journal of Physical Chemistry B*, 105(37):8963–8969, 2001.

[71] Jie Zhang and Patrick R. Unwin. Microelectrochemical measurements of electron transfer rates at the interface between two immiscible electrolyte solutions: Potential dependence of the ferro/ferricyanide-7,7,8,8-tetracyanoquinodimethane (tcnq)/tcnq[radical dot]- system. *Phys. Chem. Chem. Phys.*, 4:3820–3827, 2002.

[72] David J. Fermín, H Dung Duong, Zhifeng Ding, P-F. Brevet, and Hubert H. Girault. Photoinduced electron transfer at liquid/liquid interfaces part ii. a study of the electron transfer and recombination dynamics by intensity modulated photocurrent spectroscopy (imps). *Phys. Chem. Chem. Phys.*, 1:1461–1467, 1999.

[73] Nicolas Eugster, David J. Fermín, and Hubert H. Girault. Photoinduced electron transfer at liquid/liquid interfaces. part vi. on the thermodynamic driving force dependence of the phenomenological electron-transfer rate constant. *The Journal of Physical Chemistry B*, 106(13):3428–3433, 2002.

[74] Zhang Zhiquan, Yuan Yi, Sun Peng, Su Bin, Guo Jidong, Shao Yuanhua, and Hubert H. Study of electron-transfer reactions across an externally polarized water/1,2-dichloroethane interface by scanning electrochemical microscopy. *The Journal of Physical Chemistry B*, 106(26):6713–6717, 2002.

[75] Sun Peng, Li Fei, Chen Yong, Zhang Meiqin, Zhang Zhiquan, Gao Zhao, , and Shao Yuanhua. Observation of the marcus inverted region of electron transfer reactions at a liquid/liquid interface. *Journal of the American Chemical Society*, 125(32):9600–9601, 2003. PMID: 12904021.

[76] Hiroki Hotta, Seiko Ichikawa, Takayasu Sugihara, and Toshiyuki Osakai. Clarification of the mechanism of interfacial electron-transfer reaction between ferrocene and hexacyanoferrate(iii) by digital simulation of cyclic voltammograms. *The Journal of Physical Chemistry B*, 107(36):9717–9725, 2003.

[77] Osakai Toshiyuki, Ichikawa Seiko, Hotta Hiroki, and Nagatani Hirohisa. A true electron-transfer reaction between 5,10,15,20-tetraphenylporphyrinato cadmium(ii) and the hexacyanoferrate couple at the nitrobenzene/water interface. *Analytical Sciences*, 20(11):1567–1573, 2004.

[78] William L. Jorgensen, David S. Maxwell, and Julian Tirado-Rives. Development and testing of the opls all-atom force field on conformational energetics and properties of organic liquids. *Journal of the American Chemical Society*, 118(45):11225–11236, 1996.

[79] Chris Oostenbrink, Alessandra Villa, Alan E. Mark, and Wilfred F. Van Gunsteren. A biomolecular force field based on the free enthalpy of hydration and solvation: The gromos force-field parameter sets 53a5 and 53a6. *Journal of Computational Chemistry*, 25(13):1656–1676, 2004.

[80] Alexander D. MacKerell Jr., Nilesh Banavali, and Nicolas Foloppe. Development and current status of the charmm force field for nucleic acids. *Biopolymers*, 56(4):257–265, 2000.

[81] William C. Swope, Hans C. Andersen, Peter H. Berens, and Kent R. Wilson. A computer simulation method for the calculation of equilibrium constants for the formation of physical clusters of molecules: Application to small water clusters. *The Journal of Chemical Physics*, 76(1):637–649, 1982.

[82] H. J. C. Berendsen, J. P. M. Postma, W. F. van Gunsteren, A. DiNola, and J. R. Haak. Molecular dynamics with coupling to an external bath. *The Journal of Chemical Physics*, 81(8):3684–3690, 1984.

[83] Efrem Braun, Seyed Mohamad Moosavi, and Berend Smit. Anomalous effects of velocity rescaling algorithms: The flying ice cube effect revisited. *Journal of Chemical Theory and Computation*, 14(10):5262–5272, 2018.

PMID: 30075070.

[84] Giovanni Bussi, Davide Donadio, and Michele Parrinello. Canonical sampling through velocity rescaling. *The Journal of Chemical Physics*, 126(1):014101, 2007.

[85] D Guyomar, B Ducharne, and G Sébald. Dynamical hysteresis model of ferroelectric ceramics under electric field using fractional derivatives. *Journal of Physics D: Applied Physics*, 40(19):6048–6054, sep 2007.

[86] Lei Zhang, Xiaosong Hu, Zhenpo Wang, Fengchun Sun, and David G. Dorrell. Fractional-order modeling and state-of-charge estimation for ultracapacitors. *Journal of Power Sources*, 314:28 – 34, 2016.

[87] Changfu Zou, Lei Zhang, Xiaosong Hu, Zhenpo Wang, Torsten Wik, and Michael Pecht. A review of fractional-order techniques applied to lithium-ion batteries, lead-acid batteries, and supercapacitors. *Journal of Power Sources*, 390:286 – 296, 2018.

[88] H. Le Quoc. Electrochemical properties of the interface between two immiscible electrolyte solution. part I: Equilibrium situation and galvani potential difference. *Journal of electroanalytical chemistry, 115*, pages 159–174, 1980.

[89] J. Koryta, P. Vanysek, and Brezina M. Electrolysis with electrolyte dropping electrode. II. basic properties of the system. *Journal of electroanalytical chemistry, 75*, pages 211–228, 1977.

[90] Z. Samec, V. Marecček, J. Koryta, and W. Khalil. Investigation of ion transfer across the interface between two immiscible electrolyte solutions by cyclic voltammetry. *Journal of Electroanalytical Chemistry, 83*, pages 393–397, 1977.

[91] Z. Samec, V. Marecěk, and J. Weber. Charge transfer between two immiscible electrolyte solutions Part II. the investigation of Cs^+ ion transfer across the nitrobenzene/water interface by cyclic voltammetry with IR drop compensation. *Journal of Electroanalytical Chemistry, 100*, pages 841–852, 1978.

[92] S. Kalinowski and Z. Figaszewski. A four-electrode potentiostat-galvanostat for studies of bilayer lipid membranes. *Measure Science and Technology, 6*, pages 1050–1055, 1995.

[93] Hiroyoshi Kamogawa and Shigeki Sato. Redox photochromism of arylviologen crystals. *Bulletin of the Chemical Society of Japan*, 64(1):321–323, 1991.

[94] CHARLES C. WANG. Second-harmonic generation of light at the boundary of an isotropic medium. *Phys. Rev.*, 178:1457–1460, Feb 1969.

[95] N. Bloembergen and P. S. Pershan. Light waves at the boundary of nonlinear media. *Phys. Rev.*, 128:606–622, Oct 1962.

[96] J. M. Hicks, K. Kemnitz, K. B. Eisenthal, and T. F. Heinz. Studies of liquid surfaces by second harmonic generation. *The Journal of Physical Chemistry*, 90(4):560–562, 1986.

[97] Alonso Castro, Shaowei Ong, and Kenneth B. Eisenthal. Studies of molecular properties at the surface of a liquid jet by second harmonic generation. *Chemical Physics Letters*, 163(4):412 – 416, 1989.

[98] Daniel A. Higgins, Michael B. Abrams, Shannon K. Byerly, and Robert M. Corn. Resonant second harmonic generation studies of p-nitrophenol adsorption at condensed-phase interfaces. *Langmuir*, 8(8):1994–2000, 1992.

[99] S. G. Grubb, Mahn Won Kim, T. Rasing, and Y. R. Shen. Orientation of molecular monolayers at the liquid-liquid interface as studied by optical second harmonic generation. *Langmuir*, 4(2):452–454, 1988.

[100] Daniel A. Higgins and Robert M. Corn. Second harmonic generation studies of adsorption at a liquid-liquid electrochemical interface. *The Journal of Physical Chemistry*, 97(2):489–493, 1993.

[101] Daniel A. Higgins, Roberta R. Naujok, and Robert M. Corn. Second harmonic generation measurements of molecular orientation and coadsorption at the interface between two immiscible electrolyte solutions. *Chemical Physics Letters*, 213(5):485 – 490, 1993.

[102] John C. Conboy and Geraldine L. Richmond. Total internal reflection second harmonic generation from the interface between two immiscible electrolyte solutions. *Electrochimica Acta*, 40(18):2881 – 2886, 1995.

[103] John C. Conboy, , and Geraldine L. Richmond*. Examination of the electrochemical interface between two immiscible electrolyte solutions by second harmonic generation. *The Journal of Physical Chemistry B*, 101(6):983–990, 1997.

[104] Poul B. Petersen, , Richard J. Saykally*, Martin Mucha, , and Pavel Jungwirth*. Enhanced concentration of polarizable anions at the liquid water surface: Shg spectroscopy and md simulations of sodium thiocyanide. *The Journal of Physical Chemistry B*, 109(21):10915–10921, 2005. PMID: 16852329.

[105] Poul B. Petersen, , and Richard J. Saykally*. Evidence for an enhanced hydronium concentration at the liquid water surface. *The Journal of Physical Chemistry B*, 109(16):7976–7980, 2005. PMID: 16851932.

[106] A. A. Tamburello-Luca, Ph. Hébert, R. Antoine, P. F. Brevet, , and H. H. Girault*. Optical surface second harmonic generation study of the two acid/base equilibria of eosin b at the air/water interface. *Langmuir*, 13(16):4428–4434, 1997.

[107] Hongfei Wang, E. Borguet, and K. B. Eisenthal. Polarity of liquid interfaces by second harmonic generation spectroscopy. *The Journal of Physical*

Chemistry A, 101(4):713–718, 1997.

[108] Hongfei Wang, E. Borguet, and K. B. Eisenthal. Generalized interface polarity scale based on second harmonic spectroscopy. *The Journal of Physical Chemistry B*, 102(25):4927–4932, 1998.

[109] William H. Steel and Robert A. Walkerl. Measuring dipolar width across liquid-liquid interfaces with 'molecular rulers'. *Nature*, 424:296–299, 2003.

[110] Hirohisa Nagatani, Alexis Piron, Pierre-François Brevet, David J. Fermín, , and Hubert H. Girault. Surface second harmonic generation of cationic water-soluble porphyrins at the polarized water—1,2-dichloroethane interface. *Langmuir*, 18(17):6647–6652, 2002.

[111] Hirohisa Nagatani, Zdeněk Samec, Pierre-François Brevet, David J. Fermín, and Hubert H. Girault. Adsorption and aggregation of meso-tetrakis(4-carboxyphenyl)porphyrinato zinc(ii) at the polarized water—1,2-dichloroethane interface. *The Journal of Physical Chemistry B*, 107(3):786–790, 2003.

[112] Kazuhiko Fujiwara, Hideaki Monjushiro, and Hitoshi Watarai. Non-linear optical activity of porphyrin aggregate at the liquid/liquid interface. *Chemical Physics Letters*, 394(4–6):349 – 353, 2004.

[113] Astrid J. Olaya, Delphine Schaming, Pierre-Francois Brevet, Hirohisa Nagatani, Hai-Jun Xu, Michel Meyer, and Hubert H. Girault. Interfacial self-assembly of water-soluble cationic porphyrins for the reduction of oxygen to water. *Angewandte Chemie International Edition*, 51(26):6447–6451, 2012.

[114] Astrid J. Olaya, Delphine Schaming, Pierre-Francois Brevet, Hirohisa Nagatani, Tomas Zimmermann, Jiri Vanicek, Hai-Jun Xu, Claude P. Gros, Jean-Michel Barbe, and Hubert H. Girault. Self-assembled molecular rafts at liquid—liquid interfaces for four-electron oxygen reduction. *Journal of the American Chemical Society*, 134(1):498–506, 2012. PMID: 22107335.

[115] E. V. Sitzmann and K. B. Eisenthal. Dynamics of intermolecular electronic energy transfer at an air/liquid interface. *The Journal of Chemical Physics*, 90(5):2831–2832, 1989.

[116] Piotr Fita, Angela Punzi, and Eric Vauthey. Local viscosity of binary water+glycerol mixtures at liquid/liquid interfaces probed by time-resolved surface second harmonic generation. *The Journal of Physical Chemistry C*, 113(48):20705–20712, 2009.

[117] X. Shi, E. Borguet, A.N. Tarnovsky, and K.B. Eisenthal. Ultrafast dynamics and structure at aqueous interfaces by second harmonic generation. *Chemical Physics*, 205(1–2):167 – 178, 1996. Surface Reaction Dynamics.

[118] Angela Punzi, Gaëlle Martin-Gassin, Jakob Grilj, and Eric Vauthey. Effect of salt on the excited-state dynamics of malachite green in bulk aqueous

solutions and at air/water interfaces: a femtosecond transient absorption and surface second harmonic generation study†. *The Journal of Physical Chemistry C*, 113(27):11822–11829, 2009.

[119] W. Kunz, P. Lo Nostro, and B.W. Ninham. The present state of affairs with hofmeister effects. *Current Opinion in Colloid and Interface Science*, 9(1–2):1 – 18, 2004.

[120] Alonso Castro, Eugene V. Sitzmann, Dan Zhang, and Kenneth B. Eisenthal. Rotational relaxation at the air/water interface by time-resolved second harmonic generation. *The Journal of Physical Chemistry*, 95(18):6752–6753, 1991.

[121] R Antoine, A.A Tamburello-Luca, Ph Hébert, P.F Brevet, and H.H Girault. Picosecond dynamics of eosin b at the air/water interface by time-resolved second harmonic generation: orientational randomization and rotational relaxation. *Chemical Physics Letters*, 288(1):138 – 146, 1998.

[122] David Zimdars, J. I. Dadap, Kenneth B. Eisenthal, , and T. F. Heinz. Anisotropic orientational motion of molecular adsorbates at the air-water interface. *The Journal of Physical Chemistry B*, 103(17):3425–3433, 1999.

[123] David Zimdars, Jerry I. Dadap, Kenneth B. Eisenthal, and Tony F. Heinz. Femtosecond dynamics of solvation at the air/water interface. *Chemical Physics Letters*, 301(1–2):112 – 120, 1999.

[124] David Zimdars, , and Kenneth B. Eisenthal. Effect of solute orientation on solvation dynamics at the air/water interface. *The Journal of Physical Chemistry A*, 103(49):10567–10570, 1999.

[125] Jae-Hyung Jeon, Hector Martinez-Seara Monne, Matti Javanainen, and Ralf Metzler. Anomalous diffusion of phospholipids and cholesterols in a lipid bilayer and its origins. *Phys. Rev. Lett.*, 109:188103, Oct 2012.

[126] Carlo Manzo, Juan A. Torreno-Pina, Pietro Massignan, Gerald J. Lapeyre, Maciej Lewenstein, and Maria F. Garcia Parajo. Weak ergodicity breaking of receptor motion in living cells stemming from random diffusivity. *Phys. Rev. X*, 5:011021, Feb 2015.

[127] Jae-Hyung Jeon, Vincent Tejedor, Stas Burov, Eli Barkai, Christine Selhuber-Unkel, Kirstine Berg-Sørensen, Lene Oddershede, and Ralf Metzler. In vivo anomalous diffusion and weak ergodicity breaking of lipid granules. *Phys. Rev. Lett.*, 106:048103, Jan 2011.

[128] Stas Burov, Jae-Hyung Jeon, Ralf Metzler, and Eli Barkai. Single particle tracking in systems showing anomalous diffusion: the role of weak ergodicity breaking. *Phys. Chem. Chem. Phys.*, 13:1800–1812, 2011.

[129] Haitao Qi and Xiaoyun Jiang. Solutions of the space-time fractional cattaneo diffusion equation. *Physica A: Statistical Mechanics and its Applications*, 390(11):1876 – 1883, 2011.

[130] K. Razi Naqvi. Diffusion-controlled reactions in two-dimensional fluids: discussion of measurements of lateral diffusion of lipids in biological membranes. *Chemical Physics Letters*, 28(2):280 – 284, 1974.

[131] Charles S. Owen. Two dimensional diffusion theory: Cylindrical diffusion model applied to fluorescence quenching. *The Journal of Chemical Physics*, 62(8):3204–3207, 1975.

[132] H. S. Carslaw and J. C. Jaeger. Some two-dimensional problems in conduction of heat with circular symmetry. *Proceedings of the London Mathematical Society*, s2-46(1):361–388, 1940.

[133] Jorge Martins, Winchil L. C. Vaz, and Eurico Melo. Long-range diffusion coefficients in two-dimensional fluid media measured by the pyrene excimer reaction. *The Journal of Physical Chemistry*, 100(5):1889–1895, 1996.

[134] Cornelis A. Emeis and P. L. Fehder. Microscopic mechanism for diffusion and the rates of diffusion-controlled reactions in simple liquid solvents. *Journal of the American Chemical Society*, 92(8):2246–2252, 1970.

[135] Bin Su, Nicolas Eugster, and Hubert H. Girault. Simulations of the adsorption of ionic species at polarisable liquid/liquid interfaces. *Journal of Electroanalytical Chemistry*, 577(2):187 – 196, 2005.

[136] Takashi Kakiuchi and Mitsugi Senda. Polarizability and electrocapillary measurements of the nitrobenzene-water interface. *Bulletin of the Chemical Society of Japan*, 56(5):1322–1326, 1983.

[137] Antonín Trojánek, Alexandr Lhotský, Vladimír Mareček, and Zdeněk Samec. Limited agreement between the interfacial tension and differential capacity data for the polarised water 1,2-dichloroethane interface. *Journal of Electroanalytical Chemistry*, 565(2):243 – 250, 2004.

[138] Alexandr Lhotský, Vladimír Mareček, Stanislav Záliš, and Zdeněk Samec. Specific adsorption of tetraalkylammonium cations at the water 1,2-dichloroethane interface revisited. *Journal of Electroanalytical Chemistry*, 585(2):269 – 274, 2005.

[139] L.I. Daikhin and M. Urbakh. Double layer capacitance and a microscopic structure of electrified liquid-liquid interfaces. *Journal of Electroanalytical Chemistry*, 560(1):59 – 67, 2003.

[140] H.H. Girault. *Electrochimie Physique et Analytique*. Presse Polytechnique et Universitaires Romandes, 2007.

[141] Mario Vazdar, Eva Pluhařová, Phil E. Mason, Robert Vácha, and Pavel Jungwirth. Ions at hydrophobic aqueous interfaces: Molecular dynamics with effective polarization. *The Journal of Physical Chemistry Letters*, 3(15):2087–2091, 2012.

[142] Gosta Akerlof. Dielectric constants of some organic solvent-water mixtures at various temperatures. *Journal of the American Chemical Society*,

54(11):4125–4139, 1932.

[143] Vladislav S. Markin, Alexander G. Volkov, and Maya I. Volkova-Gugeshashvili. Structure of nonpolarizable water-nitrobenzene interface: Potential distribution, ion adsorption, and interfacial tension. *The Journal of Physical Chemistry B*, 109(34):16444–16454, 2005. PMID: 16853091.

[144] Dmitry Momotenko, Carlos M. Pereira, and Hubert H. Girault. Differential capacitance of liquid/liquid interfaces of finite thicknesses: a finite element study. *Phys. Chem. Chem. Phys.*, 14:11268–11272, 2012.

[145] Tove Sigvarsten, Bo Gestblom, Erik Noreland, and Jon Songstad. Conductometric and dielectric behaviour of solutions of tetrabutylammonium perchlorate in solvents of low and medium permittivity. *Acta. Chem. Scand.*, 43:103–115, 1989.

[146] Kasper P. Jensen and William L. Jorgensen. Halide, ammonium, and alkali metal ion parameters for modeling aqueous solutions. *Journal of Chemical Theory and Computation*, 2(6):1499–1509, 2006. PMID: 26627020.

[147] Florian Weigend and Reinhart Ahlrichs. Balanced basis sets of split valence, triple zeta valence and quadruple zeta valence quality for h to rn: Design and assessment of accuracy. *Phys. Chem. Chem. Phys.*, 7:3297–3305, 2005.

[148] Pekka Peljo, Micheál D. Scanlon, and T. Jane Stockmann. Simulations employing finite element method at liquid—liquid interfaces. *Current Opinion in Electrochemistry*, 7:200 – 207, 2018.

[149] Pekka Peljo and Hubert.H. Girault. Heterogeneous versus homogeneous electron transfer reactions at liquid–liquid interfaces: The wrong question? *Journal of Electroanalytical Chemistry*, 779:187 – 198, 2016. Special issue in honor of Koichi Aoki.

[150] Toshiyuki Osakai, Seiko Ichikawa, Hiroki Hotta, and Hirohisa Nagatani. A true electron-transfer reaction between 5,10,15,20-tetraphenylporphyrinato cadmium(ii) and the hexacyanoferrate couple at the nitrobenzene/water interface. *Analytical Sciences*, 20(11):1567–1573, 2004.

[151] C. L. Bird and A. T. Kuhn. Electrochemistry of the viologens. *Chem. Soc. Rev.*, 10:49–82, 1981.

[152] Wojciech Adamiak, Justyna Jedraszko, Olga Krysiak, Wojciech Nogala, Jonnathan C. Hidalgo-Acosta, Hubert H. Girault, and Marcin Opallo. Hydrogen and hydrogen peroxide formation in trifluorotoluene-water biphasic systems. *The Journal of Physical Chemistry C*, 118(40):23154–23161, 2014.

[153] Indra Noviandri, Kylie N. Brown, Douglas S. Fleming, Peter T. Gulyas, Peter A. Lay, Anthony F. Masters, and Leonidas Phillips. The decamethylferrocenium/decamethylferrocene redox couple: A superior redox standard to the ferrocenium/ferrocene redox couple for studying solvent effects on the thermodynamics of electron transfer. *The Journal of Physical*

Chemistry B, 103(32):6713–6722, 1999.

[154] Evgeny Smirnov, Pekka Peljo, Micheál D. Scanlon, and Hubert H. Girault. Gold nanofilm redox catalysis for oxygen reduction at soft interfaces. *Electrochimica Acta*, pages –, 2015.

[155] A. A. Stewart, J. A. Campbell, H. H. Girault, and M. Edddowes. Cyclic voltammetry for electron transfer reactions at liquid/liquid interfaces. *Berichte der Bunsengesellschaft für physikalische Chemie*, 94(1):83–87, 1990.

[156] Lucie Rivier, T. Jane Stockmann, Manuel A. Méndez, Micheál D. Scanlon, Pekka Peljo, Marcin Opallo, and Hubert H. Girault. Decamethylruthenocene hydride and hydrogen formation at liquid/liquid interfaces. *The Journal of Physical Chemistry C*, 119(46):25761–25769, 2015.

[157] Lucie Rivier, Pekka Peljo, Laurent A. C. Vannay, Grégoire C. Gschwend, Manuel A. Méndez, Clémence Corminboeuf, Micheál D. Scanlon, and Hubert H. Girault. Photoproduction of hydrogen by decamethylruthenocene combined with electrochemical recycling. *Angewandte Chemie International Edition*, 56(9):2324–2327, 2017.

[158] A. Pockels. Surface tension. *Nature*, 43:437–439, 1891.

[159] Irving Langmuir. The constituion and fundamental properties of solids and liquids. ii. liquids.1. *Journal of the American Chemical Society*, 39(9):1848–1906, 1917.

[160] E. V. Sitzmann and K. B. Eisenthal. Picosecond dynamics of a chemical reaction at the air-water interface studied by surface second harmonic generation. *The Journal of Physical Chemistry*, 92(16):4579–4580, 1988.

[161] Giuseppe Licari, Joseph S. Beckwith, Saeideh Soleimanpour, Stefan Matile, and Eric Vauthey. Detecting order and lateral pressure at biomimetic interfaces using a mechanosensitive second-harmonic-generation probe. *Phys. Chem. Chem. Phys.*, 20:9328–9336, 2018.

[162] Shoji Ishizaka, Haeng-Boo Kim, and Noboru Kitamura. Time-resolved total internal reflection fluorometry study on polarity at a liquid/liquid interface. *Analytical Chemistry*, 73(11):2421–2428, 2001.

[163] D. J. Balding and N. J. B. Green. Diffusion-controlled reactions in one dimension: Exact solutions and deterministic approximations. *Phys. Rev. A*, 40:4585–4592, Oct 1989.

[164] Jorge Martins, K. Razi Naqvi, and Eurico Melo. Kinetics of two-dimensional diffusion-controlled reactions: A monte carlo simulation of hard-disk reactants undergoing a pearson-type random walk. *The Journal of Physical Chemistry B*, 104(20):4986–4991, 2000.

[165] M.J. Saxton. Anomalous diffusion due to obstacles: a monte carlo study. *Biophysical Journal*, 66(2, Part 1):394 – 401, 1994.

[166] Hugues Berry. Monte carlo simulations of enzyme reactions in two dimensions: Fractal kinetics and spatial segregation. *Biophysical Journal*, 83(4):1891 – 1901, 2002.

[167] M. Hellmann, D. W. Heermann, and M. Weiss. Anomalous reaction kinetics and domain formation on crowded membranes. *EPL (Europhysics Letters)*, 94(1):18002, 2011.

[168] Raoul Kopelman. Fractal reaction kinetics. *Science*, 241(4873):1620–1626, 1988.

[169] D.C. Torney and H.M.M McConnel. Diffusion-limited reaction rate theory for two-dimensional systems. *Proceedings of the Royal Society of London A: Mathematical, Physical and Engineering Sciences*, 387(1792):147–170, 1983.

[170] O. Bénichou, C. Chevalier, J. Klafter, B. Meyer, and R. Voituriez. Geometry-controlled kinetics. *Nature Chemistry*, 2:472 – 477, 2010.

[171] Dusanka Milenkovic, James N. Blaza, Nils-Göran Larsson, and Judy Hirst. The enigma of the respiratory chain supercomplex. *Cell Metabolism*, 25(4):765 – 776, 2017.

[172] Helmut Kirchhoff. Diffusion of molecules and macromolecules in thylakoid membranes. *Biochimica et Biophysica Acta (BBA) - Bioenergetics*, 1837(4):495 – 502, 2014.

[173] P.D. Calvert, V.I. Govardovskii, N. Krasnoperova, R.E. Anderson, J. Lem, and C.L. Makino. Membrane protein diffusion sets the speed of rod phototransduction. *Nature*, 411:90 – 94, 2001.

[174] L. Li and L.K. Patterson. Kinetics of in-plane photoinduced electron transfer between lipid-functionalized pyrene and alkyl-substituted dipyridinium cation in lipid vesicles and langmuir films. *Journal of Physical Chemistry*, 99(43), 10 1995.

[175] F. Caruso, F. Grieser, A. Murphy, P. Thistlethwaite, R. Urquhart, M. Almgren, and E. Wistus. Determination of lateral diffusion coefficients in air-water monolayers by fluorescence quenching measurements. *Journal of the American Chemical Society*, 113(13):4838–4843, 1991.

[176] Koji Kano, Hirofumi Kawazumi, Teiichiro Ogawa, and Junzo Sunamoto. Fluorescence quenching in liposomal membranes. exciplex as a probe for investigating artificial lipid membrane properties. 85, 07 1981.

[177] Heike Kahl, Tino Wadewitz, and Jochen Winkelmann. Surface tension and interfacial tension of binary organic liquid mixtures. *Journal of Chemical & Engineering Data*, 48(6):1500–1507, 2003.

[178] K. Kalyanasundaram and M. Neumann-Spallart. Photophysical and redox properties of water-soluble porphyrins in aqueous media. *The Journal of Physical Chemistry*, 86(26):5163–5169, 1982.

[179] R.John Ellis. Macromolecular crowding: obvious but underappreciated. *Trends in Biochemical Sciences*, 26(10):597 – 604, 2001.

[180] S. Schnell and T.E. Turner. Reaction kinetics in intracellular environments with macromolecular crowding: simulations and rate laws. *Progress in Biophysics and Molecular Biology*, 85(2):235 – 260, 2004. Modelling Cellular and Tissue Function.

[181] Ralf Metzler and Joseph Klafter. The random walk's guide to anomalous diffusion: a fractional dynamics approach. *Physics Reports*, 339(1):1 – 77, 2000.

[182] Ralf Metzler, Jae-Hyung Jeon, Andrey G. Cherstvy, and Eli Barkai. Anomalous diffusion models and their properties: non-stationarity, non-ergodicity, and ageing at the centenary of single particle tracking. *Phys. Chem. Chem. Phys.*, 16:24128–24164, 2014.

[183] Hédi Soula, Bertrand Caré, Guillaume Beslon, and Hugues Berry. Anomalous versus slowed-down brownian diffusion in the ligand-binding equilibrium. *Biophysical Journal*, 105(9):2064 – 2073, 2013.

[184] G. Bel and E. Barkai. Weak ergodicity breaking in the continuous-time random walk. *Phys. Rev. Lett.*, 94:240602, Jun 2005.

[185] B.I Henry and S.L Wearne. Fractional reaction-diffusion. *Physica A: Statistical Mechanics and its Applications*, 276(3):448 – 455, 2000.

[186] Kazuhiko Seki, Mariusz Wojcik, and M. Tachiya. Fractional reaction-diffusion equation. *The Journal of Chemical Physics*, 119(4):2165–2170, 2003.

[187] B. I. Henry, T. A. M. Langlands, and S. L. Wearne. Anomalous diffusion with linear reaction dynamics: From continuous time random walks to fractional reaction-diffusion equations. *Phys. Rev. E*, 74:031116, Sep 2006.

[188] C. N. Angstmann, I. C. Donnelly, and B. I. Henry. Continuous time random walks with reactions forcing and trapping. *Mathematical Modelling of Natural Phenomena*, 8(2):17–27, 2013.

[189] Mark James Abraham, Teemu Murtola, Roland Schulz, Szilárd Páll, Jeremy C. Smith, Berk Hess, and Erik Lindahl. Gromacs: High performance molecular simulations through multi-level parallelism from laptops to supercomputers. *SoftwareX*, 1-2:19 – 25, 2015.

[190] Szilárd Páll, Mark James Abraham, Carsten Kutzner, Berk Hess, and Erik Lindahl. Tackling exascale software challenges in molecular dynamics simulations with gromacs. In Stefano Markidis and Erwin Laure, editors, *Solving Software Challenges for Exascale*, pages 3–27, Cham, 2015. Springer International Publishing.

[191] Sander Pronk, Szilárd Páll, Roland Schulz, Per Larsson, Pär Bjelkmar, Rossen Apostolov, Michael R. Shirts, Jeremy C. Smith, Peter M. Kasson,

David van der Spoel, Berk Hess, and Erik Lindahl. Gromacs 4.5: a high-throughput and highly parallel open source molecular simulation toolkit. *Bioinformatics*, 29(7):845–854, 2013.

[192] Berk Hess, Carsten Kutzner, David van der Spoel, and Erik Lindahl. Gromacs 4: Algorithms for highly efficient, load-balanced, and scalable molecular simulation. *Journal of Chemical Theory and Computation*, 4(3):435–447, 2008.

[193] Van Der Spoel David, Lindahl Erik, Hess Berk, Groenhof Gerrit, Mark Alan E., and Berendsen Herman J. C. Gromacs: Fast, flexible, and free. *Journal of Computational Chemistry*, 26(16):1701–1718, 2005.

[194] Erik Lindahl, Berk Hess, and David van der Spoel. Gromacs 3.0: a package for molecular simulation and trajectory analysis. *Molecular modeling annual*, 7(8):306–317, Aug 2001.

[195] H.J.C. Berendsen, D. van der Spoel, and R. van Drunen. Gromacs: A message-passing parallel molecular dynamics implementation. *Computer Physics Communications*, 91(1):43 – 56, 1995.

[196] Somisetti V. Sambasivarao and Orlando Acevedo. Development of opls-aa force field parameters for 68 unique ionic liquids. *Journal of Chemical Theory and Computation*, 5(4):1038–1050, 2009.

[197] I. V. Leontyev and A. A. Stuchebrukhov. Electronic continuum model for molecular dynamics simulations. *The Journal of Chemical Physics*, 130(8):085102, 2009.

[198] I. V. Leontyev and A. A. Stuchebrukhov. Electronic continuum model for molecular dynamics simulations of biological molecules. *Journal of Chemical Theory and Computation*, 6(5):1498–1508, 2010.

[199] Berk Hess. P-lincs: A parallel linear constraint solver for molecular simulation. *Journal of Chemical Theory and Computation*, 4(1):116–122, 2008.

[200] Jochen S. Hub, Bert L. de Groot, and David van der Spoel. g_wham a free weighted histogram analysis implementation including robust error and autocorrelation estimates. *Journal of Chemical Theory and Computation*, 6(12):3713–3720, 2010.

Curriculum Vitae

Grégoire C. Gschwend
EPFL Valais Wallis
Rue de l'Industrie 17
CH-1951 Sion
gregoire.gschwend@epfl.ch

Education

PhD Student (2015-2019)	École Polytechnique Fédérale de Lausanne Laboratory of Physical and Analytical Electrochemistry
Minor (Phyiscs) (2013-2014)	École Polytechnique Fédérale de Lausanne
Master (2012-2014)	École Polytechnique Fédérale de Lausanne
Bachelor (2011-2012) (2009-2011)	Imperial College London (Ersamus student) École Polytechnique Fédérale de Lausanne

Research experience

Master project (2014)	*Electron transfer at polarised interfaces: new insights* École Polytechnique Fédérale de Lausanne Pr. Hubert Girault Laboratory of Physical and Analytical Electrochemistry
Research project (2012)	*Theoretical study of fulvene and azulene radical cations in the interstellar medium.* Imperial College London Pr. Michael Bearpark Molecular Sciences Research Hub

Scientific skills

- Second harmonic generation spectroscopy, Electrochemistry at soft interfaces, Impedance spectroscopy
- Molecular simulatiom softwares: GROMACS, GAMESS, Gaussian, NW Chem, Quantum Espresso, CP2K, VMD

Publications

- G.C. Gschwend, E. Smirnov, P. Peljo and H.H. Girault, Electrovariable gold nanoparticle films at liquid–liquid interfaces: from redox electrocatalysis to Marangoni-shutters. *Faraday discussions*, 199, 565-583, 2017
- G.C. Gschwend, M. Kazmierczak, A.J. Olaya, P-F. Brevet and H.H. Girault, 2D diffusion controlled triplet-triplet annihilation kinetics, (*in press*)
- P. Peljo, E. Vladimirova, E. Smirnov, G. Gschwend, L. Rivier and H.H. Girault, Effect of Chaotropes on the transfer of ions and dyes across the liquid-liquid interface, *The Journal of Physical Chemistry C*, 122 (32), 18510-18519, 2018
- L. Rivier, P. Peljo, L. A. C. Vannay, G.C. Gschwend, M.A. Méndez, C. Corminboeuf, M.D. Scanlon, and H. H. Girault. Photoproduction of hydrogen by decamethylruthenocene combined with electrochemical recycling. *Angewandte Chemie International Edition*, 56(9):2324–2327, 2017.
- S. Gharibzadeh, F. Valduga de Almeida Camargo, C. Roldán-Carmona, G.C. Gschwend, J. Pascual, R. Tena-Zaera, G. Cerullo, G. Grancini and M.K. Nazeeruddin, Picosecond Capture of Photoexcited Electrons Improves Photovoltaic Conversion in MAPbI3:C70-Doped Planar and Mesoporous Solar Cells, *Advanced Materials*, 30 (40), 1801496
- E. Zanzola, S. Gentil, G.C. Gschwend, D. Reynard, E. Smirnov, C R Dennison and Hubert H Girault, Solid electrochemical energy storage for aqueous redox flow batteries: the case of copper hexacyanoferrate, *submited*

**Ce document a été imprimé au Centre d'impression EPFL,
imprimerie climatiquement neutre, certifiée myClimate.**